

University of Denver

Digital Commons @ DU

Electronic Theses and Dissertations

Graduate Studies

1-1-2016

Modeling and Simulation of Optical Properties of Noble Metals Triangular Nanoprisms

Soad Zahir Alsheheri
University of Denver

Follow this and additional works at: <https://digitalcommons.du.edu/etd>



Part of the [Nanoscience and Nanotechnology Commons](#)

Recommended Citation

Alsheheri, Soad Zahir, "Modeling and Simulation of Optical Properties of Noble Metals Triangular Nanoprisms" (2016). *Electronic Theses and Dissertations*. 1107.
<https://digitalcommons.du.edu/etd/1107>

This Dissertation is brought to you for free and open access by the Graduate Studies at Digital Commons @ DU. It has been accepted for inclusion in Electronic Theses and Dissertations by an authorized administrator of Digital Commons @ DU. For more information, please contact jennifer.cox@du.edu, dig-commons@du.edu.

Modeling and Simulation of Optical Properties of Noble Metals Triangular Nanoprisms

Abstract

Gold and silver has gained huge attention across the scientific community for its applications arising from its plasmonic properties. The optical properties achieved by these materials via excitation of plasmons is very unique to these materials and used as diagnostic and therapeutic agents in the field of medicine, and as sensors in a gamut of disciplines such as energy and environmental protection to name a few. Surface plasmon resonance (SPR) properties of the gold and silver are size and shape dependent. Of the various shapes reported in literature, triangular nanoprisms has tunable optical properties in the visible and near IR region by manipulating the structural features such as thickness, edge length, and morphology of tip. To understand the effect of these parameters on dipole surface plasmon resonance we have constructed triangular silver nanoprism and sandwich of gold and triangular nanoprism using Optiwave FDTD. Silver triangular nanoprism has exhibited blue shift on introduction of truncation and the blue shift continued further with depth of truncation. Similar observations were made for increase in thickness of nanoprism. In contrast, increase in edge length of the nanoprism has introduced a blue shift in dipole surface plasmon resonance. Coupling of gold and silver as sandwich with a dielectric material has introduced two plasmon resonance peaks in the visible and near IR region. In contrast to individual silver triangular nanoprism, increasing the edge length and thickness of gold and silver has introduced a red shift. Interestingly, thickness of the dielectric layer controls the wavelength of the dipole plasmon resonance of metals in the sandwich and its strength.

Document Type

Dissertation

Degree Name

Ph.D.

Department

Mechanical Engineering

First Advisor

Mohammad Matin, Ph.D.

Second Advisor

Matthew Gordon

Third Advisor

Yun Bo Yi

Keywords

Finite difference time domain, Nanoprism, Optical properties, Optiwave, Plasmonic, Simulation

Subject Categories

Nanoscience and Nanotechnology

Publication Statement

Copyright is held by the author. User is responsible for all copyright compliance.

This dissertation is available at Digital Commons @ DU: <https://digitalcommons.du.edu/etd/1107>

MODELING AND SIMULATION OF OPTICAL PROPERTIES OF NOBLE METALS
TRIANGULAR NANOPRISMS

A Dissertation

Presented to

the Faculty of the Daniel Felix Ritchie School of Engineering and Computer Science

University of Denver

In Partial Fulfillment

of the Requirements for the Degree

Doctor of Philosophy

by

Soad Alsheheri

June 2016

Advisor: Mohammad Matin

Author: Soad Alsheheri
Title: MODELING AND SIMULATION OF OPTICAL PROPERTIES OF NOBLE METALS TRIANGULAR NANOPRISMS
Advisor: Mohammad Matin
Degree Date: June 2016

Abstract

Gold and silver has gained huge attention across the scientific community for its applications arising from its plasmonic properties. The optical properties achieved by these materials via excitation of plasmons is very unique to these materials and used as diagnostic and therapeutic agents in the field of medicine, and as sensors in a gamut of disciplines such as energy and environmental protection to name a few. Surface plasmon resonance (SPR) properties of the gold and silver are size and shape dependent. Of the various shapes reported in literature, triangular nanoprisms has tunable optical properties in the visible and near IR region by manipulating the structural features such as thickness, edge length, and morphology of tip. To understand the effect of these parameters on dipole surface plasmon resonance we have constructed triangular silver nanoprism and sandwich of gold and triangular nanoprism using Optiwave FDTD. Silver triangular nanoprism has exhibited blue shift on introduction of truncation and the blue shift continued further with depth of truncation. Similar observations were made for increase in thickness of nanoprism. In contrast, increase in edge length of the nanoprism has introduced a blue shift in dipole surface plasmon resonance. Coupling of gold and silver as sandwich with a dielectric material has introduced two plasmon resonance peaks in the

visible and near IR region. In contrast to individual silver triangular nanoprism, increasing the edge length and thickness of gold and silver has introduced a red shift. Interestingly, thickness of the dielectric layer controls the wavelength of the dipole plasmon resonance of metals in the sandwich and its strength.

Acknowledgements

In acknowledgment of the personal and professional support I have received throughout the process of completing my Ph.D. study, I would like to begin by expressing my deep gratitude to Professor Mohammad Matin, my advisor. He has provided, with unfailing patience and kindness, the continuous guidance that has motivated my research and writing.

Sincere thanks are also due to the rest of my dissertation committee: Prof. Matthew Gordon, Prof. Yun-Bo Yi, and Dr. Vi Narapareddy, for maintaining their encouragement and support throughout the process. With comments and hard questions from their various perspectives, they have given me the inspiration to widen my research.

For my initial enlightenment and first glance at attempting the research, I offer my sincere thanks to Dr. Marjan Saboktakin. She has been a wonderful friend who has willingly given of her time and immense knowledge to provide me with the motivation to complete the research process.

I would also like to thank my family, my parents, my brothers, and my sisters, for supporting and encouraging me with their best wishes. A special word of thanks goes to my lovely son Mazen.

With special love and gratitude, my final thanks go to my husband, without whose support, patience, and sacrifice, I could not have completed this dissertation.

Table of Contents

Abstract.....	ii
Acknowledgements.....	iv
List of Figures.....	viii
List of Table.....	xi
Chapter One: Introduction	1
1.1 Background.....	1
1.2 Problem Statement.....	2
1.3 Objective.....	3
1.4 Scope of Research Work.....	3
1.5 Methodology.....	4
1.6 Contribution and Publications.....	4
1.7 Chapter Organization.....	5
Chapter Two: Surface Plasmon Resonances (SPRs)	7
2.1 Introducion.....	7
2.2 Mie Theory.....	16
2.3 Postulates of Mie Theory.....	16
2.4 Deviation from Sphericity.....	17
2.5 Limitation of Mie Theory.....	17
2.6 Effective Medium Theory.....	17
2.7 Discrete Dipole Approximation Method.....	25
2.8 Finite Difference Time-Domain Method (FDTD).....	28
2.8.1 One-Dimensional Simulation.....	32
2.8.2 Two-Dimensional Simulations.....	34
2.8.3 Three-Dimensional Simulation.....	35
2.9 FDTD Simulation Software.....	37
2.10 Lorentz-Drude Model (FDTD).....	39
2.11 Anisotropic Colloidal Assemblies.....	41
2.11.1 Effect of Snipping or Truncation.....	44
2.11.2 Effect of dielectric on plasmonic properties.....	44
2.12 Synthesis of Nanomaterials.....	45
2.13 Synthesis of Triangular Nanoprisms.....	47
2.14 FDTD Simulation Parameters.....	64
Chapter Three: Study of the Snip Effect in Resonance of Gold and Silver Triangular Nanoprisms	68
3.1. The effect of the edge length and thickness of perfect triangular gold and silver nanoprism.....	68

3.2 The effect of edge length and thickness of truncated triangular gold and silver nanoprism.....	72
3.3 The effect of truncation of gold and silver.....	85
3.4 Conclusion	97
Chapter Four: The Effect of Truncation and Dielectric in Plasmonic Resonance of Hybrid Plasmonic Nanosandwich Structures in Optical Range	98
4.1 Introduction.....	98
4.2 The Effect of Dielectric	100
4.3 Ag- dielectric-Au Sandwich	110
4.4 Conclusion	116
Chapter Five: Summary & Future Work	117
References.....	119
Appendix A: A List od Publication.	141

List of Figures

Figure 2.1 Size dependent colors of gold nanoparticles	8
Figure 2.2 Scheme depicting relationship between number of atoms exposed to surface to the total number of atoms in volume	9
Figure 2.3: Interaction between electromagnetic radiation and surface electrons. Reproduced from reference.....	11
Figure 2.4: Three magnetic fields originating from the common node	30
Figure 2.5 The geometry of the spherical dielectric target	31
Figure 2.6 Schematic representation of experimental set-up for preparation of nanoparticles via inert-gas condensation method	47
Figure 2.7 Synthesis of triangular gold nanoprisms along with some spherical nanoparticles	48
Figure 2.8 Scanning electron microscopy images of gold nanoprisms with various dimensions synthesized using PVP to HAuCl ₄ ratio.....	49
Figure 2.9 synthesis of triangular nanoplates after evaporation of solvent as seen in TEM	59
Figure 2.10 pH controlled synthesis of silver triangular nanoprisms at irradiation wavelength of 550 nm at pH 11.2.....	62
Figure 3.1 Effect of edge length on plasmon resonance for triangular nanoprisms of a) Ag b) Au	75
Figure 3.2 Effect of thickness on plasmon resonance for triangular nanoprism of (a) Ag (b) Au	79
Figure 3.3 Effect of edge length on plasmon resonance for truncated triangular nanoprisms of a) Ag b) Au.....	81
Figure 3.4 Effect of thickness of nanoprism on plasmon resonance for truncated triangular nanoprisms of a) Ag b) Au	82
Figure 3. 5: Comparison of effect of edgelenh on dipole plasmon resonance of perfect and truncated nanoprisms of a) Ag b) Au.....	83
Figure 3. 6: Comparison of effect of thickness on dipole plasmon resonance of perfect and truncated nanoprisms of a) Ag b) Au.....	84
Figure 3.7. Comparison of Ag and Au triangular nanoprisms for change in dipole plasmon resonance with variation in degree of truncation.	87
Figure 3.8. Effect of degree of truncation at only one vertex of Ag nanoprism on dipole plasmon resonance.	89
Figure 3.9. Plasmonic resonance of triangular Ag nanoprisms with truncation in one, two, and three vertices (A) wavelength position of the peaks. (B) absorbance strength of the peaks.....	90

Figure 3.10 FDTD simulation results showing the plasmonic resonance of nanoprism that has thickness of 30 nm and edge length of 100 nm with different degrees of truncation for (A) Ag. (B) Au.	93
Figure 3.11 The plasmonic enhancement of Ag nanoprism without snipping (a and b) and truncated nanoprism (c and d) with snip of 10 nm. The edge length (100 nm) and thickness (30nm) were maintained constant in above figure (a – d).	95
Figure 3.12 The plasmonic enhancement of Au nanoprism without snipping (a and b) and truncated nanoprism (c and d) with snip of 10 nm. The edge length (100 nm) and thickness (30nm) were maintained constant in above figure (a – d).	96
Figure 4.1 FDTD simulation results showing the absorbance spectra of Ag nanosandwich structures with edge length of 100 nm and thickness 30 nm. This figure of for dielectric thickness of 50 nm.	104
Figure 4.2 FDTD simulation results showing the absorbance spectra of Au nanosandwich structures with edge length of 100 nm and thickness 30 nm. This figure of for dielectric thickness of 50 nm.	105
Figure 4.3: Effect of refractive index on dipole plasmon resonance maximum for various thicknesses of dielectric of a) Ag b) Au.....	106
Figure 4.4: Comparison of dipole resonance maximum for Ag and Au towards change in dielectric medium with thickness of 30 nm	107
Figure 4.5. FDTD Simulation results showing the plasmonic resonance of Au and Ag nanoprism with edge length of 100 nm and thickness of 30 nm and FDTD Simulation results showing the plasmonic resonance of an Au- dielectric-Ag nanoprism with edge length of 100 nm and thickness of 30 nm for all layers. (solid black line), (A: edge length, B: height, and C: thickness)	108
Figure 4.6 (a) FDTD simulation results showing the absorbance of sandwich structure (Au/dielectric/Ag) (a) without truncation and (b) with TR= 0.1 (First peak is corresponding to Au & Second peak is corresponding to Ag).	114
Figure 4.7: Relationship between the magnitude of Ag and Au peaks and varying thickness of dielectric layer (nm) (A) Perfect sandwich structure and (B) Truncated sandwich structure.	115

List of Tables

Table 3.1: Effect of edge length on dipole plasmon resonance of triangular nanoprisms of Ag and Au truncated and non-truncated	78
Table 3.2: Effect of edge length on dipole plasmon resonance of triangular nanoprisms of Ag and Au truncated and non-truncated	78
Table 3.3: Effect of truncation on dipole plasmon resonance of triangular nanoprisms of Ag and Au	92
Table 3.4: Full Width Half Maximum of dipole plasmon resonance of truncated triangular nanoprisms of Ag and Au.....	92
Table 4.1: Summary of results investigated for effect of dielectric thickness for various refractive indices on dipole plasmon resonance	101
Table 4.2: Summary of results investigated for effect of dielectric thickness for various refractive indices on dipole plasmon resonance	101

Chapter 1

Introduction

1.1 Background

Optical sensors that operate via the generation of surface plasmons are typically known as surface plasmon resonance sensors. These optical sensors have gained huge interest in the sensing technology for the detection of analytes ranging from chemicals, biological species, environmental regulation, medical diagnostic applications etc. [1]–[5]. These surface plasmon resonance based optical sensors utilize various methods of optical excitation such as attenuated total reflection and grating coupling. Typical modulation methodologies are based on surface plasmons in wavelength [6], [7] and angular domains [8], [9]. In the broad field of sensing technology Au and Ag have received great attention due to their unique optical properties, in particular optical enhancement [10]. The optical enhancement in noble metal nanoparticles particularly in Ag and Au ensues from resonant coupling of metal conduction electrons with incident electromagnetic radiation and through strong scattering in nano-dimensions [11], [12]. Both, resonant coupling of metal conduction electrons with incident light and scattering process have their own applications. Scattering process leads to applications in diagnostics [13], [14] through imaging and therapeutic applications through thermal dissipation process leading to

localized heat from the absorbed light [15], [16]. When gold and silver are employed for applications in sensors, the changes in absorption or scattering of plasmonic resonance will be measured with respect to change in chemical and physical environment of nanoparticle surface.

Conventional biological sensors employ labels to create and augment the target signal. Labels are depending on applications, it can range from fluorophores, enzymes or radioisotopes to name a few. While the labeling methods is useful to measure signals, for studies involving understanding of biomolecules in its real-time environment are impossible with techniques that employ labels affects the biological interactions. Thus label free techniques are preferred. Additionally, presence of labels enables sensing through end-points assays only. Considering those disadvantages, it is label free surface plasmon resonance sensing is the most desired technique [17]. The prime disadvantage with label free sensing is low sensitivity. However the low sensitivity issue can be addressed through manipulation of metal nanoparticles such as size, geometry and composition [18]–[20].

1.2 Problem Statement

Although silver and gold has interesting optical properties, its potentials in plasmonic properties has been extensively investigated only as spherical particles. Further when gold and silver in spherical form offers limited opportunity to tune optical properties through variation in structure. It is desired at this moment, we need better ways to tune these materials for various sensing applications in visible and near infra-red

region. This objective can be achieved through changing the morphology of gold and silver nanoparticles from conventional spherical particles. Particularly, we believe, gold and silver has a lot to offer when they are in the form of triangular nanoprism.

1.3 Objective

The objective of our research work is, how to tune the surface plasmonic properties for various applications that uses sensors. We have discussed the advantages of triangular nanoprisms and its applications available in literature. Then, we propose here that gold and silver triangular nanoprism can offer the opportunity to tune the plasmonic properties through manipulation of dimensions.

1.4 Scope of Research Work

In this dissertation we mainly focused on identifying the advantages of gold and silver when present in the form of triangular nanoprisms to plasmonic properties. In chapter 2 we have investigated the effect of dimensions of triangular nanoprism i.e., edge length and thickness and how it can be tuned to various sensing application in infra-red region and visible region. In chapter we studied the effect of truncation and advantages of constructing a triangular nanoprism that couples dielectric, silver and gold. The studies presented in chapter 2 and chapter shed light on tunability of plasmonic properties by manipulating the dimensions of nanoprism and composition of nanoprism.

1.5 Methodology

To achieve our objectives we have used Opti-FDTD simulation software. This powerful tool was used to understand the dependence of plasmonic properties of triangular nanoprisms of gold and silver nanoparticles through simulations.

1.6 Contribution and Publications

This research is about the study of plasmonic properties of triangular nanoprisms. All of the research presented in this dissertation were submitted to peer reviewed journals. Following paragraphs will briefly summarize the content we presented for publication:

We studied the effect of truncation on the plasmonic resonance of triangular nanoprisms. Perfect Ag triangular prisms and Ag truncated triangular prisms have been designed and simulated using finite-difference time-domain (FDTD) simulation technique. Simulation results show that the increase of the truncations depth in triangular nanoprisms causes a resonance blue shift. However, for the case of truncation depth of up to 15 nm, the number of truncated corners has no effect on the position of the peak or the strength.

Hybrid plasmonic nanoprisms with and without truncation in the form of gold (Au)-dielectric- silver (Ag) sandwich nano-structures have been designed and simulated using Finite-difference time-domain (FDTD) simulation technique. Simulations results show two dipole resonant peaks for the hybrid sandwich structure. Also, a strong wavelength dependence of the plasmonic resonance peaks on the edge length and the

thickness of gold and silver layers. The increase in edge length and the decrease in thicknesses were found to cause red shift to the plasmonic peak of the nanostructures.

Moreover, the full width half maximum (FWHM) of the truncated nanoprism sandwich structure is smaller than (FWHM) for nanoprism sandwich structure without truncation. Furthermore, the resonant wavelengths and relative strength of the two-dipole plasmonic peaks are demonstrated to be tunable.

1.7 Chapter Organization

This dissertation constitutes four chapters. The layout of the chapters are as follows:

Chapter 1 includes brief background, problem statement, objective, scope and implications of the research, methods used to perform the research and finally chapter organization.

Chapter 2 offers a brief history of gold and silver in ancient days followed by discussion about importance and introduction of noble metal nanoparticles in various fields in modern days. Origin of surface plasmon resonance, role of silver and gold in plasmonic properties, size and shape dependent properties of silver and gold on plasmonic properties were discussed. Methodology (Finite Difference Time Domain) used to measure the plasmonic properties of gold and silver were discussed briefly.

Chapter 3 covers the construction of gold and silver triangular nanoprism using Opti-FDTD software. The dimensions of triangular nanoprism such as edge length and thickness and its impact on plasmonic properties were investigated. Followed by, effect

of truncation in plasmonic properties were also analyzed thoroughly and compared the results with perfect triangular nanoprisms of gold and silver.

Chapter 4 investigates the role of dielectric and its thickness on plasmonic properties of gold and silver individually. Additionally, we constructed a triangular nanosandwich prism made up of gold, silver and dielectric and analyzed for tunability of surface plasmon resonance. Effect of thickness of dielectric in truncated and perfect nanosandwich were also thoroughly studied.

Chapter 2

Surface Plasmon Resonances (SPRs)

2.1 Introduction

Gold and Silver has been the premises of exploration since the ancient days [21]. Early civilizations used these materials as medicines, utensils, plates, cups, jewelry, coins, clothes, construction materials and as disinfectant for human and water borne infections [22]. From age-old time, these metals have been part of our civilizations. Until a century ago, applications of gold and silver were primarily focused on medicinal based applications [23]–[27]. Apart from medicinal based applications, silver was explored as catalyst for reactions such as methanol to formaldehyde and ethylene oxide from ethene. Much of the applications mentioned above, based on macroscopic properties of the noble metals.

Non macroscopic properties of noble metals dates back to several centuries in the form of Lycurgus cup which exhibits ruby red in transmitted light and in reflected light it is green in color. Faraday offered the explanation for colors in Lycurgus cup was due to colloidal nature of gold particles whose interactions with light are different from bulk gold [28]. French dictionary in 18th century reported “drinkable gold” that had different

colors, (Figure 1.1) where gold is in its elementary form under extreme sub-division which is not visible to human eye [29]. Benjamin Richters explained, purple or pink colors of drinkable gold by variation in synthesis procedures [30]. Yellow color of the gold solution is observed when the gold particles are aggregated due to reduction in reflectivity for light towards the end of the spectrum [31]. Mie was the first one to offer scientific explanation of colors of gold based on its size dependence [32], [33]. The explanation offered by Mie based on phenomenon called “Surface Plasmon Resonance” [34]. Further momentum was gained to investigate the noble metal properties that depends on size came from famous lecture “There's Plenty of Room at the Bottom” by Richard Feynman and opened new era of materials called nanomaterials [35]. These nanomaterials are foundation of today’s nanoscience and nanotechnology which encompasses a broad range of interdisciplinary areas of research and transforming the ways in which materials and products are synthesized and the variety and nature of functionalities that can be derived.



Figure 2.1: Size dependent colors of gold nanoparticles [36].

Nanomaterials are defined as materials that have at least one dimension in the range of 1 to 100 nanometer (nm) [37], [38]. These materials at this scale possess unique opto- electronic, magnetic and mechanical properties [40].

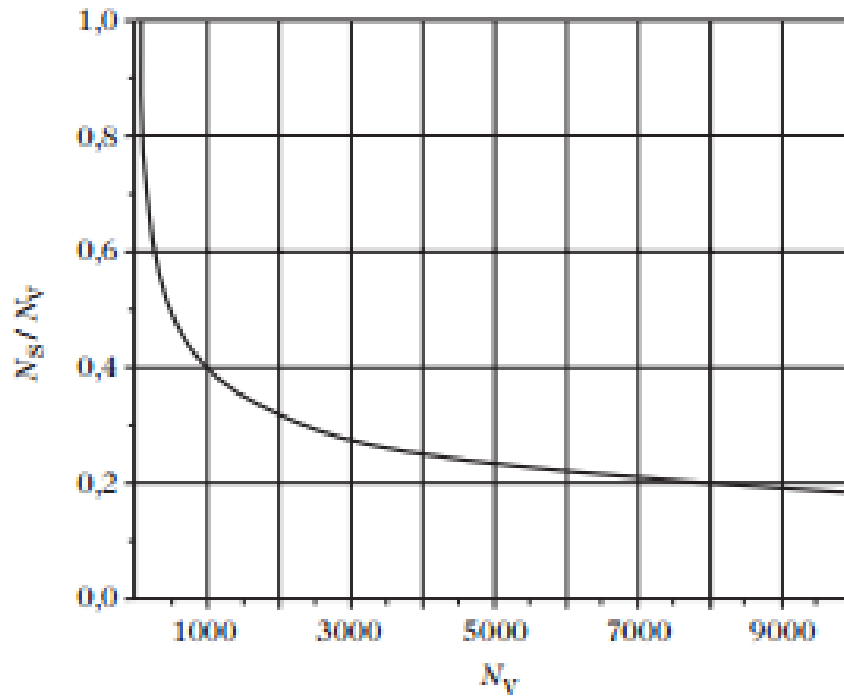


Figure 2.2: Scheme depicting relationship between number of atoms exposed to surface to the total number of atoms in volume [39].

The unique properties of nanomaterials arise from greater surface area to volume ratio [41], [42], high surface energy, spatial confinement and new quantum effects [43]. At macroscopic scale, i.e., in millimeter scale, the number of atoms exposed to surface is typically in negligible proportions compared to total number of atoms in the bulk material. Hence the surface atoms does not affect the bulk properties. However, in nano-dimension, the proportion of atoms exposed to surface, cannot be ignored. To put this in

perspective, for an object of 5 nm size, about 20% of atoms are exposed to the surface, however for nanomaterial at 2 nm dimension, roughly 50 % of atoms are exposed in the surface. The empirical relationship between the numbers of atoms exposed to surface (N_s) to total number of atoms in the volume N_v is given by the equation (1). This can be expressed in a scheme as shown in Figure 1.

$$\frac{N_s}{N_v} \approx \frac{1}{2R} \dots\dots\dots(1)$$

Nanomaterials are classified as zero dimensional (spheres and clusters), one dimensional (nanofibers), two-dimensional (2D films, plates and networks) and three-dimensional (nanoprisms, tripods, cubes) materials. These nanomaterials are synthesized by two approaches: a) top down – break or dissociate bulk materials into finer units until it attains nano-dimensions b) bottom-up – assembling atoms or molecules into nanostructured arrays [44]. Using one of the above mentioned strategies, the methods adopted to synthesize nanomaterials are mechanical grinding, sol-gel process, chemical vapor deposition, flame assisted ultrasonic spray pyrolysis, gas condensation processing, sputtered plasma processing, microwave plasma processing and laser ablation to name a few. Noble metal nanoparticles has been in limelight light since the concept of nanomaterials were evolved. The reason behind the center of attraction of silver and gold are due to applications in various genres of science and technology [45]–[53]. Of the several choices of metal nanoparticles, noble metal nanoparticles especially gold and silver unveils a intense absorption band in the visible region owing to its small particle

effect which is not seen either in bulk nor in individual atom [54]. The absorption of light by metal nanoparticles arises from the coherent oscillation of electrons from conduction band when induced by electromagnetic radiation (Figure 2.3).

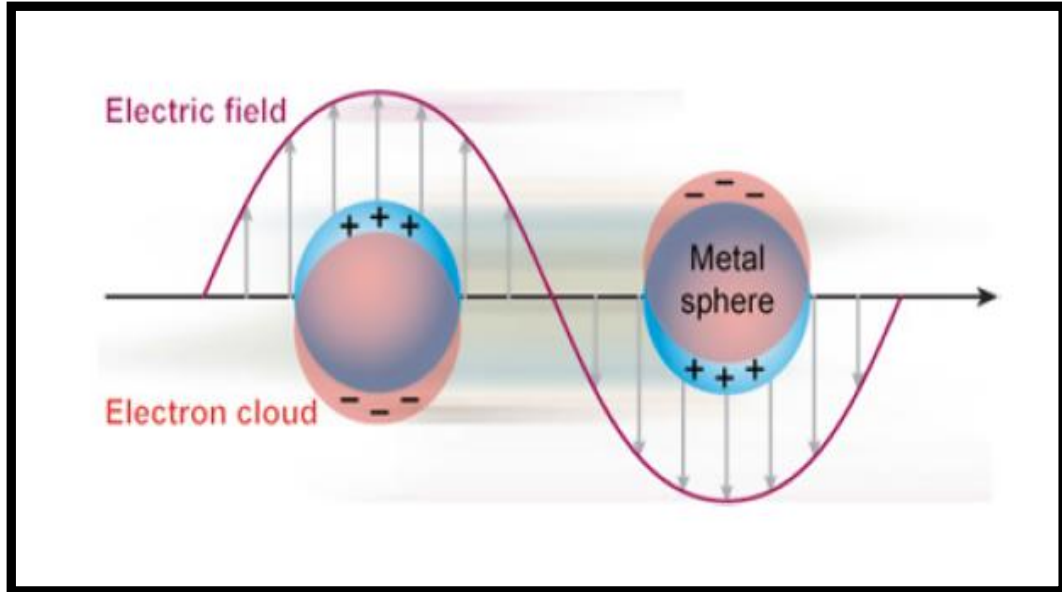


Figure 2.3: Interaction between electromagnetic radiation and surface electrons. Reproduced from reference [55]

The propagation of electromagnetic surface waves between conducting and dielectric materials over a broad range of frequencies extending from dc and radio frequencies up until the visible region. The coupling of electromagnetic field to oscillations of conduction electrons are defined as surface plasmons. The surface are very sensitive to the properties of the materials on which they propagate. The surface plasmons are characterized by strong field augmentation at the interface while electric field decays exponentially away from the surface [56]–[59] If the dimensions of conductor are in nano-dimensions, boundary and surface effects becomes very

significant, thus, the optical properties of metal nanoparticles are dominated by collective oscillation of conduction electrons [60], [61]. When the oscillation of conduction electrons are in resonant with frequency of incident photons are defined as surface plasmon resonance (SPR) [56], [57], [62].

It was in 1902, surface plasmon resonance was first observed by Wood [63]. He observed this phenomenon as an anomaly on a spectrum collected for light diffraction through a metallic diffraction grating. Later Fano accounted for anomalies observed by Wood as they were arising from excitation of surface electromagnetic waves with diffraction grating of the metal [64]. First demonstration of surface plasmon resonance through drop in reflectivity via attenuated total reflectance was given by Otto [65]. Similar observations through attenuated total reflectance were made by Raether and Kretschmann supporting the Otto's demonstration [66]. These groundbreaking observations, lead path to easy ways to create surface plasmons was developed through intense research in this field and eventually leading this phenomenon found its way into modern optics. Several reviews and books were published periodically in understanding the fundamentals of the surface plasmons [57], [58], [67]–[69].

For most common metals such as lead, tin, cadmium and indium the SPR frequency occurs in the ultraviolet region of the spectrum and hence it does not exhibit strong color effects. Further, these metals are readily oxidized under surface plasmon resonant conditions or atmospheric conditions. Contrary to common metals, the coinage metals under atmospheric conditions form stable colloids and have d-d transitions in the

visible spectrum. Additionally, imaginary part of the dielectric constant is too small hence, near-field effect is very high which makes plasmon excitation very interesting in noble metals. The surface plasmon resonance frequency is strongly dependent on dielectric properties, local environment, size, shape and interparticle interactions [70]–[75]. The oscillation frequency of nanoparticles depends on electron density, effective electron mass, shape and size of charge distribution. Particularly, plasmonic research is very exclusive to the gold and silver nanoparticles than most coinage metals due to high density of conduction electrons in these materials enables plasmon resonances at optical frequencies. High conduction electrons density enhances the electrostatic restoring force which in turn enhances the plasmon resonance frequency. Another factor which really distinguishes silver and gold from rest of the coinage metals is the plasmon losses. The plasmon losses or dissipation for gold and silver is very small when compared other coinage metals. In fact, between gold and silver, silver has the strong plasmon resonance due to least plasmon dissipation. Despite the strong plasmon resonance exhibition by silver, gold is more often used owing to its chemical and physical stability.

The electromagnetic radiation incident on nanoparticle induces a polarization of free electrons on the metal surface. During the polarization, the positive charges on the nanoparticles are immobile, whereas the electrons are in motion under the stimulus of external field which causes the separation of negative charges from the positive charges. Thus a net charge separation occurs at the nanoparticles boundaries. A consequence of this charge separation ensues a linear restoring force to the system, resulting in formation

of dipolar oscillation. Such formed dipolar oscillation are known as dipole plasmon resonance. The dipole plasmon resonance is different from plasmon excitations that originates from bulk metal surface. In surface plasmon resonance, the free electrons in the conduction band are excited in a coherent fashion that leads to in-phase oscillation [76]. Plasmons can occur in bulk as well as at the surface of the big lumps of the materials too [77], [78]. Due to mismatch in plasmon dispersion and photon of incident light in bigger particles, ordinary plane of light cannot excite the plasmons. Interestingly, in small particles plasmons can be excited by ordinary light as conservation of momentum is not required. Along with dipole plasmon resonance, multipolar resonance also exists for small clusters or individual nanoparticles. The surface charge distribution on nanoparticles alone distinguishes a dipole plasmon resonance from multipole resonance. Thus surface of the nanoparticle plays a crucial role for the surface plasmon resonance as it can alter the boundary condition for the polarizability of the metal. The electrons in the nanoparticle cluster behave as an oscillator system, while the electrons in bulk materials conduct themselves as a relaxator system.

Since the past few decades, scientists have tried to tap the rare size dependent opto-electronic properties of metal nanoparticles through simulation, fabrication and characterization [79]–[84]. When conduction electrons are confined and quantized in a small volume it enhances the opto-electronic properties in nanocrystals [85], [86]. When the wavelength of incident light is larger than nanoparticles, energy will be confined in the small spatial regions through local excitation of SPRs. The field enhancement in the

spatial regions where energy is confined are used in a wide range of applications as sensors in chemical and biological sciences [87]–[91] and Surface Enhanced Raman Scattering (SERS) [71], [92]–[95], nano-optical devices [96], [97] energy storage [98], [99] and near-field scanning optical microscopy [100]–[102]. Further, interesting field enhancement arises when one resonant particle are brought close to another resonant particle. Thus, when the resonant particles are vicinal to each other, the energy of the particles are found at the interface between the particles. Additionally, the resonant energy can transfer between the particles in vicinity leading to transport of electromagnetic energy at length scales smaller than the diffraction limit. Further particle-particle interaction also control the linear and nonlinear optical properties of nanomaterials embedded in matrices or as assembled into thin films. Thus, nanomaterials as aggregates or in the form thin films provides opportunities to exploit unique properties of these materials in electronic and optical device applications. The Mie's theory developed to solve Maxwell's equations for individual spherical nanoparticles does not hold good for aggregates of nanoparticles or for the field enhancement occurring at the interface of the particles. For such scenarios, effective medium theory proposed by Maxwell Garnett can account for optical absorbance behavior of metal nanoparticles aggregated as matrices and thin films.

2.2 Mie Theory

The variation of colors of colloidal gold nanoparticles with size is an intriguing scientific phenomenon in the early last century. Gustav Mie had applied Maxwell's

equations with suitable boundary conditions in spherical coordinates using multipole expansions of incident light's electric and magnetic fields to explain the color of colloidal gold solutions. The colloidal solution he investigated had spherical nanoparticles, however his theory can offer exact solutions for ten other geometries such as cylinder, parallelepiped, spherical shells etc. to name a few [61], [73], [75], [103]–[107].

2.3 Postulates of Mie Theory:

The Maxwell's equations of geometries mentioned above can be solved using Mie's theory with the following assumptions. 1) The bulk optical and dielectric functions of particle under investigation and its surrounding medium are extendable to nanoparticles [108], [109]. 2) The boundary conditions of nanoparticles are explained by electron density which has sharp discontinuity at the surface of the particle at radius R . 3) The optical materials function of nanoparticle and its medium are input parameters. 4) The wavelength of light interacting with metal nanoparticle should be at least twice larger than its radius. Under these assumptions, the electric component of light is constant and the interaction of light with nanoparticle will be governed by electrostatics instead of electrodynamics. Under these conditions, quasi-static approximation takes effect.

2.4 Deviation from Sphericity:

Surface plasmon oscillations of metallic nanoparticles takes a twist when they deviate from spherical to non-spherical shape [110]–[117]. When metallic nanoparticles depart from sphericity, the longitudinal resonance and transverse resonance emerging from such particles will no longer considered equivalent [110]–[112], [118]. The

longitudinal plasmon resonance will be long and red-shifted, and another peak for transverse plasmon resonance [110]. To account for this phenomenon Gans offered a modification to Mie theory.

2.5 Limitations of Mie Theory:

Mie theory was able to calculate the optical response of isolated single metal nanoparticles only by following electrodynamics. It cannot account for variation in optical properties emerging from polydispersity. Further, this theory works well under the assumption that there is no interaction between the metal nanoparticles, however, in reality new optical properties emerging from interactions between nanoparticles cannot be ignored. Another significant drawback for this theory arise from the assumption that dielectric constant of small metal nanoparticles is same as bulk, but opposite is true [119], [120].

2.6 Effective Medium Theory:

It is understood that Mie's theory does not hold well when metal nanoparticle solution is concentrated as metal-metal interaction interferes with optical properties of single metal nanoparticle. When a metal nanoparticle cluster is in close proximity to another cluster and if the cluster - cluster to distance is smaller than five times the radius of metal nanoparticle while lead to intricate extinction spectra due to single metal nanoparticle and particle – particle interactions [10], [121]–[124]. Maxwell Garnett was able to account for this observation through his effective medium theory [125]–[128]. This theory was able to account for the optical properties of metal nanoparticles that

exists as small close-packed assembly. Effective medium theory works as long as quasistatic limit is met for various shapes of particles. For small particles, optical properties are due to property of the metal as well as property of the ensemble. This condition is typically met in thin samples where the optical behavior of cluster containing N particles will be N^{th} fold of the individual. However, if ensemble is comprises large number of particles, N particle and N^{th} fold logic would not be observed. Under those circumstances, inter-particle interactions outweigh the optical properties of the cluster and isolated particle approximation does not hold good to explain the observed surface plasmon oscillation [129]. Unlike the isolated metal nanoparticles whose optical properties or surface plasmon oscillation depends on dimensions of the particle, geometrical shape etc., the aggregated cluster particles optical properties are defined by correlation length of spatial ordering, filling factors and structure of geometric ordering to name a few. Such information regarding aggregates can be obtained via a statistical average over a large number of aggregates and average volume fraction. These values typically depend on synthesis conditions of metal nanoparticle, which aggregate to form clusters. Most importantly, this theory can be generalized to several shapes of particles; however, it is valid under quasi-static approximation conditions only. Being said that, the assumptions of this theory are as follows: 1) the particle shapes are approximated to spheres and aggregate shapes should be easily treatable geometries 2) particle sizes are small such that scattering is negligible 3) the metal nanoparticles response to electromagnetic field is assumed to be linear 4) chemical structural constituents may be

reduced to minima and it has only negligible proximity effects of sample surface are present.

Based on the above assumptions, let us discuss now the quasistatic response of spherical metal nanoparticles to electric field. For a polarizable particle, the dielectric function is due to total of all contributions arising from electrical polarization that includes neighboring particles. For the particle under investigation, the surroundings are treated as homogenous on scale length that is larger than spatial correlations length, however, for the vicinal particles contribution to the local field through scattering and spatial arrangements are very significant and should be considered in detail. The dielectric properties of such nanoparticles can be effectively represented using Lorentz local field as:

$$E_{\text{local}} = E_0 + E_d + E_s + E_{\text{near}} \dots \dots \dots (2)$$

E_0 is external field; E_s is electric field arising due to polarization charges around the sphere, E_d is electric field due to charges on the external surface of the nanoparticle, E_{near} is the field arising due to dipoles inside the sphere. The above equation (2) can be represented in alternative form as

$$E_{\text{local}} = E_{\text{Maxwell}} + E_s + E_{\text{near}} \dots \dots (3)$$

where E_{maxwell} is defined as sum of external field and field from polarization charges on the surface of Lorentz sphere. Another important assumption is the dielectric function of

material ϵ_m is real and effect of impact of the contiguity or proximity of sample surface is negligible. Additionally, the Lorentz local field is assumed to act on particle as whole.

When colloidal nanoparticles are touching each other, a new embedding method is employed to solve the Maxwell's equations to understand how plasmons are affected by the crystal field. The Maxwell Garnett approximation holds good for the interacting metal nano spheres when filling fractions ($f < 10^{-3}$) are low. However, when the filling fractions are more than 10^{-3} collective properties become significant and E_{near} reduces to 0 as the scattering fields of the particles nullified via interference at the center of the sphere. However, the electric field surrounding the sphere due to polarization of charges E_s should be considered and given by the equation (4).

$$E_s = \int_0^\pi \left(\frac{P \cos \theta}{R^2} \right) \cos \theta (2R^2 \sin \theta) d\theta = \frac{4\pi}{3} P \dots\dots\dots (4)$$

Similarly, the relationship between average electric field E and polarization P for local electric field E_{local} is defined by equation (5)

$$E_{local} = E + 4\pi P/3 \dots\dots\dots (5)$$

The dipole moment, μ , and polarization of the nanoparticle are calculated using the local field. Thus dipole moment is defined as

$$\mu = \alpha E_{local} \dots\dots\dots (6)$$

Likewise, the P, the polarization is expressed as follows:

$$P = \sum_i N_i \mu_i = \sum_i N_i \alpha_i E_{\text{local}}(i) \dots \dots \dots (7)$$

in equation (7) α_i is polarizability of the i^{th} particle and N_i is number density. Substituting eqn (5) in eqn (7) we represent P as

$$P = \sum_i N_i \mu_i = \sum_i N_i \alpha_i \left(E + \frac{4\pi}{3} P \right) \dots \dots \dots (8)$$

The susceptibility (χ) and polarizability of nanoparticle with radius (r) and permittivity (ϵ) are defined by eqn (9) and eqn (10) respectively.

$$\chi = \frac{P}{E} = \frac{\sum_i N_i \alpha_i}{1 - \frac{4\pi}{3} \sum_i N_i \alpha_i} \dots \dots \dots (9)$$

$$\alpha = \frac{\epsilon - \epsilon_m}{\epsilon + 2\epsilon_m} R^3 \dots \dots \dots (10)$$

When a nanoparticle satisfies quasistatic approximation conditions, then the system will be substituted by effective medium, which behaves approximately like a homogeneous material are described by, effective dielectric function, ϵ_{eff} , of the composite samples. The effective dielectric function ϵ_{eff} , offers the linear response of sample to external field in terms of polarizable properties of the particles. This effective dielectric function remains constant even upon substitution of non-homogeneous sample

by its analogous effective medium like an intensive property. Thus ϵ_{eff} , can be represented through Clausius –Mossotti relation:

$$\alpha = \frac{\epsilon_{\text{eff}} - \epsilon_m}{\epsilon_{\text{eff}} + 2\epsilon_m} = \frac{4\pi}{3} \sum_i N_i \frac{\epsilon - \epsilon_m}{\epsilon + 2\epsilon_m} R^3 \dots\dots\dots (11)$$

When volume fraction “f” was introduced in eqn 10, it takes the form as shown in eqn (12) which a familiar version of Lorentz-Lorenz equation:

$$\frac{\epsilon_{\text{eff}} - \epsilon_m}{\epsilon_{\text{eff}} + 2\epsilon_m} = f \frac{\epsilon - \epsilon_m}{\epsilon + 2\epsilon_m} \dots\dots\dots(12)$$

If the particle under analysis is atom, then eqn (11) will be known as Clausius-Mossotti equation. However, if it is a cluster of nanoparticles then eqn (11) can be represented as shown in equation (13), which is known as Maxwell Garnett equation:

$$\epsilon_{\text{eff}} = \epsilon_m \frac{1 + 2f\Lambda}{1 - f\Lambda} \dots\dots (13)$$

Where Λ is

$$\Lambda = \frac{1}{\epsilon_m} \frac{\epsilon - \epsilon_m}{\epsilon + 2\epsilon_m} = \frac{\alpha}{3\epsilon_0 \epsilon_m V} \dots\dots (14)$$

For isolated nanoparticle, the surface plasmon absorption spectrum is given by absorption constant $\gamma_a(\omega)$,

$$\gamma_a(\omega) = \frac{\omega}{n_r c} \text{Im}\{\epsilon_{\text{eff}}\} = \frac{4\pi k}{\lambda} = \frac{2\omega}{c} \sqrt{-\frac{\epsilon_{1,\text{eff}}^2}{2} + \frac{\sqrt{\epsilon_{1,\text{eff}}^2 + \epsilon_{2,\text{eff}}^2}}{2}} \dots (15)$$

$$\text{Where, } \omega = \frac{\omega_p}{(1 + 2\epsilon_m)^{1/2}}$$

The above Maxwell Garnett equation holds good under low filling factors f , and is only applied for dilute ensembles of nanoparticles that interact via far-field and it breaks down when the nanoparticles are close enough for near-field to interact.

It is well seen now for dilute ensemble of nanoparticle aggregates, Maxwell Garnett effective medium theory is capable of explaining the optical properties by employing effective medium approximations. In the effective medium approximations, the nanoparticle cluster or aggregate was substituted by effective object whose dielectric constant is uniform. Reasonably accepted results for the optical spectra of clusters are possible when the density of ensemble is suitably low and per particle polarization is within the quasistatic approximation limits. However, when quasistatic approximation conditions were not met by aggregate, the optical properties of such spherical ensembles are explained by coupled multipoles [130]. The coupled multipoles method is able to analyze aggregates composed of few hundred particles unlike the effective medium theory which is around ten particles. For the coupled multipoles method, best results are found when the particle size is small. For sufficiently small particles, the cluster may

have up to 100000 particles, and lattice of the aggregate can be defined using Fourier transformations to find the sum of dipoles.

The optical response for aggregate of metal nanospheres to the incident light and the scattered fields from other particles are from self-consistent solution, unlike for macroscopic molecules optical response are governed by Maxwell's equations for electric and magnetic field. If nanoparticles size is less than the wavelength of the incident light, the optical response hugely depends on dipole component of electric field, provided, the higher order multipole components are not very large. The polarizability α_i of isotropic nanospheres are determined by the equation below:

$$\alpha_1 = r^3 \frac{3i}{2(kr)^3} a_1 \dots \dots \dots (16)$$

Where r is the radius of sphere, and $k=m_0(2\pi/\lambda)$ is the magnitude of wave vector for the dielectric medium; m_0 and a_1 is real refractive index and function of size parameter respectively.

As mentioned earlier, the optical response to aggregate of non-magnetic spherical nanoparticles could be evaluated by self-consistent solution of electric dipole polarizations, P_i , of every sphere in the superposed field of incident electromagnetic radiation and dipole fields of other particles. Hence, the nanospheres aggregates can be expressed as one dipole for every particle instead of several. Hence for given dipole in a position r_i ,

$$P_i = \alpha_i E_{loc}(r_i) \dots \dots \dots (17)$$

In the above equation, $E_{loc}(r_i)$ is a sum of incident plane wave and retarded fields as per the equation below:

$$-\mathbf{A}_{ij} \cdot \mathbf{P}_j = \frac{\exp(i\mathbf{k} \cdot \mathbf{r}_{ij})}{r_{ij}^3} \left[\mathbf{k}^2 r_{ij} \times (\mathbf{r}_{ij} \times \mathbf{P}_j) + \frac{(1 - i\mathbf{k}r_{ij})}{r_{ij}^2} \times \right. \\ \left. \{r_{ij}^2 \mathbf{P}_j - 3r_{ij} (\mathbf{r}_{ij} \cdot \mathbf{P}_j)\} \right] \quad (j \neq i) \\ \dots \dots \dots (18)$$

Use of retarded fields, avoids the necessity of using explicit modeling of time dependence of fields and polarizations. Hence,

$$(\alpha^{-1})\mathbf{P}_i + \sum_{j \neq i} \mathbf{A}_{ij} \cdot \mathbf{P}_j = \mathbf{E}_{inc,i} \dots \dots \dots (19)$$

Above expression provides solution for the optical response of nanospheres packed at a distance close enough to be called as aggregates.

2.7 Discrete Dipole Approximation Method (DDA):

For aggregates of metal nanoparticles the description is challenging and complicated when compared with single particles. Aggregates that has only few particles, solutions to Maxwell’s equations can be achieved using Fourier transformation methods to perform dipole sums. These calculations are often identical to discrete dipole

approximations (DDA) where each particle represents a dipole. All dipoles in the aggregate are coupled together to attain the overall polarization response of the aggregate [130]. Thus DDA facilitates to describe the arbitrary shapes, composition and sizes of aggregates which are touching or coalescing [131]–[133]. This approach divides the nanoparticle aggregate into several small polarizable cubes. Such induced dipole polarizations are used to determine extinction cross-section of the aggregate. This method was first proposed by Pennypacker and Purcell [134] and remained dormant until the theory has found applications in chemistry by Van Duyne and Schatz [135]. Now this is one of the important computational tool to investigate the optical properties of nanomaterials. The prime challenge while using this method is, too many elements are necessary to describe a small aggregate that contains around 10 particles.

Significant developments were made in DDA theory to describe nanoparticles which are not spherical using finite element discrete dipole approximation theory. This approach divide the particle into many polarizable cubes. The dipoles induced in these polarizable cubes are evaluated self-consistently, followed by extinction cross-section were determined using the induced polarizations. Huge advantage of this method is it evades the imposition of boundary conditions to the particles under investigation through dividing the particle into elements and thus it allows the elements to interact via dipole-dipole interactions only. Thus, a nanoparticle cluster under investigation is defined by a cubic array of several N point dipoles that has polarizabilities represented as α_i , centered

at position r_i and the interaction of dipole with local electric field (E_{loc}) will induce polarization are defined by equation (20).

$$P_i = \alpha_i E_{loc}(r_i) \dots \dots \dots (20)$$

However, for isolated particles, E_{loc} is defined by equation (21)

$$E_{loc}(r_i) = E_{loc,i} = E_{inc,i} + E_{dip,i} = E_0 \exp(ik \cdot r_i) - \sum_{j \neq i} A_{ij} \cdot P_j \quad (21)$$

The incident wave amplitude and wave vector are denoted as E_0 and k respectively. The interaction matrix A takes the form equation (22)

$$A_{ij} \cdot P_j = \frac{\exp(ik \cdot r_{ij})}{r_{ij}^3} \left[k^2 r_{ij} \times (r_{ij} \times P_j) + \frac{(1 - ik r_{ij})}{r_{ij}^2} \times \{r_{ij}^2 P_j - 3r_{ij} (r_{ij} \cdot P_j)\} \right] \quad (j \neq i) \quad \dots (22)$$

k in equations (21) and (22) are defined as ω/c . When equations (21) and (22) are substituted in equation (20), equation (23) will be arrived.

$$A' \cdot P = E \dots \dots \dots (23)$$

A' is the matrix derived from A in (21). Thus for equation containing a total of N dipoles, E and P have $3N$ dimensional vectors and A' is defined as $3N \times 3N$ matrix. Solving equation (23) enables solution for P . Substitution of P in equation (24) leads to calculation of extinction cross-section C_{ext}

$$C_{\text{ext}} = \frac{4\pi k}{|E_0|^2} + \sum_{j=i}^N (\mathbf{E}_{\text{loc},j}^* \cdot \mathbf{P}_j) \dots (24)$$

The above obtained solution will be exact for particles with finite size, however, for particles with irregular shape the results are off with 5% of the exact extinction cross-section when optical response of bulk dipole lattice to bulk material when calculations were converged with respect to dipole density. The downside of this approach is too many elements are required to describe even a small aggregate.

2.8 Finite Difference Time-Domain Method (FDTD):

FDTD is computational electrodynamics modeling technique to obtain the optical responses to nanoparticle aggregates of arbitrary shapes. This is arguably the simplest in terms of implementation and concept wise. This methods uses grid based differential time domain numerical modeling methods. It is capable of running simulation over a wide frequency range in a single run. If particle under investigation is smaller than the wavelength of light, efficient solutions are obtained through quasi-static approximations and ray based methods are used to solve the particles for which wavelengths are shorter than the particle under investigation.

The fundamental FDTD grid was first proposed by Kane Yee in 1966 [136] and the acronym was tossed by Allen Taflove in 1980 [137]. The key points in of this algorithm are as follows: a) all derivatives in Ampere and Faraday's laws are replaced by finite difference. Space and time are discretized such that electric and magnetic fields are distributed over both space and time. B) Evaluate electric fields and magnetic fields one-

step at a time which is also defined as leapfrog manner. FDTD is widely used computationally to address all problems related to electromagnetic wave interactions with material structures. The applications of FDTD simulations range from predicting the performance of photonic crystals, nanoplasmonics and biophotonics to name a few.

The FDTD technique divides time and space into discrete segments. Box-shaped cells are used to segment space. However, wavelength is larger than these spaces. Magnetic fields are located on the faces of the boxes while the electric fields are located on the edges. This is called the *Yee cell* field orientation which forms the foundation of the finite-difference time-domain technique [138].

This orientations quantizes time into steps that denote the amount of time a field requires to move from one cell to another. There is an offset of the field values with respect to change in time as a result of the offset in the space between the magnetic fields and the electric fields. A leap frog schematic updates the magnetic and electric fields with the magnetic fields computed after the computation of the electric fields relative to the change in time.

The FDTD mesh (or grid) is generated from the accumulation of numerous FDTD cells that together form a 3D (three-dimensional) volume [139] as shown in Figure 2. Each FDTD cell is characterized by three electric fields starting at a common node that is associated with the cells. This is the result of the overlapping of the edges and faces of the FDTD cells that are adjacent to each other. The common node of the electric fields is the origin of the three magnetic fields that characterize the faces of cell adjacent to the

node. Manipulation of the equations that compute the fields at specific locations allows the addition of materials such as dielectrics and conductors within the FDTD generated mesh. A salient example is setting the electric field computing equation to zero when adding an efficiently conducting wire segment to a given cell.

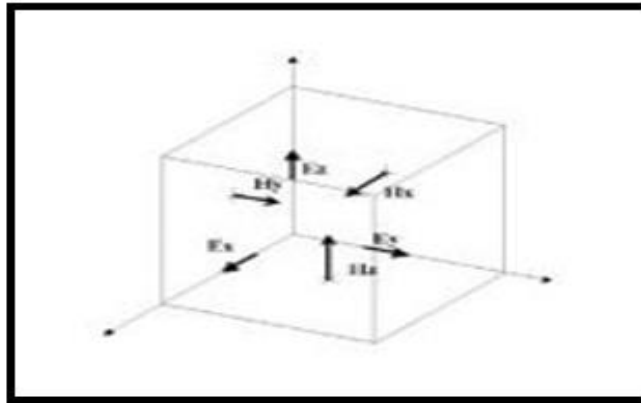


Figure 2.4: Three magnetic fields originating from the common node [139].

This is because efficiently conducting substance or wire has an electric field that is identically zero. A wire is formed by connecting the edges of numerous end-to-end cells that are defined as efficient conducting materials.

This model allows for the addition of other different materials by applying similar manipulations to the electric and magnetic field calculations, relative to the characteristics of the materials elected.

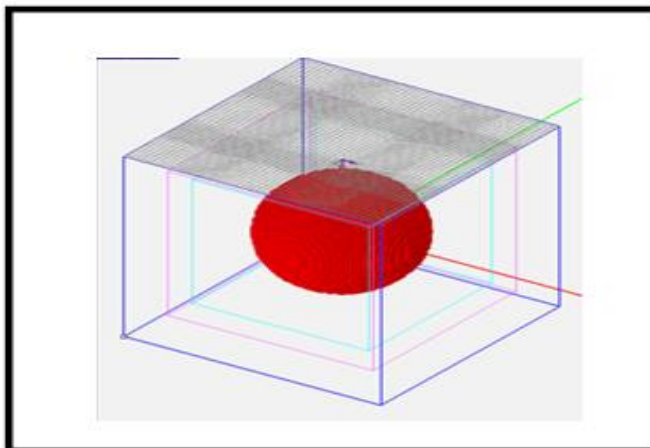


Figure 2.5: The geometry of the spherical dielectric target.

The FDTD grid allows for the generation of a geometrical structure that results from the association of numerous cell edges with the respective materials, with every box representing a single FDTD cell [140]. The value a waveform is added at each step time to the corresponding field value. The introduced waveform will be efficiently propagated throughout the FDTD grid relative to the characteristics of each individual cell.

The FDTD simulation has one important constraint, the dimensions (size) of the small box. This is because the box represents the upper frequency limit for the calculation that has been employed, as well as the time step size. This technique employs a rule of thumb that determines the minimum resolution at ten cells per wavelength. This also serves as the upper frequency limit. While this is in theory, the cell size tends to characterize a much smaller resolution which is important in resolving the features and dimension of the simulated structure. These include the length or thickness of a wire.

2.8.1 One-Dimensional Simulation

The one-dimensional simulation using the FDTD technique is applied to the simplest problems such as the simulation of a pulse propagating in a single-dimensional free space. This technique employs the Maxwell curl equations in free space that are time-dependent [141]. While the initial vectors of the equation (E and H) are three dimensional, the one dimensional approach is applied by orienting the equations of the magnetic field of the plane wave in the y direction and the electric field in the x direction.

This results in the approximation of the central differences for the spatial and temporal derivatives as;

$$\frac{E_x^{n+1/2}(k) - E_x^{n-1/2}(k)}{\Delta t} = -\frac{1}{\epsilon_0} \frac{H_y^n(k+1/2) - H_y^n(k-1/2)}{\Delta x} \dots\dots\dots(25)$$

$$\frac{H_y^{n+1}(k+1/2) - H_y^n(k+1/2)}{\Delta t} = -\frac{1}{\mu_0} \frac{E_x^{n+1/2}(k+1) - E_x^{n+1/2}(k)}{\Delta x} \dots\dots\dots(26)$$

The subscript n denote time as $t = \Delta t \cdot n$. Both equations are founded on the assumption that E and H are incorporated in both time and space. The H field is assumed to be found between the values of the E field. The n superscript indicates between which values before or after n it occurs. In the FDTD technique, time is implicit making calculations easier and more accurate.

This results in the rearranged iterative algorithm;

$$E_x^{n+1/2}(k) = E_x^{n-1/2}(k) - \frac{\Delta t}{\varepsilon_0 \cdot \Delta x} [H_y^n(k + 1/2) - H_y^n(k - 1/2)] \dots\dots\dots (27)$$

$$H_y^{n+1}(k + 1/2) = H_y^n(k + 1/2) - \frac{\Delta t}{\mu_0 \cdot \Delta x} E_x^{n+1/2}(k + 1) - E_x^{n+1/2}(k) \dots (28)$$

The calculations highlighted above are interleaved for both space and time. This is evident in the fact that the new value of E_x takes into account the most current values of H_y as well as the previous value of E_x . The one-dimensional simulation employs absorbing boundary conditions in order to mitigate the reflection of E and H fields back into the problem space [139]. This technique can also be employed in the simulation of propagation in a dielectric medium. This is achieved through the addition of the relative dielectric constant, represented by ε_r , into the Maxwell equations.

2.8.2 Two-Dimensional Simulations

2D simulations are usually conducted on either the transverse magnetic (TM) mode or the transverse electric (TE) mode. The TM Mode is comprised of E_z, H_x, H_y fields. The TE Mode is made up of the E_x, E_y, H_z fields. Two dimensional simulation also takes into account the interleaving of fields in the calculations.

Two-dimensional simulations employ the perfectly matched layer (PML) as its absorbing boundary condition (ABC). This technique is an effective way of accounting for and distinguishing the unpredictable reflections that may be generated and go back into the problem area. PML essentially states that a wave propagating in medium A impinges upon medium b, the intrinsic impedances of the two media determines the amount of reflection experienced. PML is also considerably flexible, and is represented by equation 29;

$$\Gamma = \frac{\eta_A - \eta_B}{\eta_A + \eta_B} \dots\dots\dots(29)$$

But also taking into consideration that the permeabilities μ and dielectric constants ϵ of the two media determine the above formula;

$$\eta = \frac{\mu}{\epsilon} \dots\dots\dots (30)$$

The two dimensional simulation has to take into account the two conditions that are required to form a PML. They include:

- A- There's constant impedance that moves from the background medium to the PML. Where the impedance will be 1 with normalized units.

$$\eta_0 = \eta_m = \frac{\mu_{Fx}^*}{\epsilon_{Fx}^*} = \mathbf{1} \dots\dots (31)$$

B- The relative permeability and relative dielectric constant in the direction perpendicular to the boundary has to be inverse to those in the other directions.

This is represented by;

$$\epsilon_{Fx}^* = \frac{1}{\epsilon_{Fy}^*} \dots\dots\dots (32)$$

$$\mu_{Fx}^* = \frac{1}{\mu_{Fy}^*} \dots\dots\dots (33)$$

The two-dimensional simulation has the ability to simulate a plane wave. This wave can be simulated while interacting with an object by specifying the object in terms of its electromagnetic properties, the dielectric constant involved in the problem and the conductivity. The FDTD two-dimensional simulation also has the ability to simulate a smooth transition from one medium to another. This is achieved by dividing all FDTD cell into sub cells.

2.8.3 Three-Dimensional Simulation

This type of simulation is similar to two-dimensional simulation with the only difference being the logistical problems that increase the complexity of the problem. This is because this simulation employs all vector fields, with each field in three dimensions.

The simulation starts with Maxwell equations and assumes the notations as the general assumption of normalized values is applied [139]. This will result in the production of six scalar equations represented by;

$$\frac{\partial D_x}{\partial t} = \frac{1}{\sqrt{\varepsilon_0 \mu_0}} \left(\frac{\partial H_z}{\partial y} - \frac{\partial H_y}{\partial z} \right) \dots \dots \dots (34)$$

$$\frac{\partial D_y}{\partial t} = \frac{1}{\sqrt{\varepsilon_0 \mu_0}} \left(\frac{\partial H_x}{\partial z} - \frac{\partial H_z}{\partial x} \right) \dots \dots \dots (35)$$

$$\frac{\partial D_z}{\partial t} = \frac{1}{\sqrt{\varepsilon_0 \mu_0}} \left(\frac{\partial H_y}{\partial x} - \frac{\partial H_x}{\partial y} \right) \dots \dots \dots (36)$$

$$\frac{\partial H_x}{\partial t} = \frac{1}{\sqrt{\varepsilon_0 \mu_0}} \left(\frac{\partial E_y}{\partial z} - \frac{\partial E_z}{\partial y} \right) \dots \dots \dots (37)$$

$$\frac{\partial H_y}{\partial t} = \frac{1}{\sqrt{\varepsilon_0 \mu_0}} \left(\frac{\partial E_z}{\partial x} - \frac{\partial E_x}{\partial z} \right) \dots \dots \dots (38)$$

$$\frac{\partial H_z}{\partial t} = \frac{1}{\sqrt{\varepsilon_0 \mu_0}} \left(\frac{\partial E_x}{\partial y} - \frac{\partial E_y}{\partial x} \right) \dots \dots \dots (39)$$

The relationship between E and D is the same in one-dimensional, two-dimensional and three-dimensional analysis with the difference being the presence of three equations. Three-dimensional analysis also employs the use of PML with the only difference being the introduction of three direction as opposed to two in the two-dimensional analysis. One of the key constraints of the FDTD three-dimensional analysis is the steps size for both space and time. These two elements influence accuracy, stability of the FDTD technique and the numerical dispersion.

2.9 FDTD Simulation Software:

Problems that requires solutions through FDTD analysis are typically solved by simulation software. FDTD analysis is required for applications stretching from biophotonics to design of antennas to name a few. This technique is relatively new in comparison to other analytical techniques such as method of moments, finite element method and frequency domain techniques. FDTD commercial software packages made entry as powerful research tool for simulations after satisfactory solutions for absorbing boundary was addressed. Several research institutions and companies offer software packages for FDTD simulations ranging from free to limited usage. Personal computers had seen a huge transformation with reference to speed, bits and random access memory since the beginning of this century and those developments made simulations by FDTD software packages seamless in terms of computation speed, accuracy of analysis and magnitude of problem that could be solved. Typically the bits of the computer accounts for error in analysis arise from truncation of nanoprism. Higher the bits, lesser the error. Processor speed accounts for time of analysis. The magnitude of electrical component size from electromagnetic radiation depends on random access memory. Thus, higher the random access memory of the computer, larger the variables that can be dealt by computer. Additionally, grid cell dimensions can be made smaller and smaller with increase in random access memory. While the developments in personal computation had made the FDTD analysis simpler, dedicated hardware also developed for this purpose to make the FDTD analysis further simple. However, the dedicated hardware are not

cost-effective hence it is not widely used. To alleviate the cost issues associated with hardware, graphic cards meant for FDTD computation was also developed and widely used.

Below is brief discussion about the types of software packages available for FDTD:

EZ-FDTD: It is supported in Win9x, WindowsNT, Windows2000, and WindowsME & Windows XP. Users will be able to create the models as they desire. It uses same graphical interface to create models and display results. This software is capable of generating error messages for invalid or illogical FDTD problems. It offers movies and far-field points for electrical and magnetic fields. The latest version is capable of solving problems with applications in antenna design, SAR studies, material modeling, power plane decoupling analysis and many more. It offers a 30 day trial version. The functionalities and features include Linux, and Windows platforms, voltage and current probes, boundary conditions for PML, Mur or Liao etc.

Fidelity FDTD-Based EM simulator software: This is a full 3D-electromagnetic simulator for modeling antennas, microwave circuits, waveguides etc., It can be used online as well as downloaded to personal computer. MS Windows based menu-driven graphic interface for construction of interactive 3D and planar structures. Radiating boundary conditions modeled as various absorbing boundary conditions including PML. Antenna structures can be modeled efficiently and accurately. Pre-defined coaxial port, microstrip port, rectangular waveguide port, circular waveguide port and user-defined

port allow hassle-free port definition are available. It can have both far and near field view. Integrated pre-processing and post processing are available. It is space and simulation time efficient.

In a similar note, other software packages available for FDTD simulations are Empire FDTD software package, Concerto FDTD software package, Optiwave FDTD software package, XFDTD software package, Agnora FDTD software package, MEEP FDTD software package etc. MEEP FDTD software is a free simulation software. All the softwares for FDTD simulations discussed here had more or less similar capabilities. In our research we have used Opti-FDTD software package to simulate the triangular nanoprisms we conducted.

2.10 Lorentz-Drude Model (FDTD)

The Lorentz-Drude Model is an essential tool that depicts dispersion materials that have their frequency dependent on the permittivity of the dielectric defined by the sum of multiple resonance Lorentzian functions depicted below;

$$\epsilon_r(\omega) = \epsilon_\infty + \sum_{m=1}^N \frac{\chi_0 G_m \omega_{0m}^2}{\omega_{0m}^2 + i\Gamma_m \omega - \omega^2}, \sum_{m=1}^N G_m = 1 \dots \dots \dots (40)$$

Where;

ω_{0m} are the resonant frequencies

G_m is related to the oscillator strengths

Γ_m is the damping coefficient

ϵ_∞ is the permittivity at the infinite frequency

ϵ_0 is the permittivity at $\omega = 0$

While the model exists and functions within the frequency model, FDTD is based in the time domain, and as such is a time domain technique. This difference makes it particularly suitable for simulating broadband. In order for FDTD to handle the full-wave-analysis the Lorentz-model has to be transformed to the time domain [138]. The Maxwell's equation contains the polarization philosophy which is used to complete this transformation. Within the time domain, the Lorentz-Drude Model is depicted in the following manner:

$$\mu_0 \frac{\partial H}{\partial t} = \nabla \times E \dots\dots\dots (41)$$

$$\epsilon_{r,\infty} \epsilon_0 \frac{\partial E}{\partial t} + \sum_{m=0}^M \frac{\partial P_m}{\partial t} = -\nabla \times H \dots\dots\dots (42)$$

$$\frac{\partial^2 P_m}{\partial t^2} + \Gamma_m \frac{\partial P_m}{\partial t} + \omega_m^2 P_m = \epsilon_0 G_m \Omega_m^2 E \dots\dots\dots (43)$$

When implementing the first equation into the FDTD formalism, we employ the dielectric susceptibility function. This takes into consideration the polarization equation approach. The dielectric susceptibility function is highlighted below:

$$\chi(\omega) = \frac{\chi_0 \omega_0^2}{\omega_{0m}^2 + i\Gamma_m \omega - \omega^2} \dots\dots\dots (44)$$

OptiFDTD marks Drude material using the following equation;

$$\epsilon_r = \epsilon_{r\infty} + \frac{\omega_p^2}{j\Gamma\omega - \omega^2} \dots \dots \dots (45)$$

Where;

ϵ_r represents the permittivity for infinity frequency

ω_p represents the plasma frequency

Γ represents the collision frequency [138]

In conclusion, while FDTD technique is a useful tool, there is need to increase the computation speed of the current FDTD. This procedure would programing-intensive and may include optimizing computation loops for cache, using multiple CPU of a computer in a parallel configuration.

2.11 Anisotropic Colloidal Assemblies

The huge attention gained by nanomaterials in the field of science and technology arise from dimensions of the particles. At nanoscale, due to the size, shape-dependence, surface to volume ratio, the physical, optical and electronic properties of these materials make them an indispensable components in the contemporary materials chemistry [117], [142]–[144]. Such nanoparticles are broadly classified into two types: isotropic and anisotropic. For nanomaterials with isotropic shapes have material properties same regardless of the directions. However, for anisotropic nanoparticles the physical, mechanical and optical properties differ with directions. In the recent years, significant accomplishments were made in controlling the sizes [145] of isotropic materials and

modification of surfaces of those particles [146]–[148]. Interest in synthesis of tailorable anisotropic materials such as multipods [149]–[153], nanoshells [154]–[158], disks [159]–[161], triangular nanoprisms [160], [162]–[164], rods [165]–[169], and cubes [170], [171] is gaining attention for its interesting properties. The research in this field is sheer driven by its inherent shape-dependent properties [172], [173]. for cutting-edge technological applications such as sensors, photovoltaics, surface enhanced Raman spectroscopy [174]–[177]. Some studies are promising to date to tailor these anisotropic particles towards its final structure. Additionally these anisotropic nanoparticles may serve as templates for generation of new nanostructure different from the template [178], [179]. Of the several anisotropic structures reported so far in the literature is largely in the field of nanorods. Nanorods made of combination of elements such as CdSe, CdTe and titania, or as pure metals such as Ag, and Au and few more were reported [180], [181]. Typically surface plasmon bands of nanorods exhibited a red-shift along long-axis and small blue-shift along short-axis. Further, it was demonstrated that surface plasmon resonance along long-axis is primarily affected by the aspect ratio of the rods. The promising results from nanorods has triggered research in several anisotropic material due its interesting optical properties.

Among the several shapes of anisotropic nanomaterials investigated for surface plasmon resonance (SPR) applications, triangular nanoprism have been the center of attraction owing in recent days. Triangular nanoprisms facilitates concentration of electromagnetic fields at the edges and corners due to lightning rod effect. An ideal

triangular nanoprism is defined as polygon that has three congruent edge lengths and a defined thickness. The SPRs of triangular nanoprisms are tunable across the visible and near IR region (NIR) via manipulation of nanoprism edge length, thickness and morphology of the tip. For triangular nanoprisms, multiple modes (dipole, quadrupole and octupole) of SPRs are possible unlike spherical nanoparticles. Typically dipole and quadrupole resonance are separated by 100 to 400 nm hence it can be resolved very well in triangular nanoprism. The dipole and quadrupole modes of resonance originates from direction and degree of polarization of electron cloud relative to incident electric field of the light. Dipole plasmon resonance arises when electron cloud surrounding the nanoparticle moves either parallel or anti-parallel direction to the applied electric field.

For quadrupole mode of resonance, around half of the electron cloud surrounding the nanoparticle moves parallel and other half moves anti-parallel. Higher order resonances beyond dipole and quadrupole are observed for triangular nanoprism with high aspect ratio through complex polarizations which will not be discussed here as it is beyond the scope of this dissertation.

2.10.1 Effect of Snipping or Truncation

We have discussed the interesting optical properties of triangular nanoprisms made up of noble metal nanoparticles. However, the triangular nanoprisms that are synthesized in laboratory are not perfect triangular nanoprisms instead they are mixture of particles which had different degrees of truncation along with ideal ones. When the truncation of nanoprism is huge, they no longer are categorized as triangular nanoprism

instead they are referred as nanodisks or nanohexagons. Intense research are underway by chemists to synthesize ideal triangular nanoprisms. Snipping or truncation that arises during the synthesis of triangular nanoprisms also found to impart some interesting plasmonic properties to the materials. It was observed by researchers that the snipping introduces a red or blue shift to plasmonic resonance peaks. This will be discussed in detail elsewhere in this dissertation.

2.11.2 Effect of dielectric on plasmonic properties

Apart from the structural parameters of triangular nanoprisms such as edge length, thickness and truncation, dielectric environment of the nanoprism also affect the plasmonic properties [182]–[184]. Qualitatively, plasmon wavelength and refractive index of dielectric are directly proportional to each other [117]. Further the optical properties of nanoparticles were found to be very sensitive to particle morphology. The refractive index sensitivity for spherical nanoparticles were found to be 100 nm per refractive index unit [185], however, for tetrahedral nanoparticles the sensitivity was found to be 200 nm per refractive index unit [186]. The general trend reported in literature was larger the aspect ratio of the nanoparticle, larger the sensitivity to dielectric medium. In another report by Xue et al, silver nanoprisms coated on glass substrate exhibited reversible color changes when they were wet and dry. The reversible color changes observed for silver nanoprism arise from plasmonic sensitivity to surrounding refractive indices [187].

Generally, plasmon resonance of metal nanoparticles are investigated in transparent media whose dielectric function does not interfere with optical frequency of interest. When refractive index or dielectric medium is changed, the plasmon resonance frequency changes too. Thus plasmon resonance frequency is a measure of refractive index of the surroundings of a metal nanoparticle. This phenomenon leads to molecular detection of biological molecules. Biomolecules have refractive index different from water, hence, when biomolecules bind to surface of plasmonic metal nanoparticle, shift in plasmon resonance frequency occurs which enables the detection. Thus presence of dielectric does not require fluorescent agents, radioactive or other labeling agents to monitor or detect the binding of biomolecules. Gold nanoparticles are widely used for this specific applications owing to its biocompatibility and readiness to its bio-functionalization ability with sulfur containing functional groups.

2.12 Synthesis of Nanomaterials:

Nanomaterials are conventionally synthesized by one of the following four methods described below depending on the sources of the nanomaterials or the desired features of the final product.

- 1) Inert gas condensation: in this process the precursors of the nanomaterials are decomposed at elevated temperatures followed by condensation or precipitation of nanoparticles. This method generates nanoparticles with contamination free surface with ultrafine crystallite size

- 2) Physical or chemical vapor deposition: in this process, atoms or molecules are deposited on appropriate substrate by vaporizing the precursors of the nanomaterials. This method is also suitable for producing nanocomposites by deposition of different precursors in simultaneous or consecutive fashion.
- 3) In the third method, nanomaterials are synthesized by creating imperfections (dislocations, grain boundaries) in a perfect crystal via high energy irradiation, ball milling or through shear to name a few.
- 4) Precipitation or crystallization: nanomaterials will be crystallized or precipitated from unstable condensed phase from glasses or precipitation via supersaturated solutions of liquids or solids.

The above four categories are the common ways to size nanomaterials, however several variations of these processes were to produce nanocomposites with tailorable compositions and features. Being said that, two broad and common synthetic techniques are physical and chemical methods.

The common physical methods are inert-gas evaporation technique (Figure 2.6), sputtering, mechanical deformation etc, however they suffer from poor control on features of the nanoparticles being prepared and contamination. Physical methods are useful to synthesize the nanomaterials in large scale. Chemical methods of synthesis yields nanoparticles with high homogeneity via mixing at molecular level. On that context, we are going to discuss current developments reported in the literature to synthesize anisotropic nanoprisms of gold and silver.

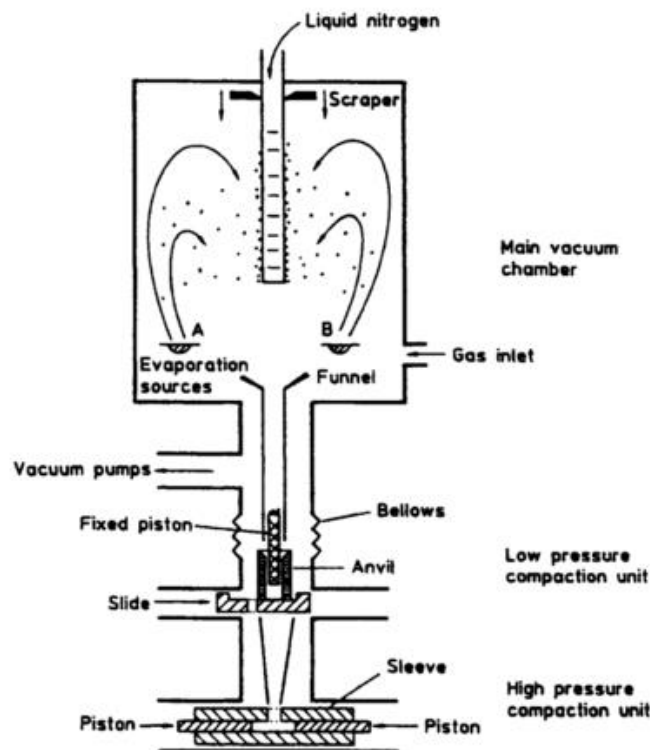


Figure 2.6: Schematic representation of experimental set-up for preparation of nanoparticles via inert-gas condensation method [188].

2.13 Synthesis of Triangular Nanoprisms:

Synthesis of triangular nanoprisms are broadly classified into two types: a) Thermal b) Photochemical. The thermal synthesis further classified into two categories based on the synthesis medium as aqueous phase and organic phase synthesis. Similarly, photochemical methods are classified into visible light methods and UV and radiolysis methods based on the wavelength of employed during the synthesis. We present here a brief discussion of both methods (thermal and photochemical) in this literature review.

On that note, we first discuss, thermal methods of synthesis of gold and silver triangular nanoprisms.

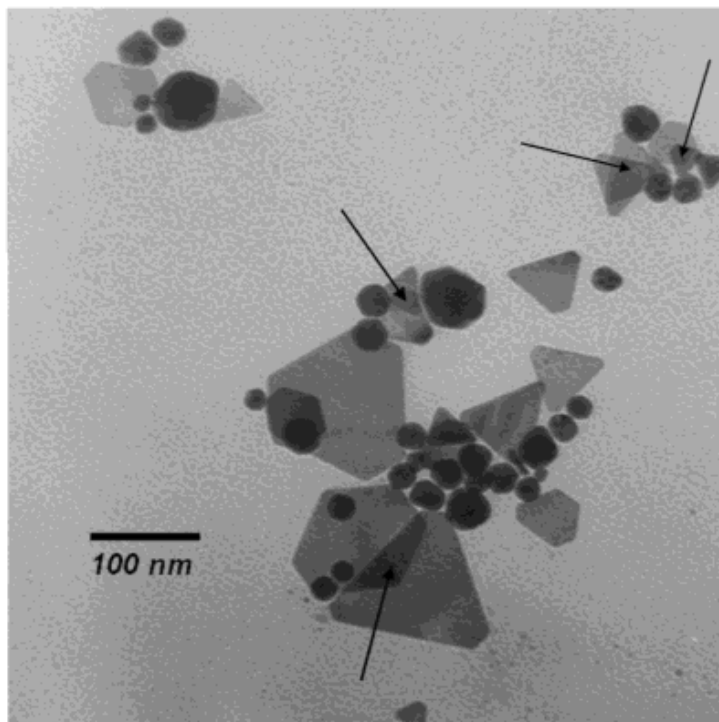


Figure 2.7: Synthesis of triangular gold nanoprisms along with some spherical nanoparticles. Figure adopted from reference [189].

First report on synthesis of triangular gold nanoprisms (Figure 2.6) as part of mixture of hexagons and pseudospherical particles when they reduced the chloroauric acid using salicylic acid were published by Malikova et al [189]. The UV-Vis spectra of the colloidal solution exhibited two SPR (surface plasmon resonance) peaks corresponding to spherical particles in the visible region and longitudinal modes of anisotropic particles in the near infra-red region. The SPR peak due to anisotropic particles were very broad due to polydispersity in size and shape of the anisotropic structures. Followed by this report, Zhang and coworkers [190] reported synthesis of

gold nanoparticles through reduction of chloroauric acid using sodium sulfide. Such synthesized particles also exhibited SPR peak in the near IR region which was accounted for anisotropic triangular nanoprism. Followed by this two initial reports, methods were developed to produce gold nanoprisms with control in size and shape by tweaking the experimental parameter. Ah et al [191], synthesized gold nanoplates using sodium citrate as reducing agent for hydrogen tetra chloraurate in presence of poly vinyl pyrrolidone(PVP). By tuning the molar ratios sodium citrate and PVP in reference to HAuCl_4 the geometric shape and size were tuned to the width between 80-500 nm and thickness ranging from 10-40 nm (Figure 2.7). Importantly they were able to gain control in dispersity of size and shape. The sodium citrate used in the synthesis generates small number of gold nuclei as seeds towards the lateral growth of the nanoprism.

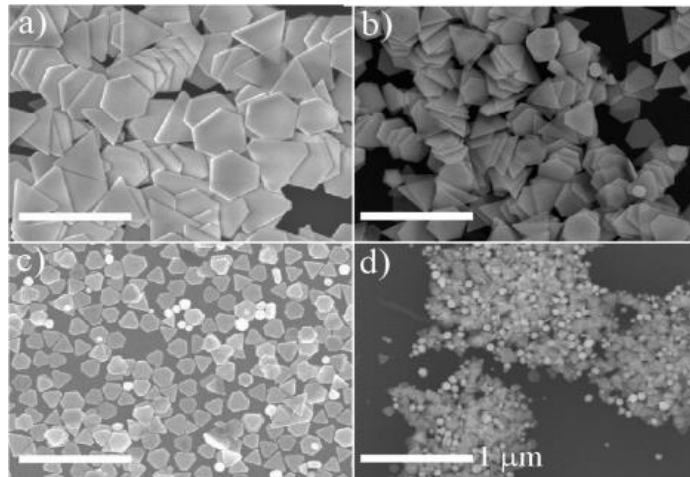


Figure 2.8: Scanning electron microscopy images of gold nanoprisms with various dimensions synthesized using PVP to HAuCl_4 ratio. Figure adopted from reference [191].

Mirkin and coworkers [192] also reported the synthesis of gold nanoparticles using cetyl trimethyl ammonium bromide (CTAB) as capping agent through three-step

growth of gold nuclei seeds in aqueous media. Ascorbic acid was employed as reducing agent. In that strategy, they were able to synthesize a mixture of spheres and triangular nanoprisms exclusively with better control in size distribution in a homogeneous way. Interestingly, the studies of optical properties of gold nanoprism exhibited optical features characteristic to dipole and quadrupole plasmon resonance. This was the first report published for observation of quadrupole plasmon resonance.

High yield synthesis of Ag triangular nanoprisms were reported by Chen et al [193]. Their synthetic strategy has two important steps: 1) seed mediated growth in presence of CTAB for preparation of truncated silver triangular nanoprism 2) aging of colloidal silver nanoprism solution. Aging process was critical in determining the shape of nanoparticles. TEM analysis of colloidal solution of silver before aging has revealed particles with size below 10 nm were spotted, which authors claim as seeds for the growth of larger particles through Ostwald ripening process. Such synthesized particles had thickness around 28 nm and diameter approximately 60 nm. In another research report published by Carroll and coworkers, had similar observations [160]. They synthesized truncated triangular silver nanoprism using ascorbic acid as reducing agent and CTAB as soft template. Synthesized particles had exhibited 4 absorption bands between 35 nm and 552 nm which corresponds to in-plane and out-of-plane dipole and quadrupole plasmon resonance. Growth of triangular silver nanoprisms were investigated by changing the metal ion to reducing agent ratio, CTAB concentrations, pH, effect of different reducing agents and seed concentrations [194].

Xia and coworkers reported the synthesis of silver triangular nanoprisms by reduction of silver nitrate via sodium borohydride reduction in presence of PVP and sodium citrate. This synthetic approach produced silver nanoprisms with less rounding. Additionally, this synthesis utilized thermal and photochemical approaches in aqueous solution. Light was found to be important for formation seeds, while heat aids the growth of seeds into larger structures. Thus far, we presented the reports on strategies to synthesize triangular silver nanoprisms in shape selective fashion. Mirkin research group reported synthesis of triangular nanoprisms via thermal method with modest control over edge length and thickness [195]. In this method, silver nitrate was reduced using trisodium citrate in presence of PVP by changing the amounts of sodium borohydride. Amount of sodium borohydride employed during the synthesis played important role in regards to the conversion of silver nanoparticles to triangular nanoprisms as well as the edge length. In addition, thickness of nanoprisms affects the optical properties significantly than the edge length. Presence of PVP prevents aggregation of anisotropic nanoparticles, whereas citrate controls the face selective growth of triangular nanoprisms.

Biological organisms, environments and molecules were also investigated in the thermal synthesis of gold and silver triangular nanoprisms to tune the structural features. *Pseudomonas stutzeri* AG259 a bacterial strain known to accumulate silver ions were employed in synthesis by Klaus et al [196]. The poles of bacterial cell had accumulated silver ions in triangular and hexagonal shapes. The silver fabricated to anisotropic structures were in elemental form and each cell had approximately 5 or less

nanostructures. The resistance to silver by *Pseudomonas stutzeri* AG259 and formation silver crystals were found to depend on physical and chemical growth parameters. pH, incubation time, effect of light, culture composition was found to tune the size and morphology of the particle. Synthesis of gold nanoprisms were reported using the extracts of plant materials [197]–[199] such as seaweed, aloe vera and lemon grass. The plant extracts serve as both reducing and capping for the synthesis of triangular nanoprism. When aurochloric acid were reduced by lemon grass, seed nanoparticles form first, followed by aggregation. The anisotropic structures arising from aggregation had its aspect ratio increasing over the time. This method yields more than 45% of gold nanoparticles in the form of triangular nanoprism. Further triangular nanoprism formed were is a mixture of perfect and truncated triangular nanoprism. For synthesis of gold nanoprisms aided by seaweed extract, yields were as high as 80 -90% and tuning of lateral nanoparticles size were achieved to the extent of 200-800 nm. The conclusion made by the authors regarding this synthesis were, neutral pH and ambient temperature were the optimal reaction conditions for high yields of nanoplates. Further, initial reactant concentrations were found to tune the particle edge length.

In addition to plant extracts, genetic materials such as proteins and nucleic acid were also employed to synthesize triangular nanoprism. These genetic materials found to control the growth of nanoparticle. Johnson and coworkers have reported the synthesis of via enzyme mediated biomineralization process. Gold (III) chloride was incubated with potassium hydroxide and sodium ascorbate under ambient conditions. Morphology

controlled synthesis of nanoprisms affected by two key factors of polypeptide: a) affinity for gold 2) possessing catalytic function. The creation of low pH environment at the vicinity of growing crystal and blockage of (111) crystal face is crucial for nanoprism formation [200].

Ultrasound and microwaves are widely used in the synthesis of nanomaterials. The cavitation produced by ultrasound creates shockwaves in synthesis solutions which affects the surface of nanoparticles leading to distinct shapes and structures [201]–[203]. Meanwhile, microwaves heat the synthesis solutions very rapidly than conventional hot plate leading to brief crystallization times and homogeneous nucleation [204]. Perfect and truncated gold triangular nanoprisms were synthesized using polyol (ethylene glycol) by microwave irradiation in a pulse or continuous wave fashion of solution containing PVP and HAuCl_4 . Such synthesized nanoparticles exhibited three bands characteristic of plate-like nanoparticles. Interestingly authors reported the square nanoprisms for the first time. Formation of nanoplates were facilitated by high temperatures achieved by microwave radiation using ethylene glycol [204].

Sonochemical methods are extensively used used for synthesis of nanomaterials. Jiang et al reported the synthesis of nanoplates by reduction of silver nitrate with dimethylformamide in presence of PVP [201]. Transmission electron microscopy and UV-Vis studies led to following observations: a) reduction of AgNO_3 yields prism-like seeds with initial dimensions of 2-5 nm spherical particles b) seeds on rapid dissolution and rapid growth form larger crystals c) larger crystals upon slow growth form

monodispersed silver nanoplates through Ostwald ripening. The ultrasound was found to accelerate the ripening process as well as control the size of as-synthesized particles. Presence of PVP induces the selective crystal growth of plate-like particles. In another study by Cai et al, ultrasound synthesis of gold nanoprisms were reported via reduction of HAuCl_4 using ethylene glycol in presence of PVP [205]. Ethylene glycol serves the role of solvent as well as reducing agent. Experimental analysis indicates PVP and ethylene glycol concentrations were crucial for formation of nanoprisms. For HAuCl_4 concentration of 0.5 mM, varying the concentrations of PVP from 100 -200 mM favors formation of nanoprism. When PVP concentration exceeds 200 mM, irregular morphologies were formed. Additionally, it was observed that aging time is crucial for manipulation of morphology. Sample synthesized through irradiation of ultrasound for 120 min that was aged for one week had nanoprism size of 70-90 nm which exhibited in-plane and out of plane dipole plasmon resonance peaks. Aging beyond one week induced for further growth in nanoprism. To the aged solution, fresh addition of HAuCl_4 found to increase the size of gold nanoprism which was confirmed by corresponding shift in optical properties of nanoprisms.

In comparison to synthesis strategies being explored for nanoprism synthesis in aqueous media, organic mediated synthesis is far from few as it requires elevated reaction conditions. Liz-Marzan et al have reported the synthesis of silver and gold nanoprism in DMF [206]. Silver nanoprisms were synthesized by reduction of silver perchlorate. Under reflux condition, the nanoparticles synthesized for found to be have homogeneous

size distribution. Heating via microwave irradiation also explored by them, which supports formation of homogeneously sized nanoparticles. Synthesis in the absence of PVP leads to aggregation of nanoparticles. For microwave induced reduction, average size of nanoparticles synthesized were independent of concentration of PVP. Molecular weight of PVP used during the synthesis found to affect the features of nanoparticles synthesized. High molecular weight PVP yields nanoparticles who bands are sharper, symmetrical which can be correlated to uniform size distribution. Lower molecular weight PVP yields larger particle size. Further, synthesized nanoparticles exhibited more stability in ethanol than water which was attributed loss of stability of PVP due to high polar nature of water. Sarkar et al also investigated the synthesis of silver nanoprisms, using formamide [207]. When polyethylene glycol (PEG) was used along with formamide, array of triangular nanoprisms were found. However, when PVP is used along with polyethylene glycol, at a ratio of 1:1, nanospheres were also formed along with nanoprisms. The ratio of PVP to PEG provided the opportunity to tune the ratio of nanospheres to nanoprisms.

So far we have presented the brief literature reports regarding the thermal synthesis of silver and gold triangular nanoprisms. Now we present a discussion of progress made in light mediated synthesis of nanoprisms. First report on synthesis of silver nanoprisms were reported by Mirkin research group [142]. It is a photo induced method for conversion of large amounts of spherical silver spheres to triangular nanoprisms. The synthesis procedure involves reduction of silver nitrate with sodium

borohydride in presence of trisodium citrate. Bis(*p*-sulfonatophenyl)phenylphosphine dihydrate dipotassium salt solution (BSPP) was added dropwise which acts as stabilizing agent and the reaction mixture was exposed to white light. A series of color changes were observed over 70 hours ranging from yellow, green and blue. During that time when reaction mixture was monitored by UV-Vis three new bands were appeared while the peak due to nanosphere was vanishing indicating the spheres were converted to nanoprisms. Synthesis can be turned on or off via tweaking the exposure of light with appropriate wavelength or presence and absence of citrate ions and rate of reaction was affected by citrate to BSPP ratio [179]. Formation of nanoprism had induction, growth and termination stages. Growth of nanoprisms were achieved through Ostwald ripening process using smaller Ag crystals as seeds and the reaction was terminated when all small particles were consumed. Formation of triangular nanoprism was subject of intense debate. Two theories were put forward were formation of nanoprisms are a) light driven ripening process through transition from silver nanospheres [208], [209] b) oxidation and re-deposition [210]–[212]. When Brus and coworkers synthesized silver triangular nanoprisms in the absence of BSPP, it had a wide size distribution of prisms formed and nanoprism conversion was incomplete. The kinetics studies indicated that nanoprisms were formed by oxidative etching of Ag and subsequently a reduction process of silver ions by citrate photooxidation. Further this studies ruled out the interference of photo induced thermal heating and optical forces [213]–[215]. If spherical nanoparticles formed initially are the ones being transformed to nanoprisms, approximately it would need

around 30 seeds to make a prism. For particles as many as 30 to come together, such a process will have complex kinetic order. Reaction kinetics studies suggested autocatalytic first order, thus fusion concept for formation of prisms were ruled out. Alternately, oxygen in the seed solution dissolves silver to form silver ions, which is supported by the fact that significant increase in pH of the growth solution. The primary role of silver seed particles is to serve as source for silver ions which can be re-deposited on aging silver nanoprisms. Additionally, the deposition and redeposition process are very crucial to size of seed particles. Typically, larger the size of nanoparticle, higher its reduction potential. Thus when silver particles go beyond a certain size, it will be tough to oxidize it, hence, prism formation will be affected [216].

Sun and Xia, reported the synthesis of silver nanoprisms using PVP as stabilizing agent and halogen lamp with UV cut-off filter [217]. They were able to achieve the triangular nanoprism morphology regardless of whether PVP is used or not during the synthesis. PVP found to affect the size distribution of silver nanoparticles being synthesized. In addition to PVP, polyvinyl alcohol and sodium dodecyl sulfate were also studied as stabilizing agent. They concluded that for successful synthesis of nanoprism, the seed particles should be kept under 10 nm. Gehlen and coworkers reported the synthesis of nanoprisms using two PVP of two different molecular weights i.e. 29000 and 58000 g mol^{-1} [217]. Molecular weights of PVP found to influence the stability of the synthesized silver nanoprisms. Low molecular weight PVP was found to yield more photostable nanoprisms than high molecular weight PVP. The other variable found to

affect the synthesis of nanoprisms are pH, use of nucleophiles and ligands [218]. Synthesis of nanoprisms via oxidative dissolution process were facilitated by use of nucleophiles. Nucleophiles used during the synthesis would build up excess negative charge in the interior of nanoparticles which aids the removal of electrons by oxidants [142], [210], [211], [219], [220].

Xue et al reported the synthesis of silver nanoprisms using gold seed particles [221]. The gold seed particles play a dual role in the synthesis as plasmonic cores as well as experimental labels to evaluate the role of plasmonic excitation in conversion of spherical silver nanoparticles to triangular nanoprisms. When a solution prepared with Au/Ag particle with particle size of 11 and 5 nm respectively at a ratio of 1:10 was irradiated with 550 nm light for 5 h, the outcome was silver nanoprism with Au core. The nanoprism had an average edge length of 76 nm and 14 nm thickness. The thickness of nanoprism was found to be dependent on diameter of the gold cores employed in synthesis. The core-shell structure of silver nanoprism formation involves two steps: 1) the dipole plasmon resonance of gold nanoparticles were excited by incident light 2) deposition of silver layers induced by gold plasmon resonance. When the gold spheres were replaced by gold triangular nanoprism as seeds, bimetallic core-shell structures were not observed at irradiation wavelength of 550 nm. However when the irradiation wavelength was changed to 1064 nm, silver nanoprism shell with gold prism core was formed. Thus through this experiments, it is concluded that excitation wavelength also plays a crucial role in formation of nanoprism.

So far we have presented the discussion on synthesis of triangular nanoprisms limited to just white light. Chergui and coworkers first investigated the effect of irradiation wavelength and shape of nanoparticles (Figure 2.8) [209]. First, spherical nanoparticles were prepared via sodium borohydride reduction of silver nitrate and they split it into multiples identical samples.

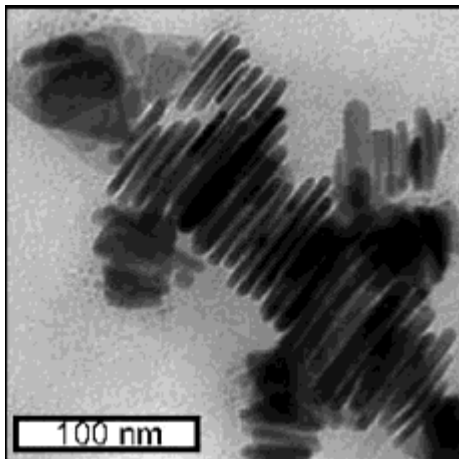


Figure 2.9: synthesis of triangular nanoplates after evaporation of solvent as seen in TEM. Figure adopted from reference [209].

Those identical samples were initially exposed to light from fluorescent tube. After an induction period, the nanoparticles color changed from yellow and green. At that point, they employed various filters to control the irradiation wavelength from the same source. Orange filter had predominantly produced triangular nanoprisms with very high aspect ratio. For broadest blue filter, triangular nanoprisms of smaller size were the major product, however when they used the narrowest blue filter, cubic and octahedral particles were formed. Effect of irradiation wavelength on shape control were explained by authors through photo-oxidation and light-induced coalescence and growth. During the

induction period photo-oxidation occurs, and growth occurs when filters were used. Interestingly they were able to pause and resume the reaction by moving the reaction solution to dark and light respectively [209].

Brus and coworkers synthesized silver nanoparticles photochemically from adsorbed silver ions in the presence of citrate using laser [212]. If colloidal seed solution has particles with different size and shape, larger particles in the seed solution grow fastest. Citrate molecule employed in the synthesis play a crucial role as capping ligand for Ag nanoparticles and to photoreducing agent. The three carboxylic acid molecules in the citrate, two of them bind with silver and the third one involves in colloid stabilization via electrostatic repulsion. Additionally citrate act as reducing agent too. The silver ions concentration in the solution determines the ultimate size of the particles and the aspect ratio is controlled via the irradiation wavelength. The aspect ratio of synthesized particles are higher when size irradiation wavelength is high and vice versa.

Mirkin and coworkers have reported anisotropic synthesis of silver nanoparticles by controlling the plasmonic excitation [219]. In that study they employed xenon lamp coupled with band pass filter. The result was prisms with bimodal distributions in size was produced. The edge lengths were found to be 70 nm and 150 nm but they had same thickness around 10 nm. Bimodal distribution can be converted to monomodal distribution when two different excitation wavelengths were used together. When primary irradiation wavelength of 550 nm was used bimodal distribution was observed. However, when secondary irradiation wavelength of 450 nm was used along with 550

nm, only unimodal size distribution size was formed. When secondary radiation wavelength was kept constant and primary irradiation wavelength were changed from 450 nm to 750 nm results in linear increase of edge length. The bimodal and unimodal particle size distributions were explained by particle fusion mechanism in an edge selective manner or growth of nanoprisms reaching the maximum size controlled by light.

In another report by Mirkin and coworkers, pH was used as a tool to synthesize the silver nanoprisms (Figure 2.9) through single-beam excitation [222]. In the previous synthesis discussion, a larger triangular nanoprism is being formed through coalescence of 4 small nanoprisms [219]. In this synthesis they prevented accumulation of 4 triangular nanoprisms coming together by controlling the pH which in turn executes inter-prism repulsion.

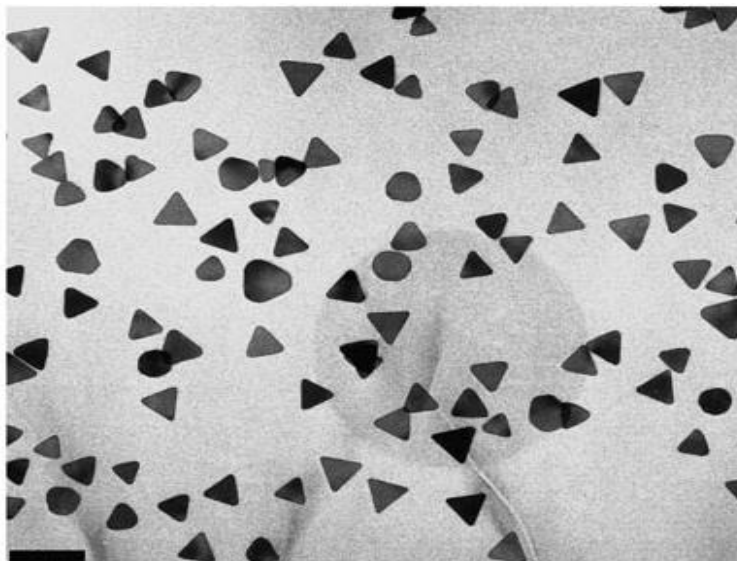


Figure 2.10: pH controlled synthesis of silver triangular nanoprisms at irradiation wavelength of 550 nm at pH 11.2. Figure adopted from reference [222].

When silver nanoparticles were irradiated with 550 nm light at an initial pH of 9.5. Bimodal particle size distribution was observed at pH of 7.4 through addition of nitric acid. However, when sodium hydroxide was added to the seed solution to raise the pH to 11.2, unimodal prisms were only observed. For such prisms the edge length corresponds to smaller prism in the bimodal mixture observed at pH of 9.2. At pH value above 12, the reaction does not yield any prisms as high hydroxide concentration effectively removes the silver ions in the solution, without it, no reaction was observed. Further at such elevated basic conditions a passive layer of silver hydroxide forms which prevents the photoreaction.

Xu and Lombardi coworkers presented an alternate pathway to tune size dispersity in triangular nanoprisms [223]. They employed monochromatic irradiation source with different laser wavelengths for irradiation of seed solution. The synthesis solution contains silver seeds, silver ions and citrate ions. They observed that both size and shape were affected frequency and power of the incident light. The optical properties exhibited by synthesized particles were found to be correlated to excitation wavelength. The mild laser power contributed to bimodal distribution, however, stronger laser power resulted in a monomodal distribution of particles. Lower laser power yielded particles that are pyramidal and pentagonal in shape, while higher laser power yielded planar triangular shape nanoparticles. The growth process of particles involves, inducing and accumulation of nanoseeds to form intermediates followed by exciting the SPR of

intermediates that drives the directional growth into nanoparticles and finally truncation and regrowth to form monodispersed silver nanoparticles.

In another interesting report by Liz-Marzan and coworkers, silver nanoprisms were synthesized by reduction using sodium borohydride in presence of trisodium citrate and PVP [208]. The reaction mixture was exposed to light emitting diodes (LED) with different wavelengths at very low intensities. The silver nanoprism irradiated with light of 653 nm, very high edge length of 242 nm. The higher temperature employed in the reaction aid for faster completion of reaction without affecting the size or shape of final particles. A quasilinear dependency of particle size was found with respect to irradiation wavelength. The nanoprisms were formed at the expense of preformed silver seeds.

Zanchet and coworkers investigated the kinetics of formation of silver nanoprisms synthesized using sodium borohydride reduction in presence of sodium citrate [224]. The spherical seeds were exposed to visible light with wavelengths of 500, 550, 600 and 650 nm in presence of excess of silver nitrate and sodium citrate. When wavelength filters were used, the silver deposition on seed particles was very slow until prism formation was observed. This was due to the fact that seed particles plasmon excitation was far from filter wavelength. Longer the wavelength used for irradiation, longer the time taken for completion of the reaction and particles had longer edge lengths. The prism morphology was seen even when little to no light was absorbed by seed particles. This observation suggests plasmon excitation is not necessary for formation of prismatic morphology. Paul et al reported the synthesis of silver nanoprisms on a solid substrate. In

that method, small nanotriangles, were embedded on the substrate followed by irradiating in the seed solution. When linearly polarized laser was irradiated, the triangular nanoprisms shown preference towards the direction with tip being parallel to polarization direction.

There was not much precedence in the literature for the synthesis of silver-dielectric-gold sandwich we proposed in this thesis. Spin coating will be an ideal starting point to investigate the surface plasmonic properties of the sandwich structure experimentally [225]. To tap the identified advantages through simulations of sandwich structures, synthesis of those materials will pose a challenge for synthetic and material chemists.

2.14 FDTD Simulation Parameters:

All FDTD simulations were performed using OptiFDTD simulation software. The triangular nanoprisms of gold and silver investigated separately and as sandwich were constructed using OptiFDTD software. The procedure for construction of triangular nanoprisms of silver and gold were same as well as the sandwiches. The first E and B nodes are taken to be zero since there are no source in the field prior to the start of the simulation. The steps we carried out to do simulation is outlined here as follows:

Layout Creation Steps: Commercial software Opti-FDTD was used for simulation of gold nanoparticles on 3D surface Plasmon. The procedure for simulation is as follows:

Layout creation steps: from the start menu OptiFDTD waveguide layout designer were opened, followed by in the programs section, optiwave software were chosen to open a waveguide layout designer window. The initial properties dialog box appeared when new project was created using OptiFDTD_Designer file menu.

Gold_Au_Lorentz_Drude_Model file was dragged from the material folder in **Master** to FDTD_dispersive folder under **Materials** in the current project. Gold_Au_Lorentz_Drude_Model was stored under this project. In the OptiFDTD_Designer1, **Channel** folder can be found under the **Profiles** folder through a right click. Choose New, followed by a **Channel Profile** dialog box pops up. In the dialog box, profile name, layer name (layer 1), width (0.1), thickness (0.1), and offset (0.0) were described. **Gold_Au_Lorentz_Drude_Model** was selected from the material list and added to the channel profile followed by click store. After this, we went back to initial properties dialog box and the following information were fed into the appropriate box: width 0.1 μm , profile as **ChannelPro1**, wafer length – 0.6 μm (z-direction), and width 0.3 μm (x-direction). Cladding material is air with thickness of 0.3 μm (y-direction) and air also serves as substrate material with thickness 0 (y-direction). **OptiFDTD Designer** window appeared after click OK in **Initial Properties** dialog box.

A nanoparticle layout was drawn as triangular nanoprism and the shape of waveguide and position was adjustable in the layout window by making double click on the sphere. The position x, y, z of sphere waveguide were chosen as 0, 0.15 μm , 0.35 μm respectively with a radius of 0.05 μm . For further simulations, only the radius was changed

from 0.01 to 0.07 with an interval of 0.01 m without changing other parameters. At this point, we can see the layout in the 3D mode under the **3D layout model** tab.

Defining Input Wave: a **Vertical Input Plane** was chosen from the **Draw** menu and the input plane properties were defined as **Gaussian Modulated Continuous Wave**, with a wavelength of 0.55 μm followed by it was set to the time domain input waveform. To the time domain input plane time offset and half width were chosen as 4.0e-15 and 0.8e-15 seconds respectively. The other general information for the Input Plane were described as follows: input field traverse – rectangular, z position – 0.2 μm , plane geometry – positive direction and finally it was labeled as **InputPlane1**. The center position setting for X,Y are 0.0 and 0.15 μm respectively with halfwidth for X and Y as 0.2 μm . The effective index was chosen as **Local** and polarization as **Linear Y** with amplitude of 1.0 (V/m^2). With that we defined all the parameters for input plane.

Defining Simulation Parameters: simulation was performed through **Simulate 3D Using 64-bit Simulator**. The mesh size along X, Y, Z were chosen as 0.004 m. The boundary conditions for X and Y direction were chosen as PBC and for Z direction as APML. The values for PML boundary condition is, anisotropic PML layer number -16, theoretical reflection coefficient – 10e -12, real anisotropic PML tensor parameter – 60.0, power of grading polynomial – 3.5 and chosen to run 4000 time steps with sampling time interval of 2. Under the **Spectrum** tab, number of samples was set to 101, start wavelength is 0.4 μm and end wavelength is set to 0.9 μm .

Observation Objects Setup: The observation point monitors the time domain and frequency domain response. The observation area is used to calculate power transmission ration and normalized power versus wavelength. The **observation XY plane** placed next to sphere in the layout with center horizontal offset along z-directions as 0.5 μm , center vertical offset along x-direction 0.0 μm , center depth y-direction as 0.15 μm , X and Y lengths as 0.3 μm and labeled as **ObservationArea1** with data components **Ex, Ey, Hx, Hy**. **ObservationArea2** was set as above with center horizontal offset along z-directions as 0.1 while maintaining all other parameters the same. Power spectral transmission function was obtained from observation 1 and observation 2 will obtain the power spectral reflection function.

Performing the 64Bit-FDTD Simulation: Now, we are ready to run the simulation, as we have defined all required parameters for simulation. When the simulation is in progress the progress window represents the status of simulation, **Snapshot** feature lets us to view the intermediate simulation results. After the simulation is done, results can be viewed in analyzer.

Chapter 3

Study of the Snip Effect in Resonance of Gold and Silver Triangular Nanoprisms

3.1 Introduction

The frequency of the LSPR however, depends on variables such as effective mass and density of the free electrons, and strongly varies with the shape and the size of the nanoparticles, as well as the wavelength-dependent permittivity of the nanoparticle and its surrounding medium [226].

Plasmonic properties of gold and silver nanoparticles in particular, have found several applications in recent years including in bio-sensing and chemical sensing [227], [228] , and in SERS spectroscopy technique [229], [230]. Significant progress and understanding has been made to explain the relationship between the plasmonic properties of gold and silver nanoparticles and their size [231]–[233]. Nevertheless, studies focusing on the effect of the various shapes of gold and silver nanoparticles on their plasmonic properties are at their inception. For example, gold and silver nanoparticles in spherical shape have been studied by many research groups [234], [235], for their interesting optical and electronic properties. However, interesting plasmonic

properties of anisotropic plasmonic nanoparticles has caused significant interest among researchers towards studying these types of nanoparticles recently. Gold and silver nanoparticles in the shapes of rods, hexagons, and triangular prisms have been among a few anisotropic structures synthesized in high yields with control over their architectural parameters. Typically, these types of nanoparticles can be synthesized by thermal, photochemical or electrochemistry based templates [169], [236]. Such synthesized structures have interesting plasmonic properties in the near infrared (near-IR) and visible regions. Generally, the method of synthesis does not seem to affect the plasmonic properties of nanoparticles as long as their size and shape remains similar. Nanoprisms synthesized by different methods were found to have similar physico-chemical properties [237].

Different shapes of metal nanoparticles tend to have unique plasmonic characteristics due to their particular geometry. In the case of triangular nanoprisms, the interest mostly arises from the multiple absorption bands in these particles associated with the multiple axes of their triangular shape as each of these axes can support propagating and localized surface plasmons [238], [239]. As a result, nanoprisms, are among the anisotropic plasmonic particles which exhibit LSPR in different orientations depending on the polarization of the incident light. Further, triangular nanoprisms provide us the opportunity of tuning their LSPR properties by suitably modifying their

structural parameters such as particle thickness, particle edge length and height [240], [241].

Studies on various methods of triangular nanoprisms synthesis have been performed [129], [209], [211], [237], [242]–[245]. Generally it was found that, synthetic parameters can tune the dimensions of the nanoprisms. The typical aspect ratio (edge length / thickness) for gold and silver triangular nanoprisms ranges from 5-40 and depending on the synthetic procedure adopted, synthesized nanoprisms may be single crystalline or polycrystalline. Other nanoparticle shapes such as polygons, hexagons and circular plates have also been synthesized and reported in the literature. However, most of the emphasis has been focused on triangular nanoprisms of gold and silver nanoparticles which have three congruent edge lengths varying from 40 nm to one μm and thicknesses varying from five to 50 nm [246]. The common tunable synthetic parameters such as surfactant concentrations, metal ion and reducing agent ratios, pH, seed particle concentration to name a few will help to tailor the nanoprism edge length, thickness, and tip morphology, which can lead to whole new physical and chemical properties, in particular, localized surface plasmon properties over the whole visible and near infra-red region [237].

The dipole and quadrupole resonances in nanoprisms arise from the difference in degree and direction of polarization of the electronic cloud relative to the incident electric field. Thus, the optical features of gold and silver nanoprisms are largely characterized by

their size, shape and distribution of nanostructures in solution. It is not surprising therefore that the frequency of the dipole and quadrupole resonant peaks shifts as the size, shape and dielectric environment of the nanoprisms are changed. However, it is observed that their resonant wavelengths are typically separated from each other by 100-400 nm [142], [194]. The observation of dipole and quadrupole resonance at separated wavelengths is very special for nanoprisms, as this characteristic cannot be seen in spherical particles since the frequencies of different oscillation modes are indistinguishable.

Despite the several advantages of triangular nanoprisms, it has been a challenge to synthesize these nanomaterials with absolute precision in edge lengths, and corner sharpness. Often times, synthesized triangular nanoprisms do not have the ideal sharp corners. Instead they are synthesized with one or more truncated corners. The truncated triangular Ag nanoprisms are more effective biocidal agents [184], [247]. Also, the truncated triangular forms are more effective than the round or rod shaped nanoparticles with regards to biological interactions. Zheng et al have reported the extinction efficiency of triangular silver nanoprisms in water [142]. They concluded that truncation has introduced blue shift and larger the truncation, higher the blue shift. Based on these results, we got curious to see the dipole plasmonic resonance behavior upon introduction of truncation in triangular nanoprisms of gold and silver and how they are affected by structural features such as edge length and thickness. Addition to effect of edge length

and thickness, we studied the effect of introducing truncation in a sequential fashion instead of introducing all at once in all vertices.

3.2. The effect of the edge length and thickness of perfect triangular gold and silver nanoprism:

In order to design the hybrid nanostructure, the edge length and the thickness of each of the Au and Ag nanoprism layers were studied individually and optimized separately. Theoretical optimization studies were performed on a single layer of Au and Ag nanoprism first. In this step, the nanoprism edge lengths were varied between 90-150 nm, and the thickness of each metal layer was varied between 10 nm and 30 nm in order to optimize the thickness and the length of the layers which exhibit strong dipole resonance. Simulation results showing the plasmonic absorbance resonance of a single layer of Ag, and Au nanoprisms with different edge lengths and thicknesses are shown in Figure 3.1 & Figure 3.2. The simulation results shows that the plasmonic resonance of Au and Ag nanoprisms varies as the edge length of the nanoprisms changes. Figure 3.1a shows the FDTD simulation results for silver nanoprisms with varying edge lengths between 90 and 150 nm each having a thickness of 30 nm. The simulation results shows peaks characteristic of both the quadrupole and dipole resonance. Quadrupole resonance peak observed at shorter wavelengths in comparison to dipole resonance peak. The results demonstrates that the dipole resonance peak is the more intense peak compared to

the quadrupole resonance peak and this observation was independent of the edge length of the nanoprism. Since the quadrupole peak is weak relative to the dipole peak, we have mainly focused our study and discussion on the dipole resonant peak. As shown in Figure 3.1a, the dipole plasmonic resonance of Ag nanoprism increased from 538 nm to 647 nm when nanoprism edge length increased from 90 nm to 150 nm. Thus dipole resonance peak in Ag nanoprisms experienced a red shift as the edge length of the Ag nanoprism increased. The observed red shift is due to electron accumulation in the corners of the nanoprism and the large distance between the electrons and positive ions in the electronic cloud of the nanoprisms which supports lower energy (i.e. longer wavelength) oscillations [248]. In a study conducted by Millstone *et al*, triangular nanoprisms of Ag and Au synthesized through nucleation approach, had exhibited a red shift in dipole resonance peak with increase in the edge length of the prism [192]. The red shift they observed was verified by DDA simulations too. Our observations of red shift with increase in edge length of triangular nanoprisms of Ag and Au are in good agreement with the report by Millstone *et al*. Similar to edge lengths, the intensity of dipole plasmon resonance increased with increasing edge length in the Ag nanoprisms which is simply due to larger number of electrons participating in the oscillations. The simulation experiments performed for nanoprisms with edge lengths larger than 150 nm, the shift in the dipole resonant peak becomes small as the nanoprism edge length changes. This is due to the fact that as the length of the nanoprism becomes longer, the quantum effect on

the electron's oscillation length becomes less prominent [21,22]. Thus we have limited our investigation to nanoprisms with edge lengths of less than 150 nm. On the other hand, simulation results show that in triangular nanoprisms with edge lengths smaller than 90 nm, the dipole peak loses its strength compared to higher order resonances (i.e. quadrupole and higher) which limits applications for real world experiments. As a result, edge lengths between 90 nm and 150 nm were selected for our hybrid nanoprism structure tunability study. It is important to note that along with dipole resonance, several higher order multiple resonance peaks were also observed for all edge lengths in our study. However, their intensities was negligible in comparison with the dipole resonance peak for the edge lengths we between 90 nm and 150 nm. Similar to Ag nanoprisms, the effect of varying the edge lengths for Au nanoprisms on the plasmonic resonance peak were also investigated (Figure 3.1b). The dimensions of Au nanoprism were maintained exactly same as Ag nanoprism. As shown in Figure 3.1b, the plasmonic resonance of Au nanoprism varies from 549 nm to nm to 604 nm with increasing nanoprism edge length. Similar to the trend observed for Ag nanoprisms, the plasmonic peaks of Au nanoprism also experienced a red shift with increase in the nanoprism edge length (Figure 3.1b). Summary of finding are presented in Table 3.1 and Table 3.2.

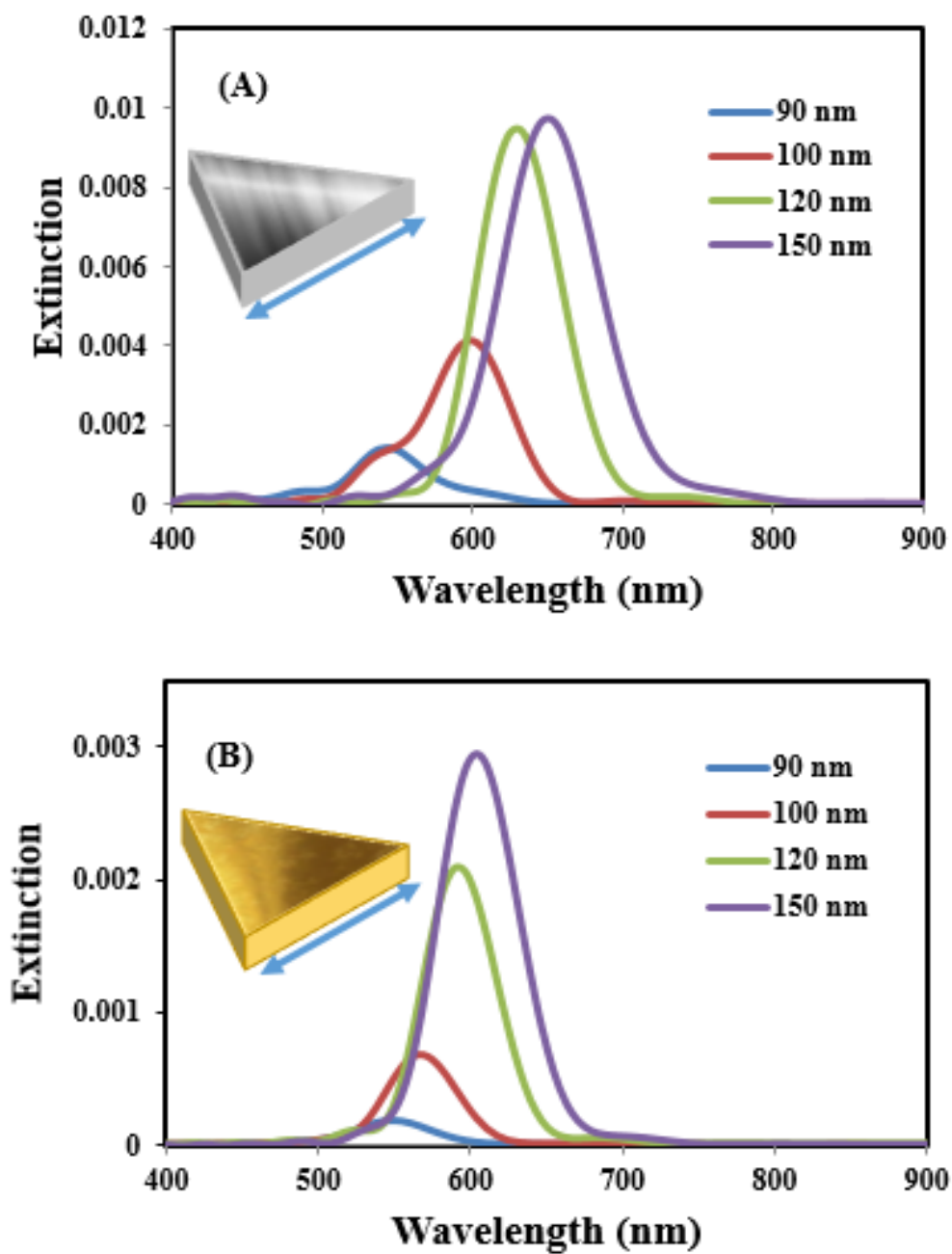


Figure 3.1 Effect of edge length on plasmon resonance for triangular nanoprisms of a) Ag
b) Au

After the effect of edge length analysis, simulations were performed on standalone Au and Ag nanoprisms to study the effect of thickness variation on the wavelength of the dipole resonant peaks. The results of this study show that both the position and strength of the nanoprism plasmonic peaks have a strong dependence on the thickness of the metal layer. Figure 3.2a shows simulation results performed for Ag nanostructures with thicknesses 10, 15, 20 and 30 nm while the edge length of the nanoprisms were held constant at 100 nm. The plasmonic dipole resonance peaks for Ag nanoprisms shifted from 597 nm to 705 nm when thickness decreased from 30 nm to 10 nm. Similar to silver, the effect of thickness variation in the dipole plasmonic resonance in Au nanoprisms were investigated for the edge length of 100 nm. The thickness of Au nanoparticles were changed between 10 nm and 30 nm. The results of the simulations indicate that the dipole resonance peak for Au nanoparticles have experienced a blue shift from 624 nm corresponding to the thickness of 10 nm to 566 nm corresponding to the thickness of 30 nm (Figure 3.2b). Again, the blue shift with increase in thickness of the nanoprism are consistent with observations made by Millstone et al for triangular nanoprisms of Ag and Au. As the thickness of a structure with a constant edge length increases, the structure can support higher energy oscillations in the direction perpendicular to the edge length (i.e. the thickness), giving rise to higher energy oscillations, which cause a blue shift in the resonance wavelength. To conclude, the results of our study has shown that the increasing the edge length of both Ag and Au

nanoprism imparted a red shift in the dipole surface plasmon resonance of the nanoprisms while increasing their thickness caused a blue shift in their dipole plasmonic resonance. Based on the results of our simulation studies, we chose an edge length of 100 nm with a thickness of 30 nm for Au and Ag to construct hybrid sandwich structure since they exhibited the strongest dipole resonant peak in the visible region, which is the range of resonance frequency with most applications.

Table 3.1: Effect of edge length on dipole plasmon resonance of triangular nanoprisms of Ag and Au truncated and non-truncated

Edge Length (nm)	Dipole Plasmon Resonance Maximum (nm)			
	Perfect Ag	Truncated Ag	Perfect Au	Truncated Au
90 nm	538	481	549	508
100 nm	597	513	566	518
120 nm	624	549	590	543
150 nm	647	617	604	590

Table 3.2: Effect of thickness on dipole plasmon resonance of triangular nanoprisms of Ag and Au truncated and non-truncated

Thickness (nm)	Dipole Plasmon Resonance Maximum (nm)			
	Perfect Ag	Truncated Ag	Perfect Au	Truncated Au
10 nm	705	549	624	548
15 nm	639	543	590	538
20 nm	617	528	578	527
30 nm	597	513	566	508

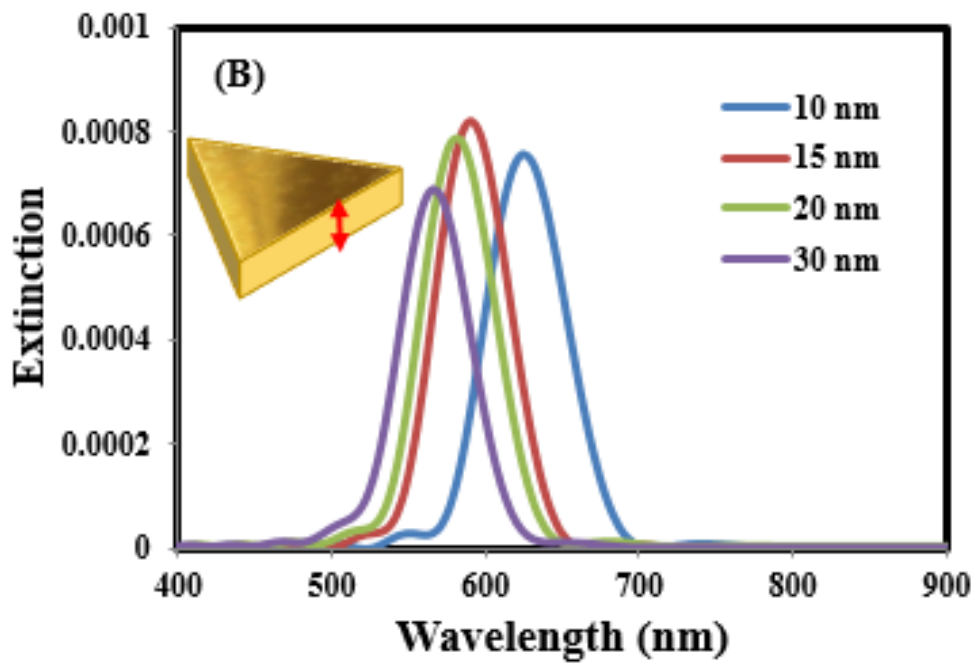
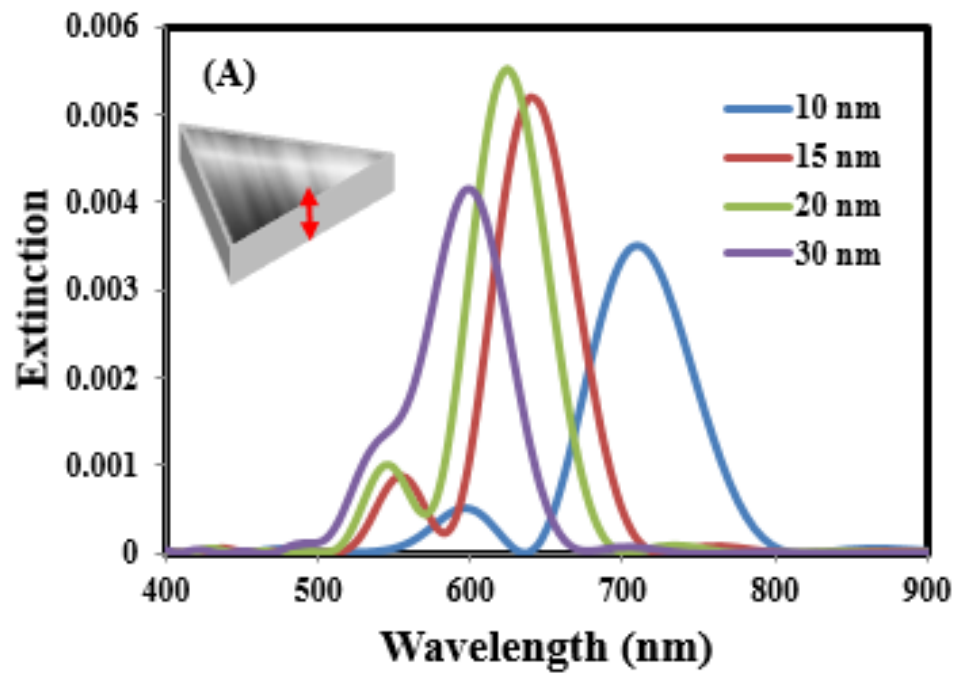


Figure 3.2 Effect of thickness on plasmon resonance for triangular nanoprism of (a) Ag (b) Au

3.2 The effect of edge length and thickness of truncated triangular gold and silver nanoprism:

The effect of edge length and thickness for truncated nanoprisms of Au and Ag were also investigated and compared the observations with reference to perfect nanoprisms (Figure 3.5 & Figure 3.6) The trends were exactly the same as for non-truncated prisms of Au and Ag i.e., a red shift in dipole plasmon resonance was observed for increase in edge length (Figure 3.3) and a blue shift is observed for increase in thickness of nanoprism (Figure 3.4). Summary of findings are presented in Table 3.1 and Table 3.2. The dipole plasmon resonance maximum for truncated nanoprisms of Au and Ag occurred at lower wavelengths than the corresponding perfect prisms. Similar trends were observed for optimization of thickness too. Truncated nanoprisms had dipole resonance maximum at lower wavelengths when compared to perfect prism. In the same note, perfect and truncated gold nanoprisms exhibited dipole plasmon resonance maximum at lower wavelengths than the corresponding silver nanoprisms. As expected, the strength of dipole plasmon resonance of Ag was observed to be more than Au.

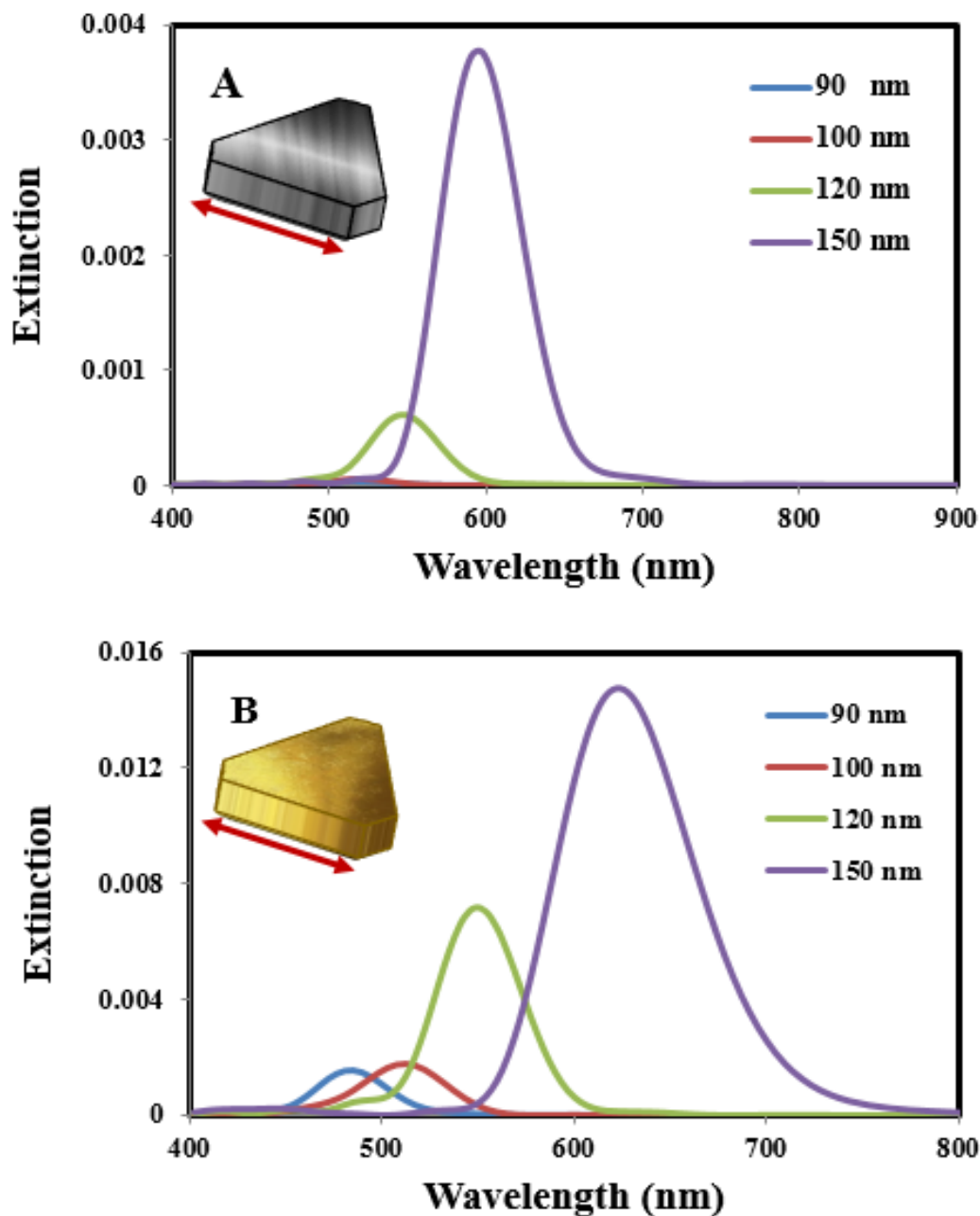


Figure 3.3 Effect of edge length on plasmon resonance for truncated triangular nanoprisms of a) Ag b) Au

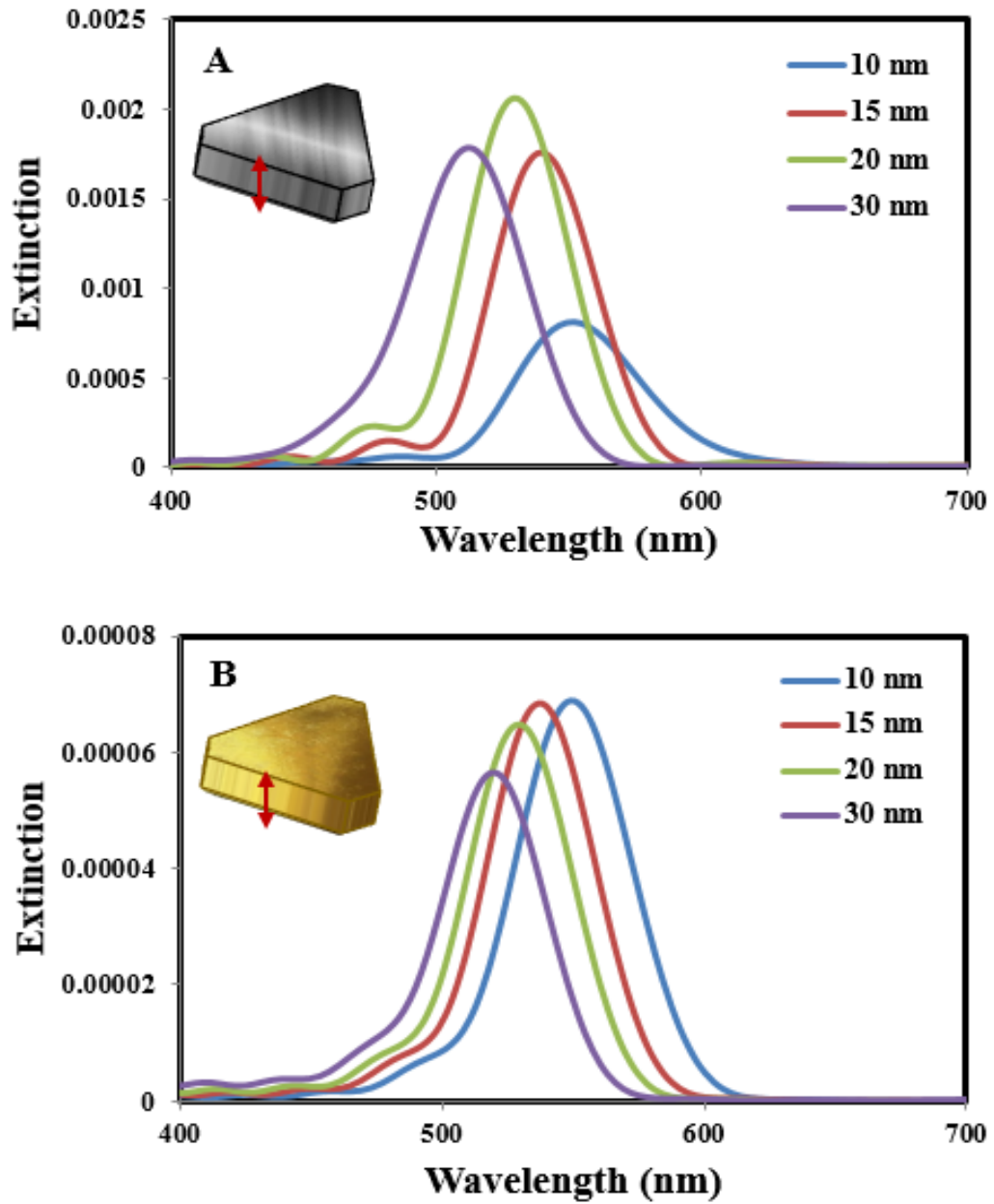


Figure 3.4 Effect of thickness of nanoprism on plasmon resonance for truncated triangular nanoprisms of a) Ag b) Au

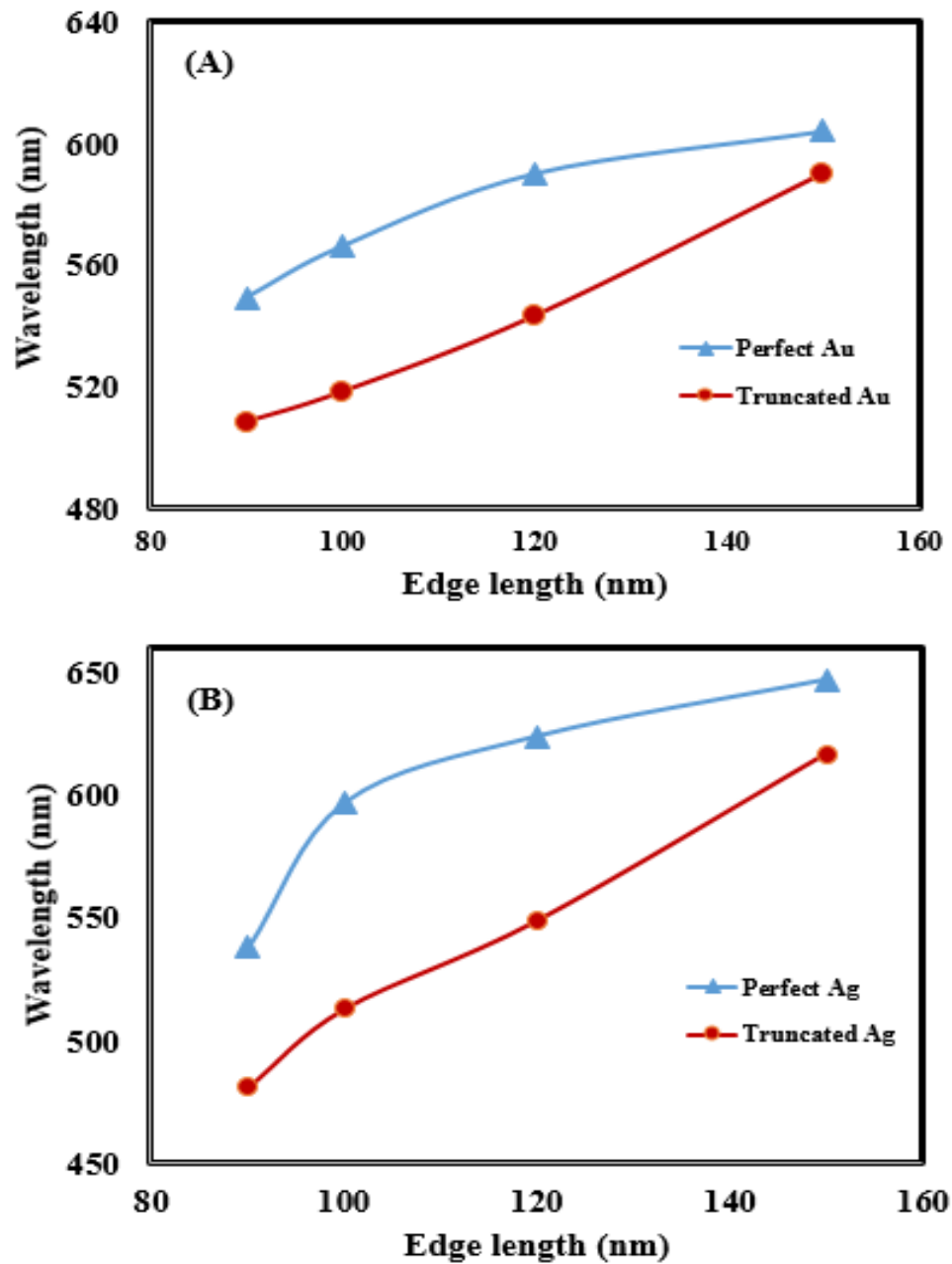


Figure 3. 5: Comparison of effect of edge length on dipole plasmon resonance of perfect and truncated nanoprisms of a) Ag b) Au

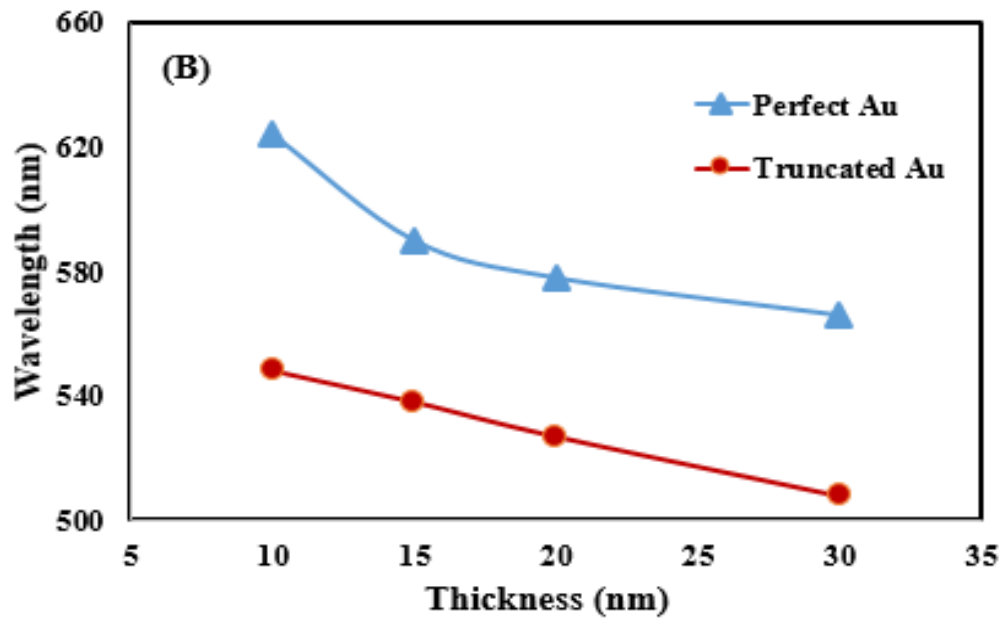
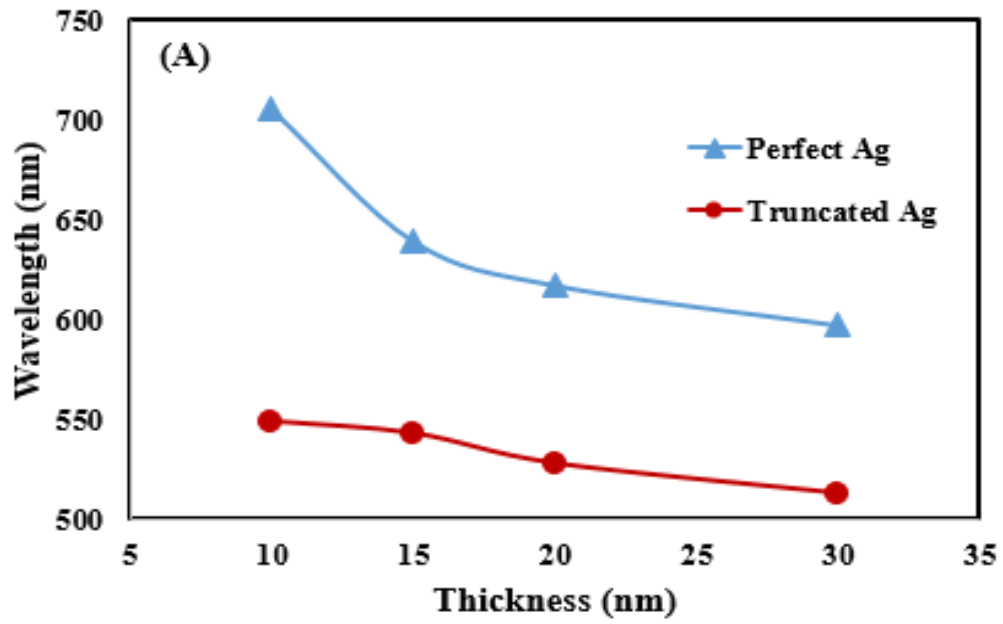


Figure 3. 6: Comparison of effect of thickness on dipole plasmon resonance of perfect and truncated nanoprisms of a) Ag b) Au

3.3 The effect of truncation of gold and silver:

Ag and Au triangular nanoprisms were investigated individually for various degree of truncation (TR) and observations were compared (Figure 3.7). TR, is defined as a/L where a is the depth of the truncation with respect to the edge of the nanoprisms (also called snip), and L is the edge length of the nanoprisms (100 nm) (i.e. $TR = a/L = 5/100 = 0.05$) as depicted in inset of the Figure 3.10 The TR values studied were 0, 0.05, 0.1, 0.2 and 0.25, which corresponds to the snips: $a = 0, 5, 10, 20$ and 25 nm, respectively for the edge length of 100 nm (Table 3.3). The plasmonic resonance of Ag and Au nanoprisms were presented in Figure 3.10. The perfect nanoprism with no truncation had dipole resonance peak at 579 nm (for Ag nanoprisms) and 566 nm (for Au nanoprisms). Introduction of snipping ($TR = 0.05$) to the nanoprisms causes a significant blue shift for the dipole plasmon resonance of both Au and Ag nanoprisms [251]. For Ag nanoprisms a 30nm blue shift in the plasmonic peak was observed which was from 579 nm ($TR = 0$) to 549 nm ($TR = 0.05$). Similarly for Au nanoprisms, a blue shift of 20 nm was observed i.e., from 566 nm ($TR = 0$) to 546 nm ($TR = 0.05$); which is a relatively smaller shift compared to Ag nanoprisms. This blue shift effect in the truncated nanoprisms occurs because the length of the quantum box for electron oscillation is smaller in the truncated nanoprisms (Figure 3.10A). In addition, the electron density in the corners of a nanoparticle plays an important role in determining the resonant wavelength [252] and this blue shift effect is partly attributed to the lower electronic density in the corners as

they are snipped away. The blue shift continued as the truncation of the corners of the nanoprisms become deeper for both Ag and Au nanoprisms

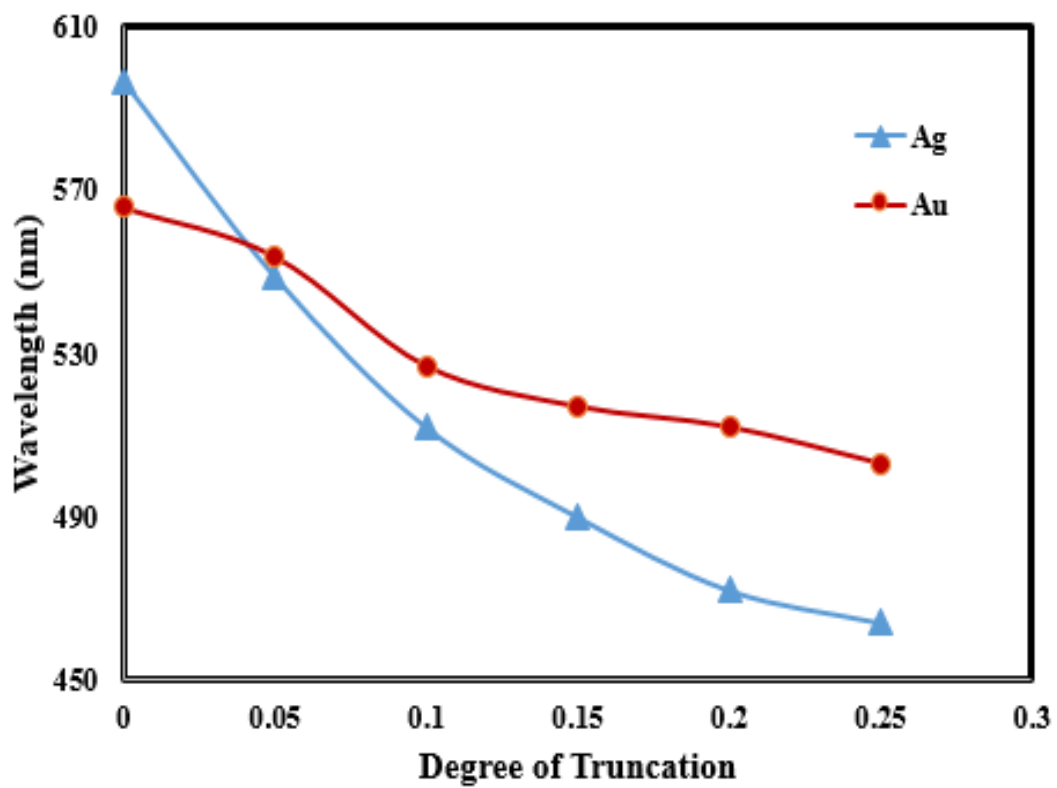


Figure 3.7. Comparison of Ag and Au triangular nanoprisms for change in dipole plasmon resonance with variation in degree of truncation.

Upon introduction of truncation, the strength of dipole plasmon resonance peak dropped significantly for both gold and silver (Figure 3.10B). This result is to be expected as by introducing the snip to the nanostructure, we have effectively removed the accumulation of free electrons at the corners which play an important role in supporting the plasmonic resonance causing a decrease in the strength of plasmonic oscillations (also known as the “lightning rod effect”) [253]. The strength of the signal kept dropping with increase in truncation for Ag nanoprisms. For Au nanoprism, the drop in strength of the dipole resonance peak was extended only until truncation of 0.1. Additional increase in truncation does not result in drop of the strength of the signal, instead, they fairly remained constant.

Initially, we studied the effect of various depths of truncation in an Ag nanoprism with only one truncated corner. Figure 3.8 is an illustration of the effects of various depths of corner truncations in the Ag nanoprism with edge length of 150 nm. Increasing the depth of corner truncation in the Ag nanoprism causes a plasmonic blue shift from 764 nm for the case of no truncation (TR=0) to 696 nm for the case of a truncation depth of 20 nm (TR= 0.13). Further the intensity of dipole plasmon resonance of untruncated triangular nanoprism is smaller than the truncated nanoprisms. The enhancement in the signal intensity of truncated nanoprisms might be due to “lightning rod effect”.

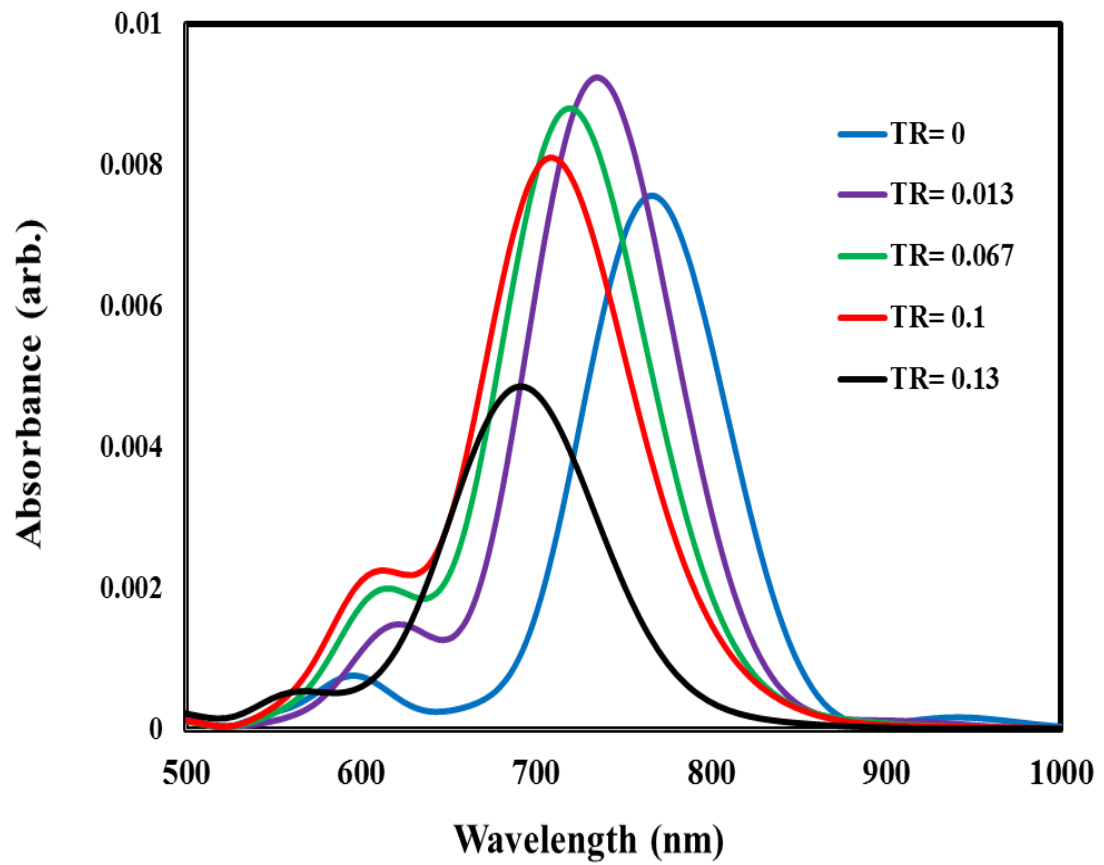


Figure 3.8. Effect of degree of truncation at only one vertex of Ag nanoprism on dipole plasmon resonance.

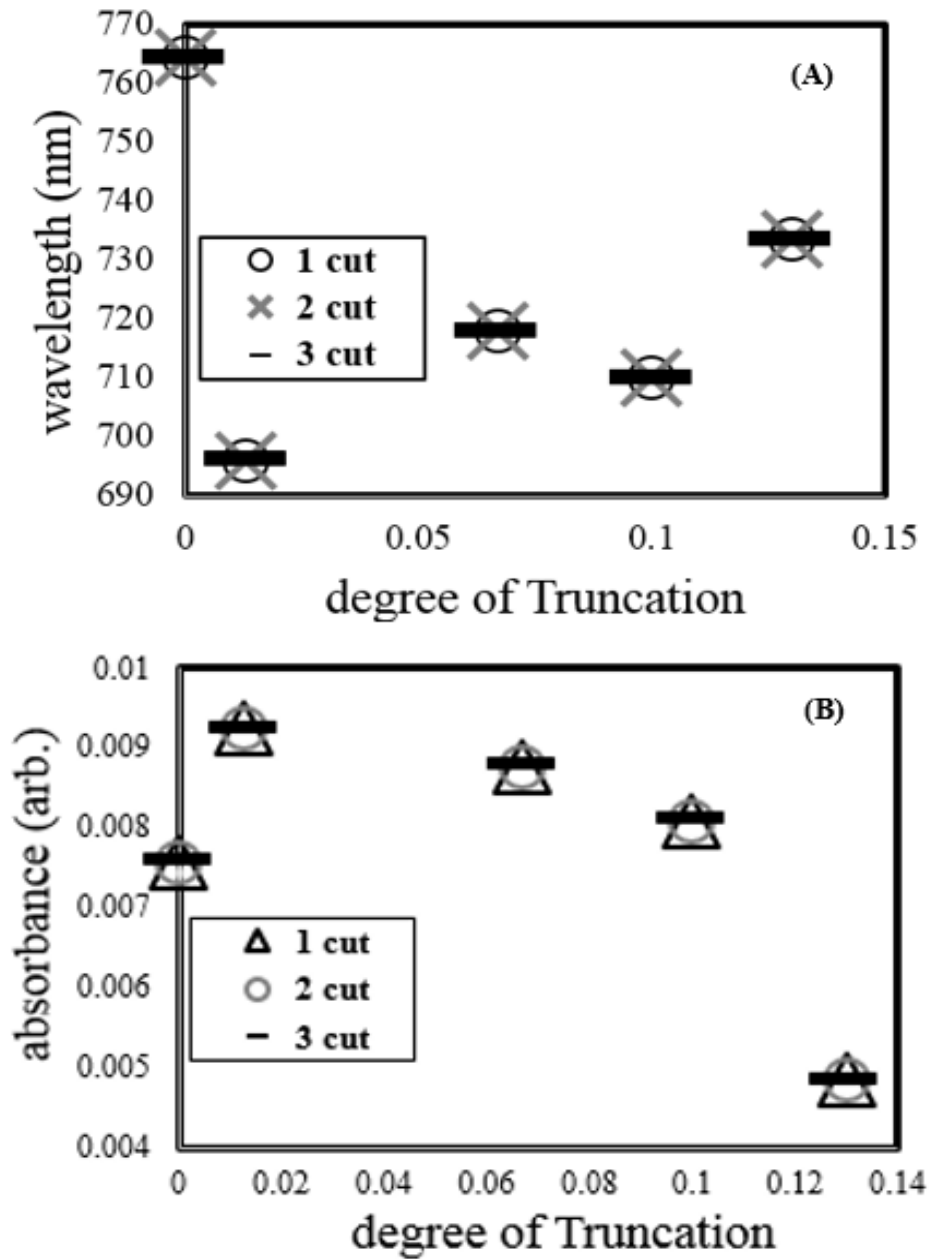


Figure 3.9. Plasmonic resonance of triangular Ag nanoprisms with truncation in one, two, and three vertices (A) wavelength position of the peaks. (B) absorbance strength of the peaks [251].

Next, we studied Ag triangular nanoprism with two and three truncated corners to determine the effect of the number of truncated corners on the plasmonic resonance shift and the strength of the plasmonic peaks. Ag nanoprisms were investigated for various TR values for one, two, or three truncated corners. These TR values were 0.05, 0.1, and 0.15, which corresponded to the snips: $a = 5, 10, \text{ and } 15 \text{ nm}$, respectively for a nanoprism with edge length of 150 nm. Figure 3.9A presents the absorbance of Ag nanoprisms with no truncated corners as well as truncated Ag nanoprisms with one, two or all three truncated corners with various degrees of truncation. Simulation results showed that removing one, two, or three tips of triangular nanoprism up to 15 nm of truncation depth has no effect on the position of the dipole plasmon peak (Figure 3.9A) or the strength of Ag nanoprisms (Figure 3.9B). It is important to note that the blue shifting of the resonant wavelengths continue as increase the depth of truncation. However, the resonance strength maximizes at $TR=0.02$ and drops as we increase the truncation depth.

The full width at half maximum (FWHM) for Ag and Au plasmonic peaks were measured for the TR values mentioned previously and tabulated in Table 3.4. The FWHM has decreased with increase in TR values for both Au and Ag resulting in narrower peaks.

Table 3.3: Effect of truncation on dipole plasmon resonance of triangular nanoprisms of Ag and Au

Degree of Truncation	Dipole Plasmon Resonance Maximum	
	Ag	Au
0	597	566
0.05	549	554
0.1	512	527
0.15	490	517
0.2	472	512
0.25	464	503

Table 3.4: Full Width Half Maximum of dipole plasmon resonance of truncated triangular nanoprisms of Ag and Au

Degree of Truncation	Full Width at Half Maximum (FWHM)	
	Ag (nm)	Au (nm)
0	48.35	53.54
0.05	47.06	44.27
0.1	45.59	42.54
0.2	43.38	41.26

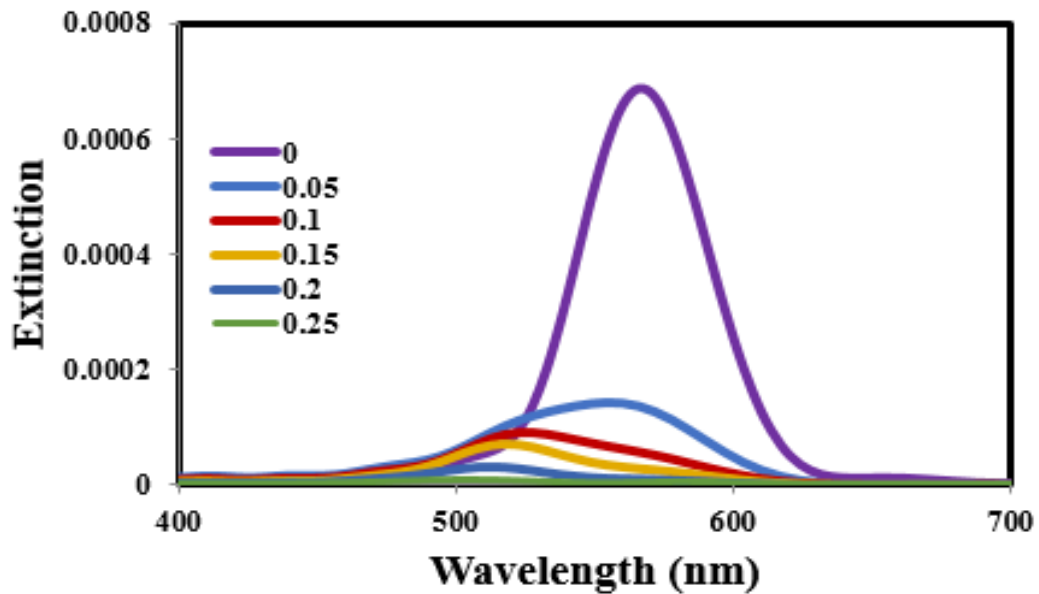
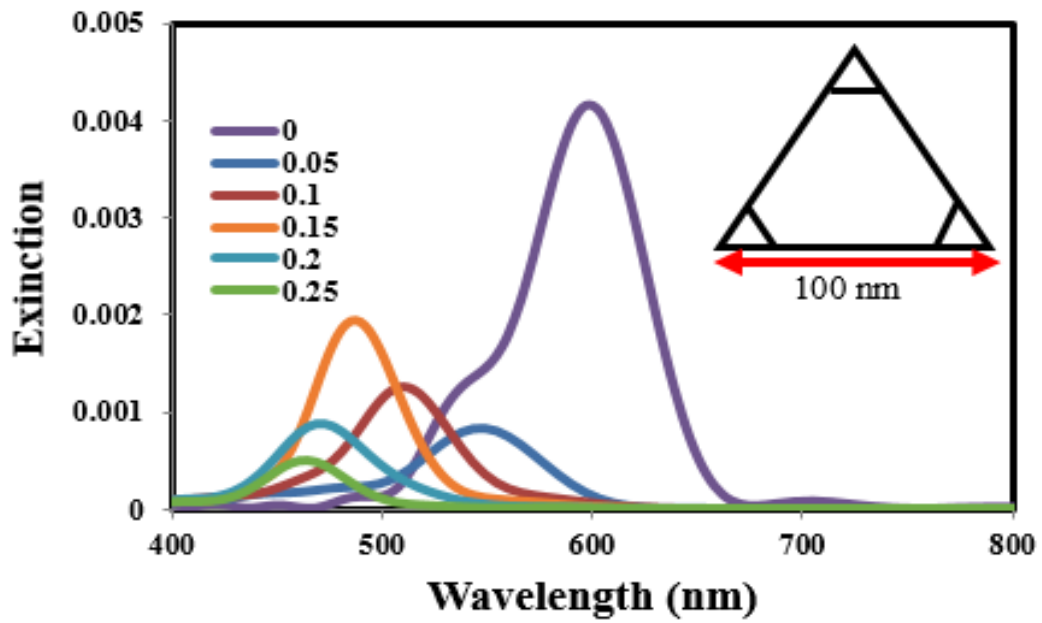


Figure 3.10 FDTD simulation results showing the plasmonic resonance of nanoprism that has thickness of 30 nm and edge length of 100 nm with different degrees of truncation for (A) Ag. (B) Au.

The plasmonic enhancements for Ag nanoprisms with and without truncation were investigated. In Figure 3.11 (a-b) is ideal triangular Ag nanoprism without truncation, while Figure 3.11 (c-d) a snip of 10 nm was introduced. For Figure 3.11(a-d) the thickness and edge length were 30 nm and 100 nm respectively. In Figure 3.11 a and c the incident light is perpendicular to the polarization plane, whereas, for Figure 3.11 b and d the incident light is parallel to the polarization place. The enhancement factor = $(|E|^2_{\text{in the presence of prism}})/(|E|^2_{\text{in the absence}})$ was found to be significantly higher in ideal triangular nanoprism than for the nanoprism with snipping. Further for both triangular nanoprisms with and without snipping, enhancement was very significant when incident light was perpendicular to the polarization plane than parallel to polarization plane. The enhancement factors calculated for the prisms in Figure 3.11 (a-d) are 4.75, 3.88, 1.92 and 0.8 respectively. The reason for higher plasmonic enhancement in triangular silver nanoprism without snipping was due to “lightning rod effect” as the edges are sharper in this case than the truncated nanoprism.

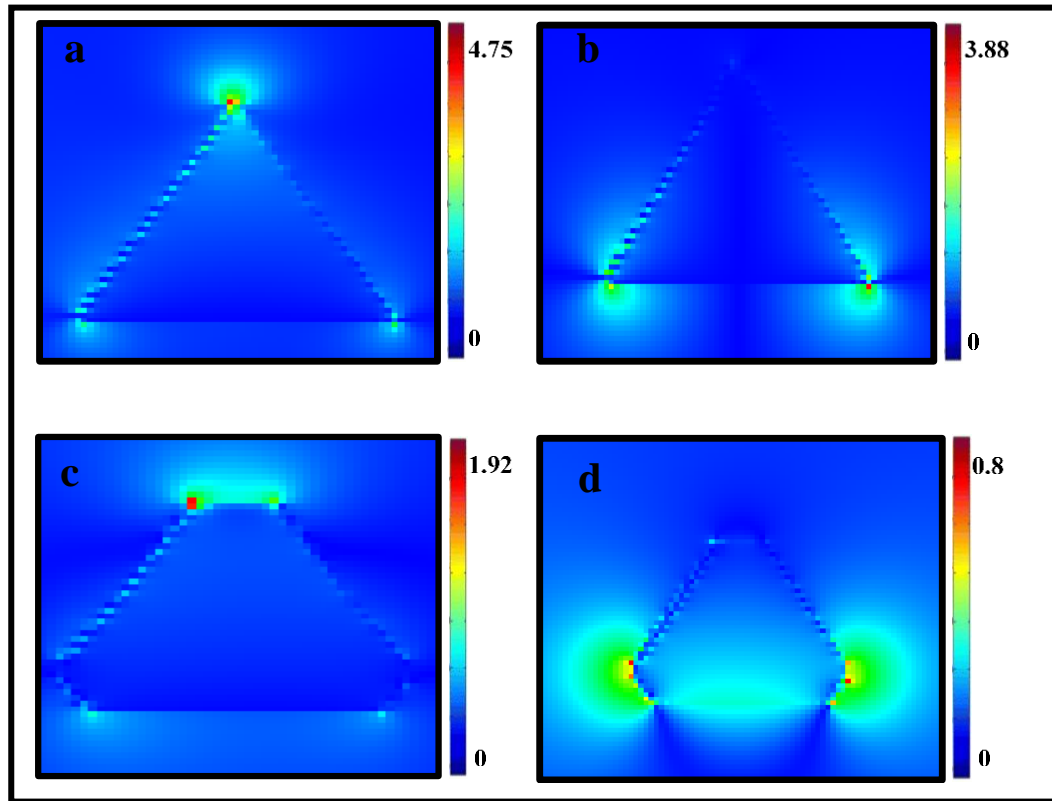


Figure 3.11 The plasmonic enhancement of Ag nanoprism without snipping (a and b) and truncated nanoprism (c and d) with snip of 10 nm. The edge length (100 nm) and thickness (30nm) were maintained constant in above figure (a – d).

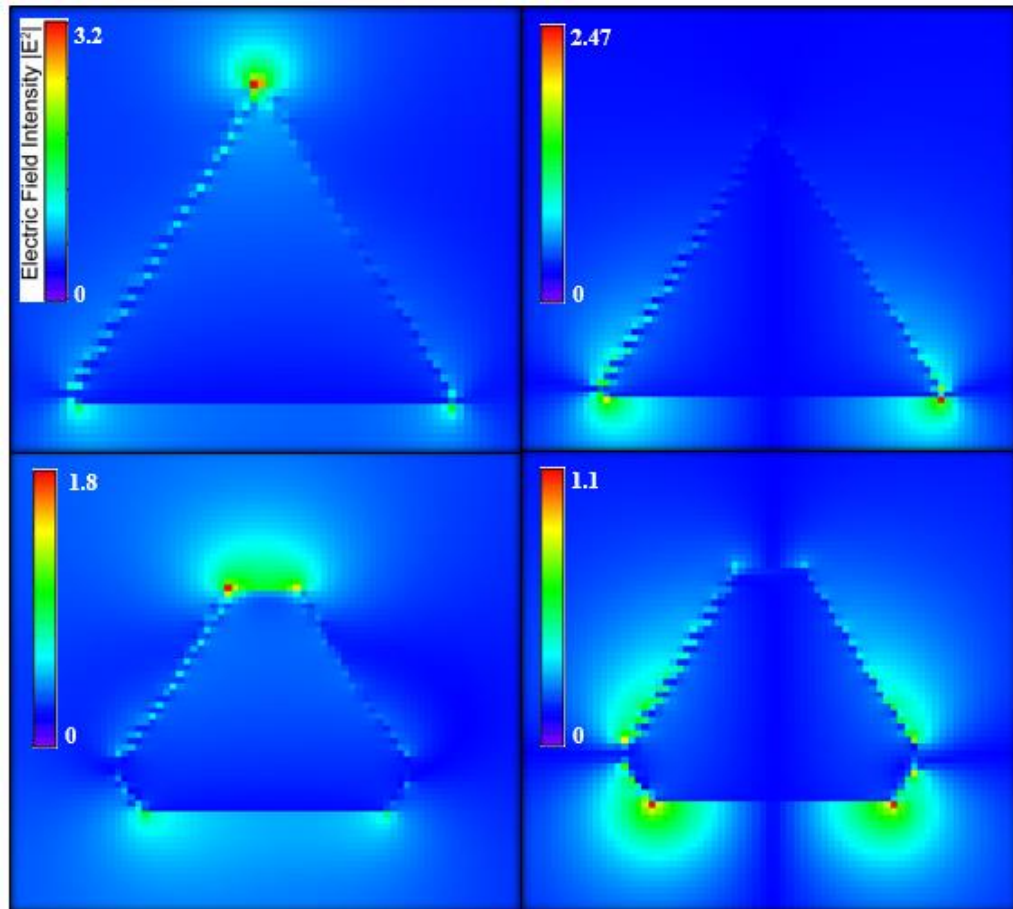


Figure 3.12 The plasmonic enhancement of Au nanoprism without snipping (a and b) and truncated nanoprism (c and d) with snip of 10 nm. The edge length (100 nm) and thickness (30nm) were maintained constant in above figure (a – d).

3.4 CONCLUSIONS

Finite-difference time-domain (FDTD) simulations, were performed on triangular nanoprisms of Au and Ag for perfect and truncated nanoprisms to understand the role of structural parameters such as edge length, thickness, and truncation. Increasing the edge length of triangular nanoprisms of Au and Ag truncated and non-truncated had introduced a red shift while, the increase in thickness had introduced a blue shift. The dipole plasmon resonance maximum occurred at lower wavelengths for Au gold nanoprisms than Ag. Similarly, the dipole plasmon resonance of truncated nanoprism occurred at lower wavelengths than the non-truncated prism. The strength of dipole plasmon resonance silver nanoprisms are higher than gold as it had least losses.

Chapter 4

The Effect of Truncation and Dielectric in Plasmonic Resonance of Hybrid Plasmonic Nanosandwich Structures in Optical Range

4.1 Introduction:

Since the days scientists found the strong absorption band of gold nanoparticle in the visible region, noble metal nanoparticles had been a great subject of investigation [32], [254], Thus observed strong absorption band of gold was explained by Mie through finding solutions for Maxwell's equations using suitable boundary settings. The material related functions found in Mie's theory are dielectric function of the metal and surrounding medium's dielectric constant. Surrounding medium also known as capping material, plays a crucial role in plasmonic properties exhibited by nanomaterials as it prevents aggregation prevailing during the synthesis conditions [255], [256], The absorption spectra of metal nanoparticles and its strength are intertwined with refractive index of the surroundings. Thus the sensitivity of nanoparticles to refractive index has opened new avenue of study called biosensors [257]–[259].

Metal nanoparticles coupled to target molecule receptors have surface plasmon properties shifted, curbed or enriched in presence of target molecules. The degree of

response by nanoparticles to target molecules depends on thickness of refractive index and sensitivity of dipole plasmon resonance to changes in bulk environment's refractive index. Several research groups are actively pursuing studies experimentally as well as theoretically to understand the surface plasmon resonance dependence to bulk and local refractive index and several reports were already published towards that direction [146], [260]–[262]. The general observation on articles published was, dipole plasmon resonance had a red shift with increase in refractive index for a range of nanoparticle shapes [263], [264]. Further, the magnitude of sensitivities depends on shape, size and composition of nanoparticles. Owing the reasons described in the introduction of the dissertation, we pursued the FDTD simulations to understand the effect of refractive index sensitivity in triangular nanoprisms of gold and silver. Effect of surrounding medium refractive medium and its impact on surface plasmon resonance are abundant [265], [266]. For single silver nanoparticles, the change in surface plasmon resonance were studied by addition and removal of oil surrounding it. The color of silver nanoparticles changed from blue to green with addition of oil indicating a red shift and the color were reverted to blue by removing the oil [267]. Van Duyne, studied the scattering of single silver nanoparticles dispersed in solvents such as ethanol, nitrogen, n-propanol, benzene and chloroform [268]. Increase in dielectric constant of medium produced a linear increase in red shift of dipole plasmon resonance maximum. In another study, gold nanoparticles with different shapes and surface modifications were studied.

Between spherical, triangular and rod-like particles, rods exhibited more sensitivity to surrounding medium and this observation was in direct correlation to aspect ratio of the material investigated.

Hybrid nanoprisms which take advantage of two different noble metals in their structures have become increasingly important as they can combine plasmonic dipole peaks associated with gold as well as silver, and thereby create additional dipole plasmonic peaks which have a higher intensity level. The additional peaks can provide a higher degree of control over the tunability of nanoprism resonance and can potentially be beneficial in various applications [178], [269]. With that in mind, in this paper, we introduce a simple hybrid nanoprism structure consisting of Au and Ag metallic nanoprisms layers separated by a dielectric layer.

4.2 The effect of dielectric:

The effect of adding a dielectric layer to either Ag or Au metal layers on dipole plasmon resonance was investigated. Addition of dielectric layer to Au or Ag metal layers facilitates the shift of dipole plasmonic resonant peak even further and tune the plasmonic properties of the nanoprisms at will. Ag nanoprism with edge length of 100 nm and thicknesses of 30 nm were chosen for investigation to understand the role of dielectric. The thickness of the dielectric layer was varied between 10 nm and 60 nm. For each dielectric thickness, refractive index values from 1 to 3 were thoroughly analyzed.

Table 4.1: Summary of results investigated for effect of dielectric thickness for various refractive indices on dipole plasmon resonance

Refractive index	Dipole plasmon resonance maximum of Ag dielectric sandwich for thickness (nm)				
	10	30	50	70	90
1	610	610	610	610	610
1.5	632	654	662	662	662
2	646	670	679	679	679
2.5	687	724	733	743	743
3	705	786	809	812	812

Table 4.2: Summary of results investigated for effect of dielectric thickness for various refractive indices on dipole plasmon resonance

Refractive index	Dipole plasmon resonance maximum of Au dielectric sandwich for thickness (nm)				
	10	30	50	70	90
1	572	572	572	572	572
1.5	590	597	603	603	603
2	604	610	617	624	624
2.5	624	638	646	654	654
3	639	670	678	687	687

Silver nanoprism coupled with dielectric thickness of 10 nm, the dipole plasmon resonance maximum of the sandwich had a red shift when refractive index changed from 1 to 3 (Figure 4.1). Summary of results were presented in Table 4.1 and Figure 4.3. For refractive index value of 1, 1.5, 2, 2.5 and 3 nm the dipole plasmon resonance maximum was 610, 632, 660, 687, and 705 nm respectively. Similar red shift was observed for dielectric thickness of 30, 50, 70, and 90 nm respectively. For refractive index of 1, no change in dipole plasmon resonance wavelength was observed when thickness changed 10 nm to 90 nm. However, for the refractive index of 1.5, 2, 2.5, and 3 dipole plasmon resonance maximum found a red shift with increase in thickness of dielectric. Interestingly, the magnitude of red shift has increased with increase in the refractive index for the thickness of dielectric investigated. Thus, the magnitude of dipole plasmon resonance shift for the refractive indices of 1, 1.5, 2, 2.5 and 3 are 0, 30, 33, 56 and 107 nm respectively for the variation of dielectric thickness. Additionally, the observed red shift for a given refractive index was observed only for variation in thickness of dielectric from 10 nm to 50 nm only. For all the refractive indices investigated, when dielectric thickness changed from 50 nm to 90 nm, the wavelength of dipole plasmon resonance remained constant. Further, for a nanoprism with similar dimensions and refractive index of 1.5 without the dielectric had dipole plasmon resonance maximum at lower wavelength than the nanoprism with dielectric. Similar to the observations made for Ag,

Au nanoprism also exhibited exactly the same trend for change in dielectric thickness with respect to refractive index (Figure 4.2). The results are summarized in Table 4.2 and Figure 4.3. The only difference observed was, the magnitude of red shift was relatively lower for Au than Ag (Figure 4.4).

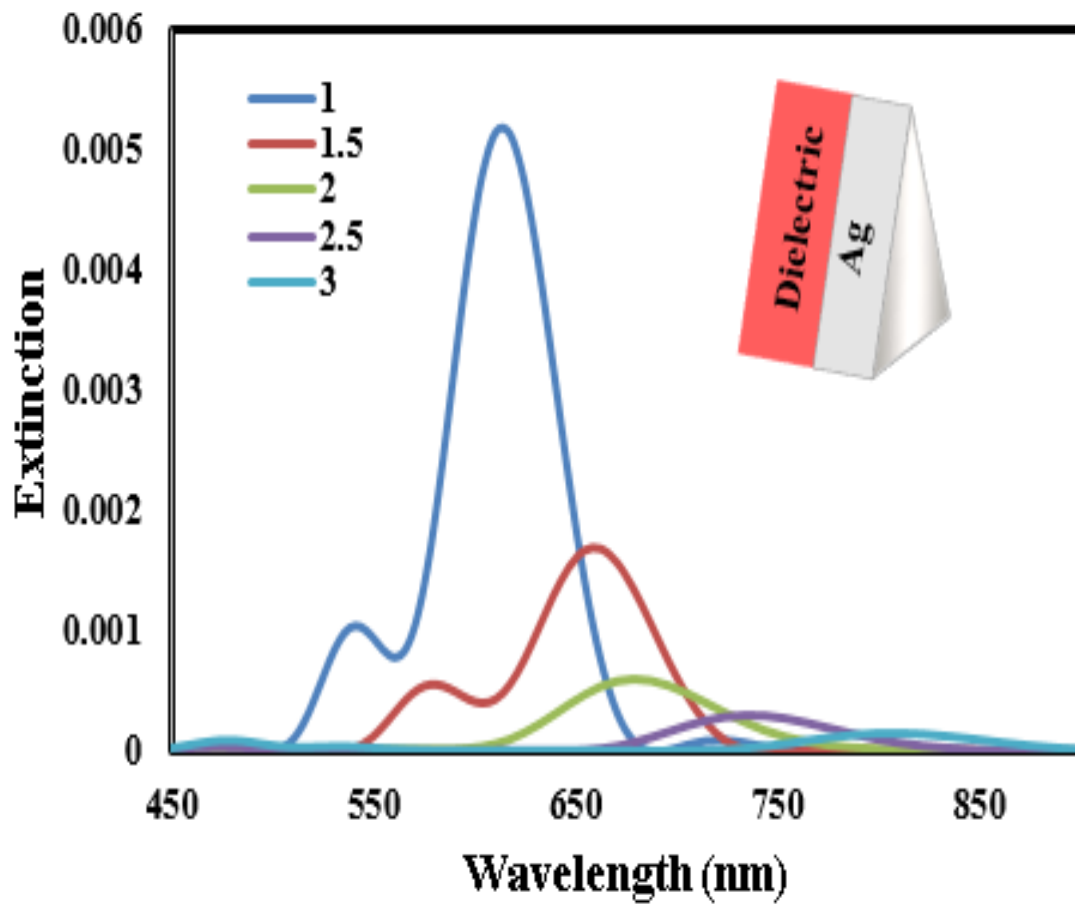


Figure 4.1 FDTD simulation results showing the absorbance spectra of Ag nanosandwich structures with edge length of 100 nm and thickness 30 nm. This figure of for dielectric thickness of 50 nm.

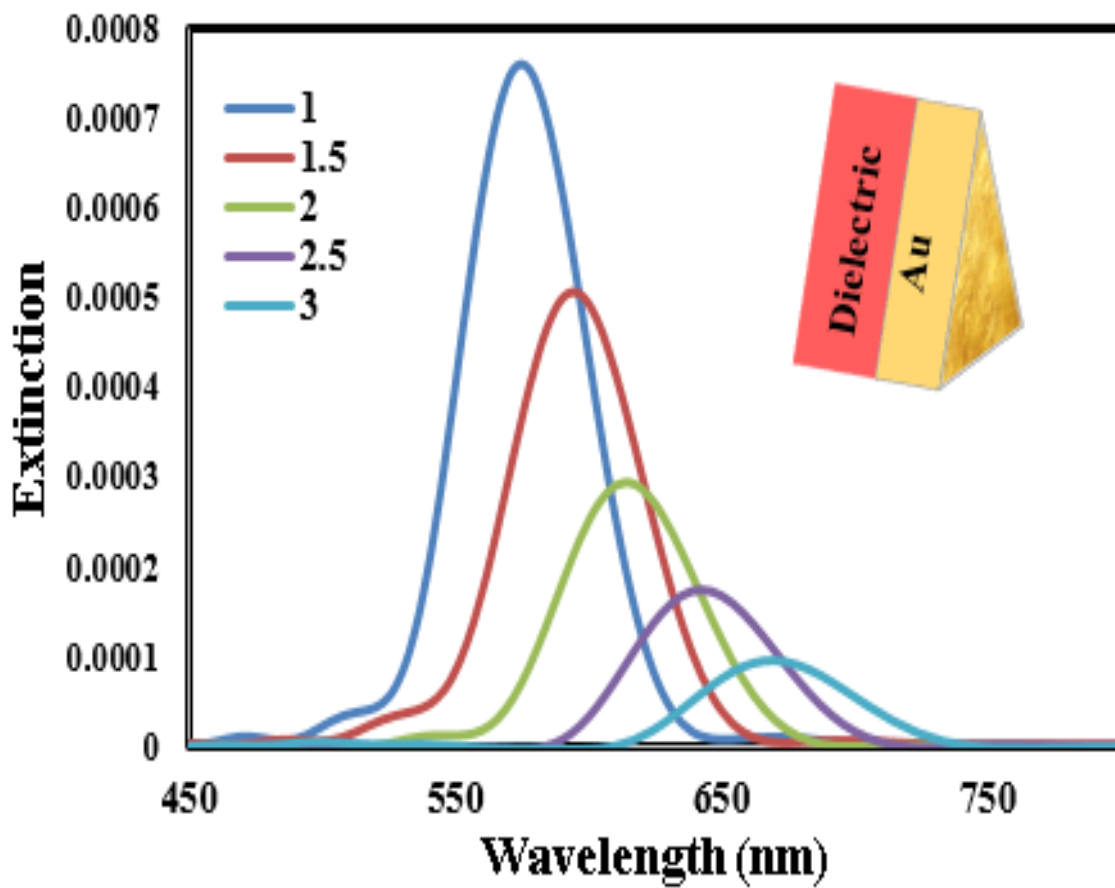


Figure 4.2 FDTD simulation results showing the absorbance spectra of Au nanosandwich structures with edge length of 100 nm and thickness 30 nm. This figure of for dielectric thickness of 50 nm.

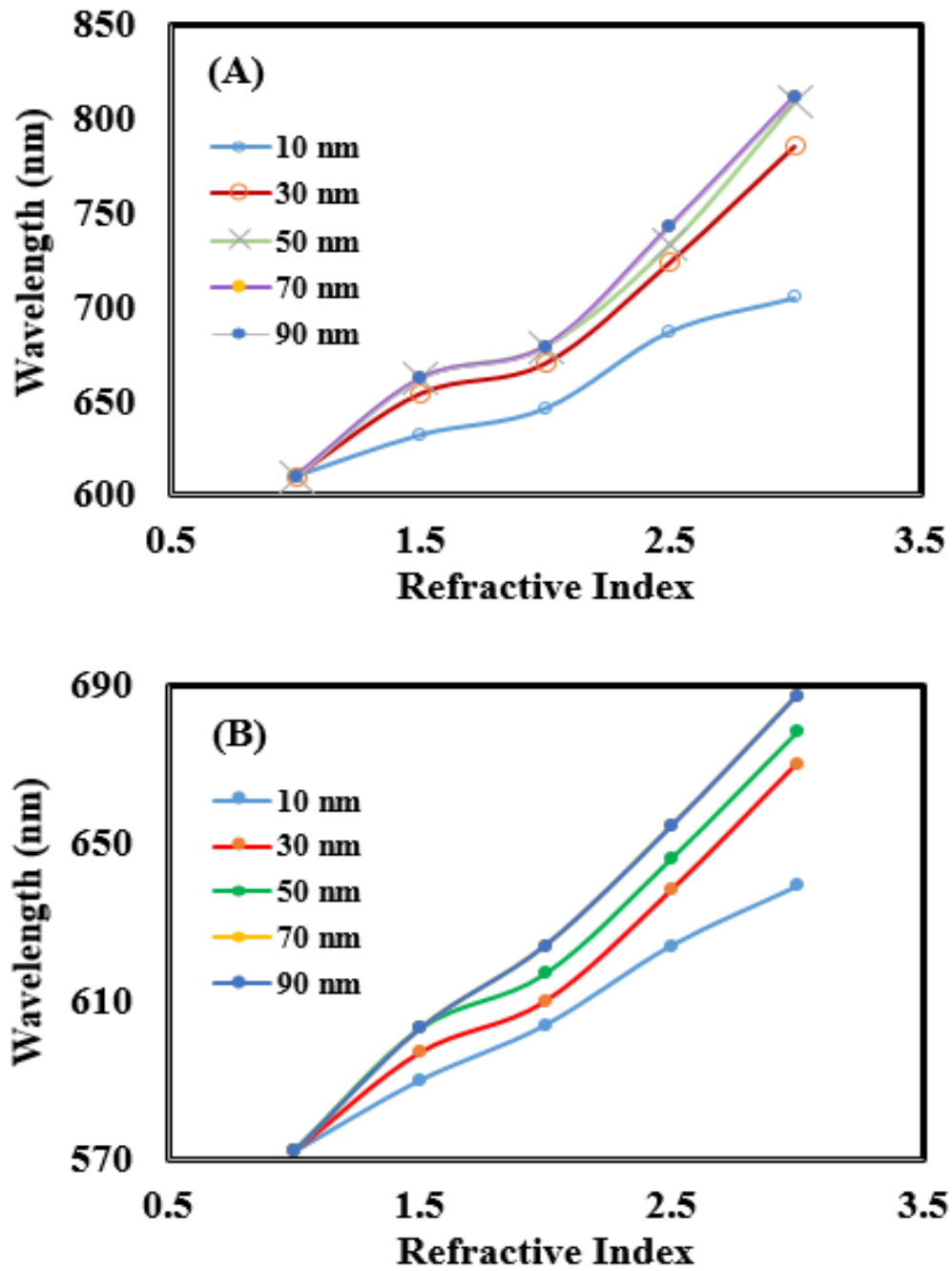


Figure 4.3: Effect of refractive index on dipole plasmon resonance maximum for various thicknesses of dielectric of a) Ag b) Au

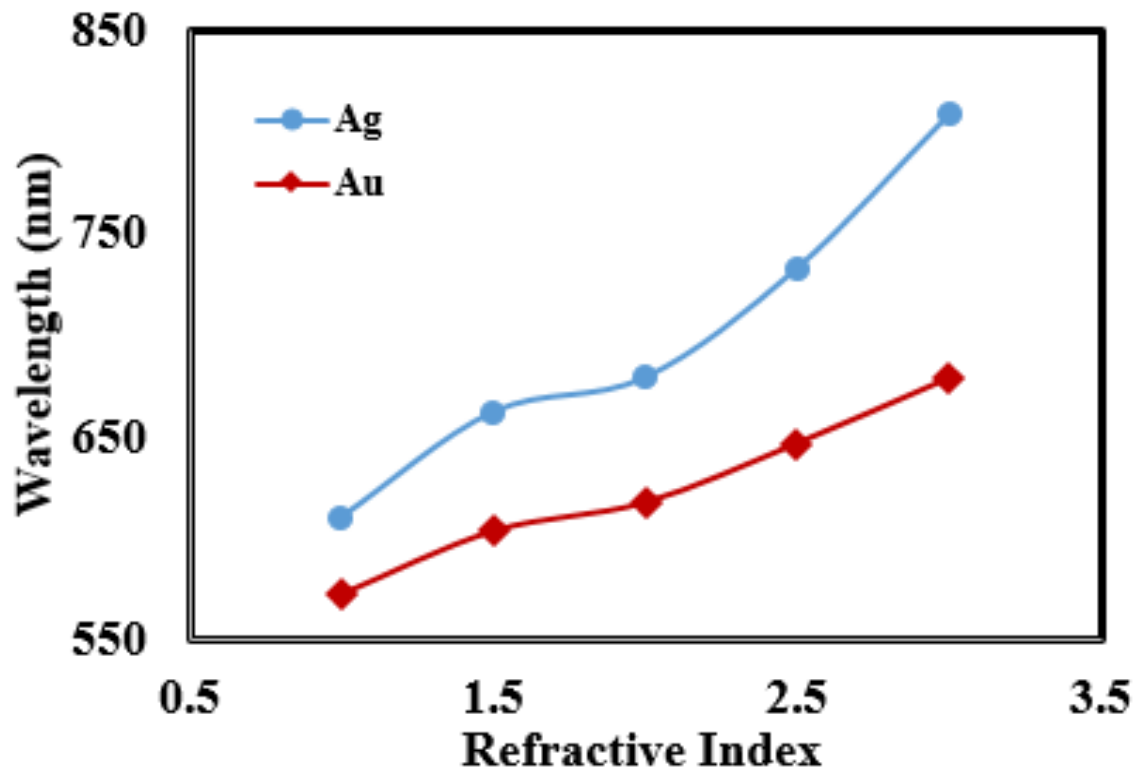


Figure 4.4: Comparison of dipole resonance maximum for Ag and Au towards change in dielectric medium with thickness of 30 nm.

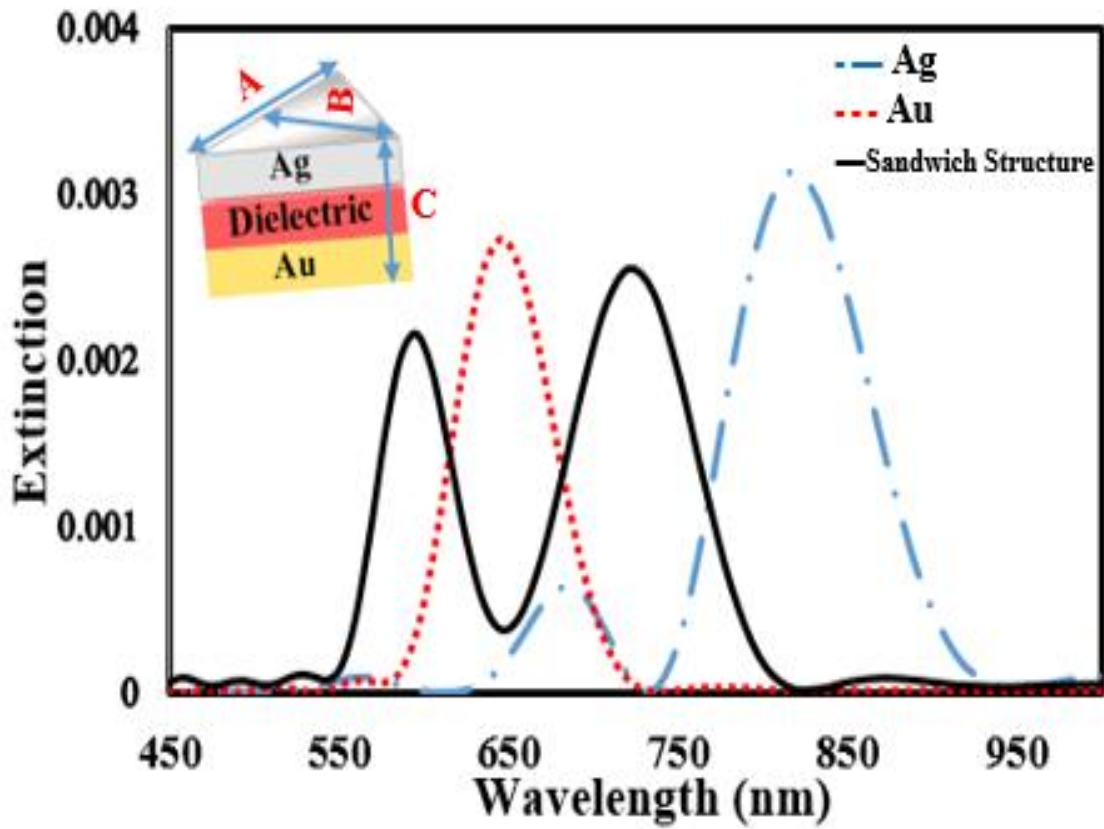


Figure 4.5. FDTD Simulation results showing the plasmonic resonance of Au and Ag nanoprism with edge length of 100 nm and thickness of 30 nm and FDTD Simulation results showing the plasmonic resonance of an Au- dielectric-Ag nanoprism with edge length of 100 nm and thickness of 30 nm for all layers. (solid black line), (A: edge length, B: height, and C: thickness) .

The hybrid nano-sandwich structure studied in this paper consists of three material layers namely a silver layer, a dielectric separating layer, and a gold layer (Figure 4.5, inset). As described above, plasmonic properties of the nanoprisms strongly depend on their shape and size as well as their material properties. To show the advantage of using a three-layered nanoprism, we have constructed the triangular nanoprism as explained above using OptiFDTD software. A single layer of Au or Ag nanoprism can only support a single dipole plasmonic resonance. This resonant peak occurs at ~646 nm for an Au nanoprism with an edge length of 100 nm and a thickness of 30 nm while it occurs at ~815 nm for an Ag nanoprism of the same size and shape (Figure 4.5). In contrast, a hybrid nanoprism made with a layer of Au and a layer of Ag in addition to a silica separating dielectric layer of 30 nm thick can support two dipole plasmonic peaks as illustrated in Figure 4.5.

4.3 Ag-dielectric-Au Sandwich:

Bi-metallic triangular nanosandwich was constructed with Au and Ag using silica as dielectric layer with an aim to extend the scope of investigation beyond individual metallic triangular nanoprisms for tuning the plasmonic properties. Tuning the plasmonic properties of triangular nanoprism sandwiches helps us to tailor materials for need based specific applications. The edge length of dielectric and metal was chosen 100 nm and thickness of Ag and Au 30 nm. The thickness of dielectric layer was changed between 5 nm to 100 nm.

The reason for adding dielectric between Ag and Au is to enhance tunability of the sandwich structure. The plasmonic peak of the entire structure can be tweaked just by changing the thickness of the dielectric separating layer [270].

As previously stated, the advantage of constructing an Ag-dielectric-Au sandwich structure is the ability to tune the wavelength of the two plasmonic peaks in addition to the relative strength of the two peaks with respect to each other.

The hybrid Ag-dielectric-Au nanoprism sandwich was constructed with edge length of 100 nm for Au, Ag and dielectric and thickness of Ag and Au are 30 nm in the simulation study is a structure as described above. The refractive index of the dielectric layer was 1.5.

The findings of the simulation study for the above constructed sandwich as follows: as the thickness of dielectric layer changed in the sandwich nanoprism structure,

the strength of the two plasmonic peaks with respect to each other changed as well. For the sandwich structure, with a dielectric layer of 5 nm thickness, the plasmonic peak due to Ag is much stronger than the plasmonic peak due to Au (Figure 4.6A). However, when the thickness of the dielectric layer increased from 5 nm to 20 nm dipole plasmon resonance peak of Au increased significantly, yet the intensity of Ag nanoprisms was stronger relatively. When the thickness of the dielectric layer was further increased to 30 nm, the strength of the peaks due to Ag and Au became almost equal. Further increase in the dielectric layer thickness to 60 nm and 100 nm caused the dipole resonant peak due to Au become more intense in comparison with the Ag peak (Figure 4.6A). The intensities of dipole plasmon resonance peak of Ag and Au for perfect and truncated sandwich was presented in It is very evident that dipole plasmon resonance of Ag is always more intense than Au due to less radiative losses. However, for the dielectric thickness of 60 nm and 100 nm the dipole plasmon resonance peak of Au was observed to be more intense than Ag. This observation requires further investigation.

Next, truncation was introduced to the nanosandwich structure. The degree of truncation of the nanosandwich structure was chosen as

$$T = \frac{a}{L} = \frac{10 \text{ nm}}{100 \text{ nm}} = 0.1$$

The edge length of the nanosandwich is fixed at 100 nm. Our simulation results indicate that both Au and Ag plasmonic peaks in the sandwich structure experienced a blue shift

upon introduction of truncation (Figure 4.6B). This is consistent with our previous observations made for the truncated standalone Au and Ag nanoprisms. Further we have observed a reduction in the distance between the two peaks in the truncated nanosandwich structure. This reduction is due to the fact that Ag plasmonic peak which is located at longer wavelengths, generally experiences a larger blue shift compared to the Au plasmonic peak as truncation is introduced to the structure causing the distance between the two peaks to decrease. The blue shift of two plasmonic peaks bring both Au and Ag peaks of the nanosandwich structure within the visible range which is ideal for many biological, medical and electronic applications. Further, similar to the single metal layer nanoprism, introduction of truncation to the nanosandwich structure causes a narrowing in the FWHM of the plasmonic peaks. This narrowing is due to the fact that shortening the edge length of the structure reduces the number of resonances supported by the structure at each length causing a narrowing the range of resonance energies. Additionally, we have two peaks in the sandwich structures we constructed. The advantage of having two plasmonic peaks will help us to design materials that are capable of sensing multiple analytes. Further the applications of these sandwich structures can be used in up conversion of phosphors and plasmonic enhancement of fluorescent materials. For fluorescent materials, one peak enhances the emission rate and other one enhances the absorption rate. Interestingly, having two peaks avoids the use of mixture of triangular nanoprisms with different edge lengths to sense two different analytes. Further,

for analysis that involves triangular nanoprisms in closer proximity, might pose a challenge. Those challenges are well addressed via sandwich structures.

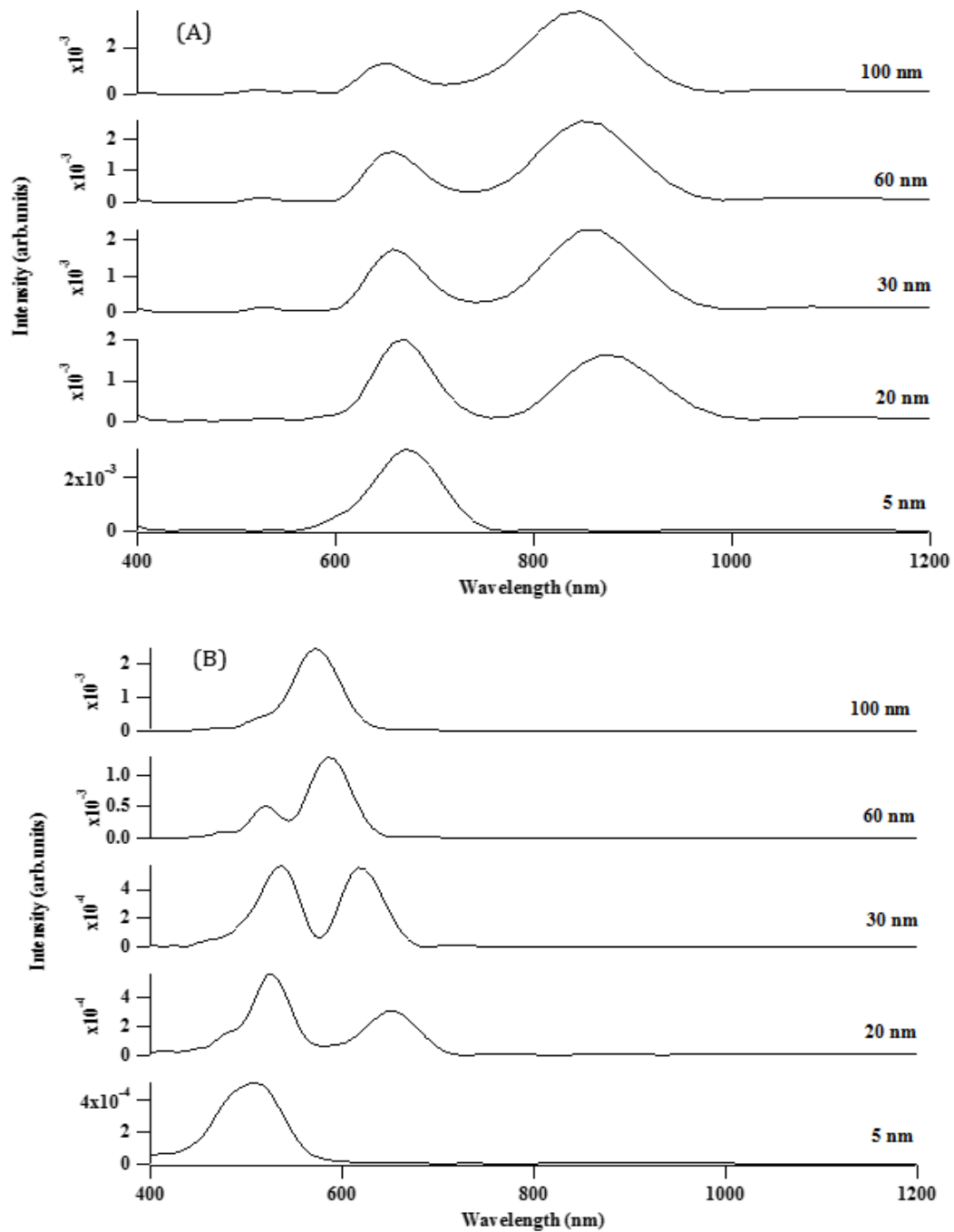


Figure 4.6 (a) FDTD simulation results showing the absorbance of sandwich structure (Au/dielectric/Ag) (a) without truncation and (b) with $TR = 0.1$ (First peak is corresponding to Au & Second peak is corresponding to Ag) [271].

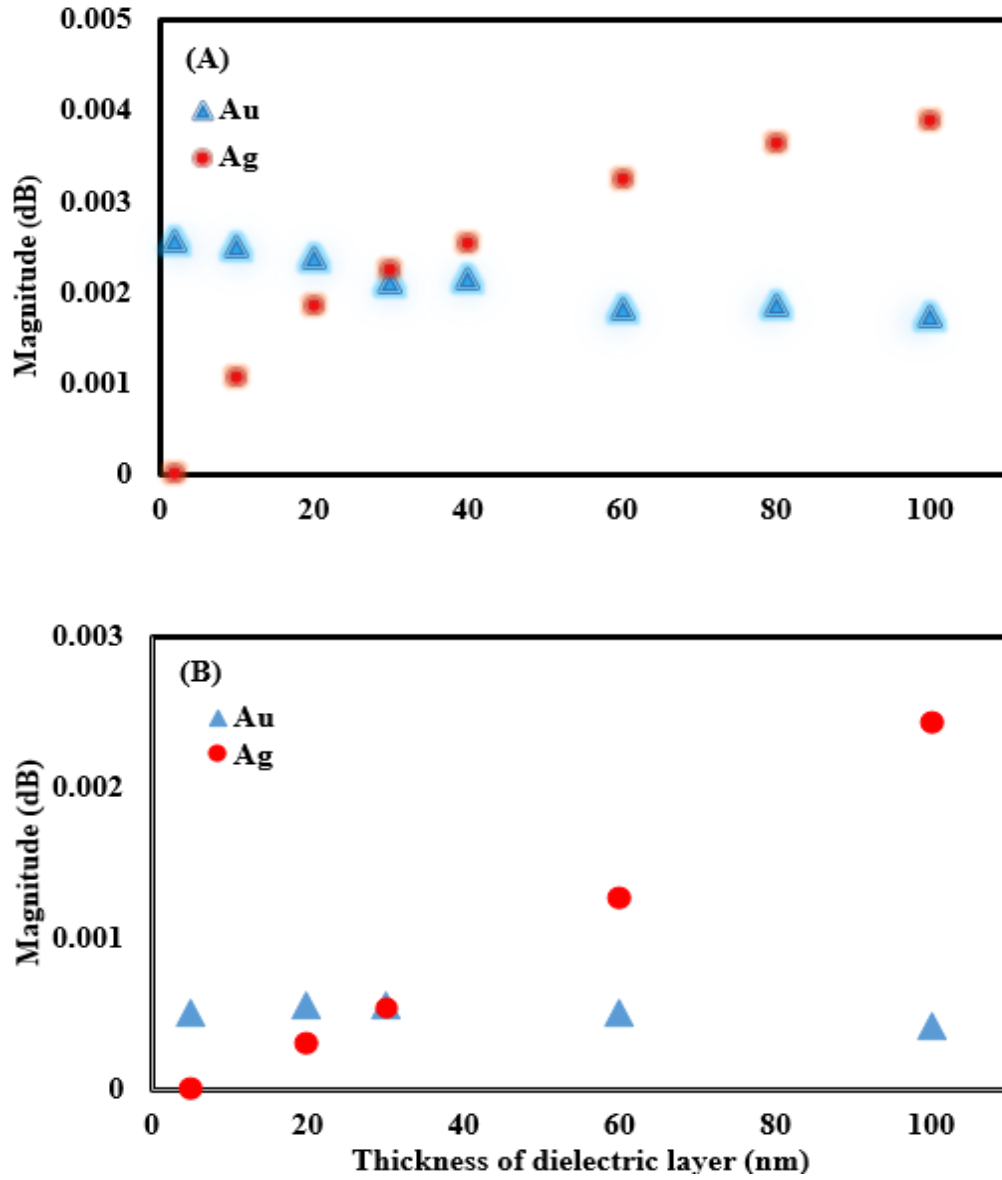


Figure 4.7: Relationship between the magnitude of Ag and Au peaks and varying thickness of dielectric layer (nm) (A) Perfect sandwich structure and (B) Truncated sandwich structure

4.4 Conclusion:

In this chapter, we have investigated effect of dielectric on dipole plasmon resonance when coupled with Au and Ag. Addition of dielectric has increased the wavelength at which dipole plasmon resonance occurs. Further, when the thickness of dielectric layer was increased red shift was observed. Additionally, the magnitude of red shift was increased with increase in refractive index medium. Next we constructed the hybrid nanoprism structures truncated and non-truncated exhibited two dipole plasmonic peaks in the visible frequency range which can be tuned by changing the thickness of the dielectric layer which effects both the strength of each of the peak as well as the wavelength position of the peak. Our simulations show high level of control on the tunability of these parameters which can be beneficial in various applications.

Chapter 5

Conclusions and Future Work

In this thesis, we have presented state of the art techniques available to synthesize anisotropic triangular nanoprisms. Further we have constructed the triangular nanoprisms of gold and silver and studied the effect of structural parameters such as edge length, thickness, truncation and dielectric on plasmonic properties using FDTD simulations. FDTD simulations revealed that increasing the edge length of both Au and Ag nanoprisms introduced a red shift, while increasing the thickness introduced a blue shift, it was conversely noted that the dipole plasmon resonance maximum occurred at lower wavelengths for Au than for Ag. Similarly, the dipole plasmon resonance of the truncated nanoprisms occurred at lower wavelengths than for the non-truncated nanoprisms. Furthermore, the strength of the dipole plasmon resonance of the Ag nanoprisms was higher than for the Au nanoprisms, as Ag showed the least losses.

The addition of dielectric increased the wavelength at which dipole plasmon resonance occurred. When the thickness of the dielectric layer was increased, a red shift was observed. It was also noted that the magnitude of the red shift was increased with a corresponding increase in the refractive index medium. Finally, we constructed the hybrid nanoprism structures, truncated and non-truncated. This study exhibited two

dipole plasmonic peaks in the visible frequency range that could be tuned by changing the thickness of the dielectric layer. This change affected both the strength of each peak as well as the wavelength position of the peak. This investigation showed a high level of control on the tunability of the established parameters that can be useful in various applications. The preliminary results we obtained through FDTD simulations will encourage future researchers to construct triangular nanoprism sandwich structures to take advantage of all the surface plasmon features we observed.

While the results from FDTD simulations are very promising and motivating to investigate it experimentally, it would be appropriate to remember that FDTD requires that the entire computational domain be gridded, and the grid spatial discretization must be sufficiently fine to resolve both the smallest electromagnetic wavelength and the smallest geometrical feature in the model, very large computational domains can be developed, which results in very long solution times. Models with long, thin features, (like wires) are difficult to model in FDTD because of the excessively large computational domain required.

References

- [1] D. N. Adrian Huber, Salvatore Demartis, “The use of biosensor technology for the engineering of antibodies and enzymes,” *J. Mol. Recognit.*, vol. 12, no. 3, pp. 198–216, 1999.
- [2] M. N. Weiss, R. Srivastava, H. Groger, P. Lo, and S.-F. Luo, “A theoretical investigation of environmental monitoring using surface plasmon resonance waveguide sensors,” *Sensors Actuators A Phys.*, vol. 51, no. 2–3, pp. 211–217, Nov. 1995.
- [3] D. SHANKARAN, K. GOBI, and N. MIURA, “Recent advancements in surface plasmon resonance immunosensors for detection of small molecules of biomedical, food and environmental interest,” *Sensors Actuators B Chem.*, vol. 121, no. 1, pp. 158–177, Jan. 2007.
- [4] J. Homola, *Surface Plasmon Resonance Based Sensors*, vol. 4. Berlin, Heidelberg: Springer Berlin Heidelberg, 2006.
- [5] J. Homola, “Surface Plasmon Resonance Sensors for Detection of Chemical and Biological Species,” *Chem. Rev.*, vol. 108, no. 2, pp. 462–493, Feb. 2008.
- [6] G. G. Nenninger, M. Piliarik, and J. Homola, “Data analysis for optical sensors based on spectroscopy of surface plasmons,” *Meas. Sci. Technol.*, vol. 13, no. 12, pp. 2038–2046, Dec. 2002.
- [7] R. Karlsson and A. Fält, “Experimental design for kinetic analysis of protein-protein interactions with surface plasmon resonance biosensors,” *J. Immunol. Methods*, vol. 200, no. 1–2, pp. 121–133, Jan. 1997.
- [8] J. Dostálek and J. Homola, “Surface plasmon resonance sensor based on an array of diffraction gratings for highly parallelized observation of biomolecular interactions,” *Sensors Actuators B Chem.*, vol. 129, no. 1, pp. 303–310, Jan. 2008.
- [9] J. T. Hastings, J. Guo, P. D. Keathley, P. B. Kumaresh, Y. Wei, S. Law, and L. G. Bachas, “Optimal self-referenced sensing using long- and short- range surface plasmons,” *Opt. Express*, vol. 15, no. 26, p. 17661, 2007.
- [10] U. Kreibig and M. Vollmer, *Optical Properties of Metal Clusters*. Springer

Science & Business Media, 2013.

- [11] P. K. Jain, K. S. Lee, I. H. El-Sayed, and M. A. El-Sayed, “Calculated Absorption and Scattering Properties of Gold Nanoparticles of Different Size, Shape, and Composition: Applications in Biological Imaging and Biomedicine,” *J. Phys. Chem. B*, vol. 110, no. 14, pp. 7238–7248, Apr. 2006.
- [12] M. A. van Dijk, M. Lippitz, and M. Orrit, “Far-Field Optical Microscopy of Single Metal Nanoparticles,” *Acc. Chem. Res.*, vol. 38, no. 7, pp. 594–601, Jul. 2005.
- [13] L. R. Hirsch, R. J. Stafford, J. A. Bankson, S. R. Sershen, B. Rivera, R. E. Price, J. D. Hazle, N. J. Halas, and J. L. West, “Nanoshell-mediated near-infrared thermal therapy of tumors under magnetic resonance guidance,” *Proc. Natl. Acad. Sci.*, vol. 100, no. 23, pp. 13549–13554, Nov. 2003.
- [14] I. H. El-Sayed, X. Huang, and M. A. El-Sayed, “Surface Plasmon Resonance Scattering and Absorption of anti-EGFR Antibody Conjugated Gold Nanoparticles in Cancer Diagnostics: Applications in Oral Cancer,” *Nano Lett.*, vol. 5, no. 5, pp. 829–834, May 2005.
- [15] I. ELSAYED, X. HUANG, and M. ELSAYED, “Selective laser photo-thermal therapy of epithelial carcinoma using anti-EGFR antibody conjugated gold nanoparticles,” *Cancer Lett.*, vol. 239, no. 1, pp. 129–135, Jul. 2006.
- [16] C. Loo, A. Lowery, N. Halas, J. West, and R. Drezek, “Immunotargeted Nanoshells for Integrated Cancer Imaging and Therapy,” *Nano Lett.*, vol. 5, no. 4, pp. 709–711, Apr. 2005.
- [17] K. M. Mayer and J. H. Hafner, “Localized surface plasmon resonance sensors,” *Chem. Rev.*, vol. 111, no. 6, pp. 3828–3857, 2011.
- [18] F. Tam, C. Moran, and N. Halas, “Geometrical Parameters Controlling Sensitivity of Nanoshell Plasmon Resonances to Changes in Dielectric Environment,” *J. Phys. Chem. B*, vol. 108, no. 45, pp. 17290–17294, Nov. 2004.
- [19] S. Link, Z. L. Wang, and M. A. El-Sayed, “Alloy Formation of Gold–Silver Nanoparticles and the Dependence of the Plasmon Absorption on Their Composition,” *J. Phys. Chem. B*, vol. 103, no. 18, pp. 3529–3533, May 1999.
- [20] G. Raschke, S. Brogl, A. S. Susha, A. L. Rogach, T. A. Klar, J. Feldmann, B. Fieres, N. Petkov, T. Bein, A. Nichtl, and K. Kürzinger, “Gold Nanoshells Improve Single Nanoparticle Molecular Sensors,” *Nano Lett.*, vol. 4, no. 10, pp. 1853–1857, Oct. 2004.
- [21] D. Compton, L. Comish, and E. van der Lingen, “The third order nonlinear optical properties of gold nanoparticles in glasses, part I,” *Gold Bull.*, vol. 36, no. 10–16, pp. 51–58, 2003.

- [22] K. Kalishwaralal, V. Deepak, S. Ram Kumar Pandian, M. Kottaisamy, S. BarathManiKanth, B. Kartikeyan, and S. Gurunathan, "Biosynthesis of silver and gold nanoparticles using *Brevibacterium casei*," *Colloids Surfaces B Biointerfaces*, vol. 77, no. 2, pp. 257–262, 2010.
- [23] F. Antonii, "'Panacea aurea-auro potabile,'" *Hambg. Ex Bibliopolio Frobeniano*, p. 250, 1618.
- [24] R. Kahn, "Serum Diagnosis for Syphilis.," *Colloid Chem.*, vol. 2, p. 757, 1928.
- [25] E. A. Hauser, "Aurum potabile," *J. Chem. Educ.*, vol. 29, no. 9, p. 456, Sep. 1952.
- [26] D. H. Brown and W. E. Smith, "The chemistry of the gold drugs used in the treatment of rheumatoid arthritis," *Chem. Soc. Rev.*, vol. 9, no. 2, p. 217, 1980.
- [27] A. D. Hyatt and B. Eaton, *Immuno-gold electron microscopy in virus diagnosis and research*. CRC Press, 1992.
- [28] M. Faraday, "The Bakerian Lecture: Experimental Relations of Gold (and Other Metals) to Light," *Philos. Trans. R. Soc. London*, vol. 147, pp. 145–181, 1857.
- [29] The Royal Institution's Faraday Museum, *The Royal Institution of Great Britain*. London, UK.: 21 Albemarle Street.
- [30] W. Ostwald, "Zur Geschichte des Colloiden Goldes.," *Kolloid Polym. Sci.*, vol. 4, no. 1, pp. 5–14, 1909.
- [31] C. Cretu and E. Van Der Lingen, "Coloured Gold Alloys," *Gold Bull.*, vol. 32, no. September, pp. 115–126, 1999.
- [32] G. Mie, "Beiträge zur Optik trüber Medien, speziell kolloidaler Metallösungen," *Ann. Phys.*, vol. 25, no. 3, pp. 377–445, 1908.
- [33] M. Kerker, *The Scattering of Light and other Electromagnetic Radiation*. Academic Press: New York, 1969.
- [34] W. Hergert and T. Wriedt, *The Mie Theory*, vol. 169. 2012.
- [35] R. Feynman, "Miniaturization," *Reinhold, New York*, pp. 282–296, 1961.
- [36] "Gold Nanoparticles: Properties and Applications | Sigma-Aldrich." [Online]. Available: <https://www.sigmaaldrich.com/materials-science/nanomaterials/gold-nanoparticles.html>. [Accessed: 24-Apr-2016].
- [37] U. Kreibig and M. Vollmer, *Optical Properties of Metal Clusters*. Springer Science & Business Media, 2013.
- [38] G. Schmid, *Clusters and Colloids - From Theory to Applications*. VCH: Weinheim, Germany, 1994.
- [39] C. Brechignac, P. Houdy, and M. Lahmani, *Nanomaterials and nanochemistry*.

2007.

- [40] H. A. Atwater, "The Promise of Plasmonics," *Sci. Am.*, vol. 296, no. 4, pp. 56–62, Apr. 2007.
- [41] S. K. Ghosh, A. Pal, S. Kundu, S. Nath, and T. Pal, "Fluorescence quenching of 1-methylaminopyrene near gold nanoparticles: size regime dependence of the small metallic particles," *Chem. Phys. Lett.*, vol. 395, no. 4–6, pp. 366–372, Sep. 2004.
- [42] S. K. Ghosh, S. Kundu, M. Mandal, and T. Pal, "Silver and Gold Nanocluster Catalyzed Reduction of Methylene Blue by Arsine in a Micellar Medium," *Langmuir*, vol. 18, no. 23, pp. 8756–8760, Nov. 2002.
- [43] R. Kubo, "Electronic Properties of Metallic Fine Particles. I.," *J. Phys. Soc. Japan*, vol. 17, no. 6, pp. 975–986, 1962.
- [44] P. R. Sajanlal, T. S. Sreepasad, A. K. Samal, and T. Pradeep, "Anisotropic nanomaterials: structure, growth, assembly, and functions," *Nano Rev.*, vol. 2, no. 0, pp. 1–62, 2011.
- [45] S. Chen and R. Pei, "Ion-Induced Rectification of Nanoparticle Quantized Capacitance Charging in Aqueous Solutions," *J. Am. Chem. Soc.*, vol. 123, no. 43, pp. 10607–10615, Oct. 2001.
- [46] A. Henglein and M. Giersig, "Optical and Chemical Observations on Gold–Mercury Nanoparticles in Aqueous Solution," *J. Phys. Chem. B*, vol. 104, no. 21, pp. 5056–5060, Jun. 2000.
- [47] S. Park, P. Yang, P. Corredor, and M. J. Weaver, "Transition Metal-Coated Nanoparticle Films: Vibrational Characterization with Surface-Enhanced Raman Scattering," *J. Am. Chem. Soc.*, vol. 124, no. 11, pp. 2428–2429, Mar. 2002.
- [48] J.-I. Park and J. Cheon, "Synthesis of 'Solid Solution' and 'Core-Shell' Type Cobalt–Platinum Magnetic Nanoparticles via Transmetalation Reactions," *J. Am. Chem. Soc.*, vol. 123, no. 24, pp. 5743–5746, Jun. 2001.
- [49] Z. L. Wang, "Transmission Electron Microscopy of Shape-Controlled Nanocrystals and Their Assemblies," *J. Phys. Chem. B*, vol. 104, no. 6, pp. 1153–1175, Feb. 2000.
- [50] J. T. Krug, G. D. Wang, S. R. Emory, and S. Nie, "Efficient Raman Enhancement and Intermittent Light Emission Observed in Single Gold Nanocrystals," *J. Am. Chem. Soc.*, vol. 121, no. 39, pp. 9208–9214, Oct. 1999.
- [51] A. C. Templeton, M. J. Hostetler, E. K. Warmoth, S. Chen, C. M. Hartshorn, V. M. Krishnamurthy, M. D. E. Forbes, and R. W. Murray, "Gateway Reactions to Diverse, Polyfunctional Monolayer-Protected Gold Clusters," *J. Am. Chem. Soc.*, vol. 120, no. 19, pp. 4845–4849, May 1998.

- [52] M. P. Pileni, A. Taleb, and C. Petit, "Silver metal nanosized particles: Control of particle size, self assemblies in 2D and 3D superlattices and optical properties," *J. Dispers. Sci. Technol.*, vol. 19, no. 2–3, pp. 185–206, Jan. 1998.
- [53] A. Henglein, "Colloidal Palladium Nanoparticles: Reduction of Pd(II) by H₂; Pd Core Au Shell Ag Shell Particles," *J. Phys. Chem. B*, vol. 104, no. 29, pp. 6683–6685, Jul. 2000.
- [54] M. M. Alvarez, J. T. Khoury, T. G. Schaaff, M. N. Shafiqullin, R. L. Whetten, and I. Vezmar, "Optical Absorption Spectra of Nanocrystal Gold Molecules," *J. Phys. Chem. B*, vol. 101, no. 19, pp. 3706–3712, 1997.
- [55] Y. Li, C. Jing, L. Zhang, and Y.-T. Long, "Resonance scattering particles as biological nanosensors in vitro and in vivo.," *Chem. Soc. Rev.*, vol. 41, no. 2, pp. 632–42, Jan. 2012.
- [56] R. H. Ritchie, "Plasma Losses by Fast Electrons in Thin Films," *Phys. Rev.*, vol. 106, no. 5, pp. 874–881, 1957.
- [57] H. Raether, "Surface-Plasmons on Smooth and Rough Surfaces and on Gratings," *Springer Tracts in Modern Physics*, vol. 111. pp. 1–133, 1988.
- [58] H. Raether, *Surface Plasmons ed G Hohler*. Berlin: Springer, 1988.
- [59] W. L. Barnes, A. Dereux, and T. W. Ebbesen, "Surface plasmon subwavelength optics.," *Nature*, vol. 424, no. 6950, pp. 824–30, Aug. 2003.
- [60] M. Moskovits, "Surface-enhanced spectroscopy," *Rev. Mod. Phys.*, vol. 57, no. 3, pp. 783–826, Jul. 1985.
- [61] H. Metiu and P. Das, "The Electromagnetic Theory of Surface Enhanced Spectroscopy," *Annu. Rev. Phys. Chem.*, vol. 35, no. 1, pp. 507–536, Oct. 1984.
- [62] W. L. Barnes, a. Dereux, and T. W. Ebbesen, "Surface plasmon subwavelength optics," *Nature*, vol. 424, no. 6950, pp. 824–30, 2003.
- [63] R. W. Wood, "XLII. On a remarkable case of uneven distribution of light in a diffraction grating spectrum," *Philos. Mag. Ser. 6*, vol. 4, no. 21, pp. 396–402, Sep. 1902.
- [64] U. FANO, "The Theory of Anomalous Diffraction Gratings and of Quasi-Stationary Waves on Metallic Surfaces (Sommerfeld's Waves)," *J. Opt. Soc. Am.*, vol. 31, no. 3, p. 213, Mar. 1941.
- [65] A. Otto, "Excitation of nonradiative surface plasma waves in silver by the method of frustrated total reflection," *Zeitschrift für Phys.*, vol. 216, no. 4, pp. 398–410, Aug. 1968.
- [66] E. Kretschmann and H. Raether, "Notizen: Radiative Decay of Non Radiative

- Surface Plasmons Excited by Light,” *Zeitschrift für Naturforsch. A*, vol. 23, no. 12, pp. 2135–2136, Jan. 1968.
- [67] A. D. Boardman, *Electromagnetic Surface Modes*. Chichester, UK: Wiley, 1980.
- [68] A. Ishimaru, S. Jaruwatanadilok, and Y. Kuga, “GENERALIZED SURFACE PLASMON RESONANCE SENSORS USING METAMATERIALS AND NEGATIVE INDEX MATERIALS,” *Prog. Electromagn. Res.*, vol. 51, pp. 139–152, 2005.
- [69] J. M. Pitarke, V. M. Silkin, E. V Chulkov, and P. M. Echenique, “Theory of surface plasmons and surface-plasmon polaritons,” *Reports Prog. Phys.*, vol. 70, no. 1, pp. 1–87, Jan. 2007.
- [70] S. Efrima and H. Metiu, “Classical theory of light scattering by an adsorbed molecule. I. Theory,” *J. Chem. Phys.*, vol. 70, no. 4, p. 1602, Jul. 1979.
- [71] P. K. Aravind and H. Metiu, “The enhancement of raman and fluorescent intensity by small surface roughness. changes in dipole emission,” *Chem. Phys. Lett.*, vol. 74, no. 2, pp. 301–305, Sep. 1980.
- [72] M. Mirkin, CA and Ratner, “Controlled synthesis and quantum-size effect in gold-coated nanoparticles,” *Annu Rev Phys Chem*, vol. 101, p. 1593, 1997.
- [73] J. Gersten and A. Nitzan, “Electromagnetic theory of enhanced Raman scattering by molecules adsorbed on rough surfaces,” *J. Chem. Phys.*, vol. 73, no. 7, p. 3023, 1980.
- [74] M. A. Rampi, O. J. A. Schueller, and G. M. Whitesides, “Alkanethiol self-assembled monolayers as the dielectric of capacitors with nanoscale thickness,” *Appl. Phys. Lett.*, vol. 72, no. 14, p. 1781, Apr. 1998.
- [75] D.-S. Wang, H. Chew, and M. Kerker, “Enhanced Raman scattering at the surface (SERS) of a spherical particle,” *Appl. Opt.*, vol. 19, no. 14, p. 2256, Jul. 1980.
- [76] M. Brack, “The physics of simple metal clusters: self-consistent jellium model and semiclassical approaches,” *Rev. Mod. Phys.*, vol. 65, no. 3, pp. 677–732, Jul. 1993.
- [77] A. Adams, R. W. Rendell, R. W. Garnett, P. K. Hansma, and H. Metiu, “Effect of metal film thickness on surface-atom coupling,” *Opt. Commun.*, vol. 34, no. 3, pp. 417–420, Sep. 1980.
- [78] A. Adams, R. W. Rendell, W. P. West, H. P. Broida, P. K. Hansma, and H. Metiu, “Luminescence and nonradiative energy transfer to surfaces,” *Phys. Rev. B*, vol. 21, no. 12, pp. 5565–5571, Jun. 1980.
- [79] A. Wokaun, J. P. Gordon, and P. F. Liao, “Radiation Damping in Surface-Enhanced Raman Scattering,” *Phys. Rev. Lett.*, vol. 48, no. 14, pp. 957–960, Apr. 1982.

- [80] L. Genzel, T. P. Martin, and U. Kreibig, “Dielectric function and plasma resonances of small metal particles,” *Zeitschrift für Phys. B Condens. Matter Quanta*, vol. 21, no. 4, pp. 339–346, Dec. 1975.
- [81] C. C. Lam, P. T. Leung, and K. Young, “Explicit asymptotic formulas for the positions, widths, and strengths of resonances in Mie scattering,” *J. Opt. Soc. Am. B*, vol. 9, no. 9, p. 1585, Sep. 1992.
- [82] M. Meier and A. Wokaun, “Enhanced fields on large metal particles: dynamic depolarization,” *Opt. Lett.*, vol. 8, no. 11, p. 581, Nov. 1983.
- [83] U. Kreibig and C. v. Fragstein, “The limitation of electron mean free path in small silver particles,” *Zeitschrift für Phys.*, vol. 224, no. 4, pp. 307–323, Aug. 1969.
- [84] R. H. Doremus and P. Rao, “Optical properties of nanosized gold particles,” *J. Mater. Res.*, vol. 11, no. 11, pp. 2834–2840, Jan. 2011.
- [85] “Special issue: Nanostructured Materials,” *Chem. Mater.*, vol. 8, p. 1569, 1996.
- [86] J. R. and others Heath, “The chemistry of size and order on the nanometer scale,” *Sci. YORK THEN Washingt.*, vol. 270, p. 1315, 1995.
- [87] J. J. Storhoff, R. Elghanian, R. C. Mucic, C. A. Mirkin, and R. L. Letsinger, “One-Pot Colorimetric Differentiation of Polynucleotides with Single Base Imperfections Using Gold Nanoparticle Probes,” *J. Am. Chem. Soc.*, vol. 120, no. 9, pp. 1959–1964, Mar. 1998.
- [88] M. Duval Malinsky, K. L. Kelly, G. C. Schatz, and R. P. Van Duyne, “Nanosphere Lithography: Effect of Substrate on the Localized Surface Plasmon Resonance Spectrum of Silver Nanoparticles,” *J. Phys. Chem. B*, vol. 105, no. 12, pp. 2343–2350, Mar. 2001.
- [89] R. P. Van Duyne, J. C. Hulteen, and D. A. Treichel, “Atomic force microscopy and surface-enhanced Raman spectroscopy. I. Ag island films and Ag film over polymer nanosphere surfaces supported on glass,” *J. Chem. Phys.*, vol. 99, no. 3, p. 2101, Aug. 1993.
- [90] U. Kreibig, M. Gartz, and A. Hilger, “Mie resonances: Sensors for physical and chemical cluster interface properties,” *Berichte der Bunsengesellschaft für Phys. Chemie*, vol. 101, no. 11, pp. 1593–1604, Nov. 1997.
- [91] R. Elghanian, “Selective Colorimetric Detection of Polynucleotides Based on the Distance-Dependent Optical Properties of Gold Nanoparticles,” *Science (80-)*, vol. 277, no. 5329, pp. 1078–1081, Aug. 1997.
- [92] A. Otto, “Raman scattering from adsorbates on silver,” *Surf. Sci.*, vol. 92, no. 1, pp. 145–152, Feb. 1980.
- [93] R. Dornhaus, R. E. Benner, R. K. Chang, and I. Chabay, “Surface plasmon

- contribution to SERS,” *Surf. Sci.*, vol. 101, no. 1–3, pp. 367–373, Dec. 1980.
- [94] S. Nie, “Probing Single Molecules and Single Nanoparticles by Surface-Enhanced Raman Scattering,” *Science* (80-.), vol. 275, no. 5303, pp. 1102–1106, Feb. 1997.
- [95] C. Y. Chen and E. Burstein, “Giant Raman Scattering by Molecules at Metal-Island Films,” *Phys. Rev. Lett.*, vol. 45, no. 15, pp. 1287–1291, Oct. 1980.
- [96] M. Quinten, A. Leitner, J. R. Krenn, and F. R. Aussenegg, “Electromagnetic energy transport via linear chains of silver nanoparticles,” *Opt. Lett.*, vol. 23, no. 17, p. 1331, Sep. 1998.
- [97] S. A. Maier, P. G. Kik, and H. A. Atwater, “Optical pulse propagation in metal nanoparticle chain waveguides,” *Phys. Rev. B*, vol. 67, no. 20, p. 205402, May 2003.
- [98] J. R. Krenn, A. Dereux, J. C. Weeber, E. Bourillot, Y. Lacroute, J. P. Goudonnet, G. Schider, W. Gotschy, A. Leitner, F. R. Aussenegg, and C. Girard, “Squeezing the Optical Near-Field Zone by Plasmon Coupling of Metallic Nanoparticles,” *Phys. Rev. Lett.*, vol. 82, no. 12, pp. 2590–2593, Mar. 1999.
- [99] J. Pendry, “APPLIED PHYSICS:Enhanced: Playing Tricks with Light,” *Science* (80-.), vol. 285, no. 5434, pp. 1687–1688, Sep. 1999.
- [100] E. Betzig and J. K. Trautman, “Near-field optics: microscopy, spectroscopy, and surface modification beyond the diffraction limit.,” *Science*, vol. 257, no. 5067, pp. 189–95, Jul. 1992.
- [101] R. D. Grober, T. D. Harris, J. K. Trautman, E. Betzig, W. Wegscheider, L. Pfeiffer, and K. West, “Optical spectroscopy of a GaAs/AlGaAs quantum wire structure using near-field scanning optical microscopy,” *Appl. Phys. Lett.*, vol. 64, no. 11, p. 1421, Mar. 1994.
- [102] S. K. Buratto, J. W. P. Hsu, J. K. Trautman, E. Betzig, R. B. Bylisma, C. C. Bahr, and M. J. Cardillo, “Imaging InGaAsP quantum-well lasers using near-field scanning optical microscopy,” *J. Appl. Phys.*, vol. 76, no. 12, p. 7720, Dec. 1994.
- [103] J. I. Gersten, “The effect of surface roughness on surface enhanced Raman scattering,” *J. Chem. Phys.*, vol. 72, no. 10, p. 5779, 1980.
- [104] M. Moskovits, “Surface roughness and the enhanced intensity of Raman scattering by molecules adsorbed on metals,” *J. Chem. Phys.*, vol. 69, no. 9, p. 4159, 1978.
- [105] M. Moskovits, “Enhanced Raman scattering by molecules adsorbed on electrodes—a theoretical model,” *Solid State Commun.*, vol. 32, no. 1, pp. 59–62, Oct. 1979.
- [106] M. Kerker, D.-S. Wang, and H. Chew, “Surface enhanced Raman scattering (SERS) by molecules adsorbed at spherical particles: errata,” *Appl. Opt.*, vol. 19, no. 24, p. 4159, Dec. 1980.

- [107] B. PETTINGER, G. PICARDI, R. SCHUSTER, and G. ERTL, "Surface Enhanced Raman Spectroscopy : Towards Single Molecule Spectroscopy," *Electrochemistry*, vol. 68, no. 12, p. 942, 2000.
- [108] V. Bonacic-Koutecky, P. Fantucci, and J. Koutecky, "Quantum chemistry of small clusters of elements of groups Ia, Ib, and IIa: fundamental concepts, predictions, and interpretation of experiments," *Chem. Rev.*, vol. 91, no. 5, pp. 1035–1108, Jul. 1991.
- [109] K.-P. Charlé, F. Frank, and W. Schulze, "The Optical Properties of Silver Microcrystallites in Dependence on Size and the Influence of the Matrix Environment," *Berichte der Bunsengesellschaft für Phys. Chemie*, vol. 88, no. 4, pp. 350–354, Apr. 1984.
- [110] J. A. A. J. Perenboom, P. Wyder, and F. Meier, "Electronic properties of small metallic particles," *Phys. Rep.*, vol. 78, no. 2, pp. 173–292, Nov. 1981.
- [111] T. G. Schaaff, M. N. Shafigullin, J. T. Houry, I. Vezmar, R. L. Whetten, W. G. Cullen, P. N. First, C. Gutiérrez-Wing, J. Ascensio, and M. J. Jose-Yacamán, "Isolation of Smaller Nanocrystal Au Molecules: Robust Quantum Effects in Optical Spectra," *J. Phys. Chem. B*, vol. 101, no. 40, pp. 7885–7891, Oct. 1997.
- [112] B. M. I. van der Zande, M. R. Böhmer, L. G. J. Fokkink, and C. Schönenberger, "Aqueous Gold Sols of Rod-Shaped Particles," *J. Phys. Chem. B*, vol. 101, no. 6, pp. 852–854, Feb. 1997.
- [113] T. G. Schaaff, G. Knight, M. N. Shafigullin, R. F. Borkman, and R. L. Whetten, "Isolation and Selected Properties of a 10.4 kDa Gold:Glutathione Cluster Compound," *J. Phys. Chem. B*, vol. 102, no. 52, pp. 10643–10646, Dec. 1998.
- [114] A. J. Nozik and R. Memming, "Physical Chemistry of Semiconductor–Liquid Interfaces," *J. Phys. Chem.*, vol. 100, no. 31, pp. 13061–13078, Jan. 1996.
- [115] S. Link, M. B. Mohamed, and M. A. El-Sayed, "Simulation of the Optical Absorption Spectra of Gold Nanorods as a Function of Their Aspect Ratio and the Effect of the Medium Dielectric Constant," *J. Phys. Chem. B*, vol. 103, no. 16, pp. 3073–3077, 1999.
- [116] Yu, S.-S. Chang, C.-L. Lee, and C. R. C. Wang, "Gold Nanorods: Electrochemical Synthesis and Optical Properties," *J. Phys. Chem. B*, vol. 101, no. 34, pp. 6661–6664, Aug. 1997.
- [117] K. L. Kelly, E. Coronado, L. L. Zhao, and G. C. Schatz, "The Optical Properties of Metal Nanoparticles: The Influence of Size, Shape, and Dielectric Environment," *J. Phys. Chem. B*, vol. 107, no. 3, pp. 668–677, Jan. 2003.
- [118] R. P. Devaty and A. J. Sievers, "Possibility of observing quantum size effects in

- the electromagnetic absorption spectrum of small metal particles,” *Phys. Rev. B*, vol. 32, no. 4, pp. 1951–1954, Aug. 1985.
- [119] M. Kubo and S. Nakamura, “The Dielectric Constant of Dispersion of Spherical Particles,” *Bull. Chem. Soc. Jpn.*, vol. 26, no. 6, pp. 318–322, 1953.
- [120] T. Maniv and H. Metiu, “Electrodynamics at a metal surface with applications to the spectroscopy of adsorbed molecules. I. General theory,” *Phys. Rev. B*, vol. 22, no. 10, pp. 4731–4738, Nov. 1980.
- [121] G. C. Papavassiliou, “Optical properties of small inorganic and organic metal particles,” *Prog. Solid State Chem.*, vol. 12, no. 3–4, pp. 185–271, Jan. 1979.
- [122] P. K. Aravind, A. Nitzan, and H. Metiu, “The interaction between electromagnetic resonances and its role in spectroscopic studies of molecules adsorbed on colloidal particles or metal spheres,” *Surf. Sci.*, vol. 110, no. 1, pp. 189–204, Sep. 1981.
- [123] M. Quinten and U. Kreibig, “Absorption and elastic scattering of light by particle aggregates,” *Appl. Opt.*, vol. 32, no. 30, p. 6173, Oct. 1993.
- [124] M. Quinten and U. Kreibig, “Optical properties of aggregates of small metal particles,” *Surf. Sci.*, vol. 172, no. 3, pp. 557–577, Jul. 1986.
- [125] J. C. Maxwell Garnett, “Colours in Metal Glasses and in Metallic Films.II,” *proceeding R. Soc. London*, vol. 73, pp. 443–445, 1904.
- [126] J. C. M. Garnett, “Colours in Metal Glasses, in Metallic Films, and in Metallic Solutions. II,” *Philos. Trans. R. Soc. A Math. Phys. Eng. Sci.*, vol. 205, no. 387–401, pp. 237–288, 1906.
- [127] C. A. Foss, G. L. Hornyak, J. A. Stockert, and C. R. Martin, “Optical properties of composite membranes containing arrays of nanoscopic gold cylinders,” *J. Phys. Chem.*, vol. 96, no. 19, pp. 7497–7499, Sep. 1992.
- [128] G. L. Hornyak, C. J. Patrissi, and C. R. Martin, “Fabrication, Characterization, and Optical Properties of Gold Nanoparticle/Porous Alumina Composites: The Nonscattering Maxwell–Garnett Limit,” *J. Phys. Chem. B*, vol. 101, no. 9, pp. 1548–1555, Feb. 1997.
- [129] J. Belloni, M. Mostafavi, H. Remita, J.-L. Marignier, and M.-O. Delcourt, “Radiation-induced synthesis of mono- and multi-metallic clusters and nanocolloids,” *New Journal of Chemistry*, vol. 22, pp. 1239–1255, 1998.
- [130] G. C. Schatz, “Electrodynamics of nonspherical noble metal nanoparticles and nanoparticle aggregates,” *J. Mol. Struct. THEOCHEM*, vol. 573, no. 1–3, pp. 73–80, Oct. 2001.
- [131] P. W. Barber and S. C. Hill, *Light Scattering by Particles: Computational Methods*. World Scientific, 1990.

- [132] B. T. Draine and P. J. Flatau, “Discrete-dipole approximation for scattering calculations,” *J. Opt. Soc. Am. A*, vol. 11, no. 4, p. 1491, Apr. 1994.
- [133] M. M. Miller and A. A. Lazarides, “Sensitivity of metal nanoparticle surface plasmon resonance to the dielectric environment,” *J. Phys. Chem. B.*, vol. 109, no. 46, pp. 21556–21565, 2005.
- [134] C. R. Purcell, Edward M and Pennypacker, “Scattering and absorption of light by nonspherical dielectric grains,” *Astrophys. J.*, vol. 186, pp. 705–714, 1973.
- [135] T. R. Jensen, M. L. Duval, K. L. Kelly, A. A. Lazarides, G. C. Schatz, and R. P. Van Duyne, “Nanosphere Lithography: Effect of the External Dielectric Medium on the Surface Plasmon Resonance Spectrum of a Periodic Array of Silver Nanoparticles,” *J. Phys. Chem. B*, vol. 103, no. 45, pp. 9846–9853, Nov. 1999.
- [136] K. Yee, “Numerical solution of initial boundary value problems involving Maxwell’s equations in isotropic media,” *Antennas and Propagation, IEEE Transactions on*, vol. 14, no. 3. pp. 302–307, 1966.
- [137] A. Taflove, “Application of the Finite-Difference Time-Domain Method to Sinusoidal Steady-State Electromagnetic-Penetration Problems,” *IEEE Trans. Electromagn. Compat.*, vol. EMC-22, no. 3, pp. 191–202, Aug. 1980.
- [138] Optiwave, “OptiFDTD,” 2012.
- [139] J. a. Pereda, A. Grande, O. González, and Á. Vegas, “The 1D ADI-FDTD method in lossy media,” *IEEE Antennas Wirel. Propag. Lett.*, vol. 7, no. FEBRUARY, pp. 477–480, 2008.
- [140] D. M. Sullivan, *Electromagnetic Simulation Using the FDTD Method*. John Wiley & Sons, 2013.
- [141] J. B. Schneider, “Understanding the Finite-Difference Time-Domain Method,” *Self Publ.*, 2013.
- [142] R. Jin, Y. Cao, C. a Mirkin, K. L. Kelly, G. C. Schatz, and J. G. Zheng, “Photoinduced conversion of silver nanospheres to nanoprisms.,” *Science*, vol. 294, no. 5548, pp. 1901–1903, 2001.
- [143] B. O. Dabbousi, J. Rodriguez, F. V Mikulec, J. R. Heine, H. Mattoussi, R. Ober, K. F. Jensen, and M. G. Bawendi, “(CdSe)ZnS Core - Shell Quantum Dots : Synthesis and Characterization of a Size Series of Highly Luminescent Nanocrystallites,” *J. Phys. Chem. B*, vol. 101, no. 97, pp. 9463–9475, 1997.
- [144] A. P. Alivisatos, “Perspectives on the Physical Chemistry of Semiconductor Nanocrystals,” *J. Phys. Chem.*, vol. 100, no. 31, pp. 13226–13239, Jan. 1996.
- [145] C. B. Murray, D. J. Norris, and M. G. Bawendi, “Synthesis and characterization of nearly monodisperse CdE (E = sulfur, selenium, tellurium) semiconductor

- nanocrystallites,” *J. Am. Chem. Soc.*, vol. 115, no. 19, pp. 8706–8715, Sep. 1993.
- [146] A. C. Templeton, J. J. Pietron, R. W. Murray, P. Mulvaney, K. Laboratories, V. Uni, C. Hill, and N. Carolina, “Solvent Refractive Index and Core Charge Influences on the Surface Plasmon Absorbance of Alkanethiolate Monolayer-Protected Gold Clusters,” *J. Phys. Chem. B*, vol. 104, no. 3, pp. 564–570, 2000.
- [147] M. Gao, S. Kirstein, H. Möhwald, A. L. Rogach, A. Kornowski, A. Eychmüller, and H. Weller, “Strongly Photoluminescent CdTe Nanocrystals by Proper Surface Modification,” *J. Phys. Chem. B*, vol. 102, no. 43, pp. 8360–8363, Oct. 1998.
- [148] X. Peng, M. C. Schlamp, A. V. Kadavanich, and A. P. Alivisatos, “Epitaxial Growth of Highly Luminescent CdSe/CdS Core/Shell Nanocrystals with Photostability and Electronic Accessibility,” *J. Am. Chem. Soc.*, vol. 119, no. 30, pp. 7019–7029, Jul. 1997.
- [149] S.-M. Lee, Y. Jun, S.-N. Cho, and J. Cheon, “Single-Crystalline Star-Shaped Nanocrystals and Their Evolution: Programming the Geometry of Nano-Building Blocks,” *J. Am. Chem. Soc.*, vol. 124, no. 38, pp. 11244–11245, Sep. 2002.
- [150] S. Chen, Z. L. Wang, J. Ballato, S. H. Foulger, and D. L. Carroll, “Monopod, Bipod, Tripod, and Tetrapod Gold Nanocrystals,” *J. Am. Chem. Soc.*, vol. 125, no. 52, pp. 16186–16187, Dec. 2003.
- [151] E. Hao, R. C. Bailey, G. C. Schatz, J. T. Hupp, and S. Li, “Synthesis and Optical Properties of ‘Branched’ Gold Nanocrystals,” *Nano Lett.*, vol. 4, no. 2, pp. 327–330, Feb. 2004.
- [152] L. Manna, E. C. Scher, and A. P. Alivisatos, “Synthesis of Soluble and Processable Rod-, Arrow-, Teardrop-, and Tetrapod-Shaped CdSe Nanocrystals,” *J. Am. Chem. Soc.*, vol. 122, no. 51, pp. 12700–12706, Dec. 2000.
- [153] L. Manna, D. J. Milliron, A. Meisel, E. C. Scher, and A. P. Alivisatos, “Controlled growth of tetrapod-branched inorganic nanocrystals,” *Nat. Mater.*, vol. 2, no. 6, pp. 382–385, Jun. 2003.
- [154] Y. Jin and S. Dong, “One-Pot Synthesis and Characterization of Novel Silver–Gold Bimetallic Nanostructures with Hollow Interiors and Bearing Nanospikes,” *J. Phys. Chem. B*, vol. 107, no. 47, pp. 12902–12905, Nov. 2003.
- [155] S. . Oldenburg, R. . Averitt, S. . Westcott, and N. . Halas, “Nanoengineering of optical resonances,” *Chem. Phys. Lett.*, vol. 288, no. 2–4, pp. 243–247, May 1998.
- [156] S. J. Oldenburg, J. B. Jackson, S. L. Westcott, and N. J. Halas, “Infrared extinction properties of gold nanoshells,” *Appl. Phys. Lett.*, vol. 75, no. 19, p. 2897, 1999.
- [157] C. Graf and A. van Blaaderen, “Metallo-dielectric Colloidal Core–Shell Particles for Photonic Applications,” *Langmuir*, vol. 18, no. 2, pp. 524–534, Jan. 2002.

- [158] J. B. Jackson and N. J. Halas, "Silver Nanoshells: Variations in Morphologies and Optical Properties," *J. Phys. Chem. B*, vol. 105, no. 14, pp. 2743–2746, Apr. 2001.
- [159] V. F. Puntes, D. Zanchet, C. K. Erdonmez, and A. P. Alivisatos, "Synthesis of hcp-Co Nanodisks," *J. Am. Chem. Soc.*, vol. 124, no. 43, pp. 12874–12880, Oct. 2002.
- [160] S. Chen, Z. Fan, and D. L. Carroll, "Silver Nanodisks: Synthesis, Characterization, and Self-Assembly," *J. Phys. Chem. B*, vol. 106, no. 42, pp. 10777–10781, Oct. 2002.
- [161] M.-P. and others Maillard, Mathieu and Giorgio, Suzanne and Pileni, "Silver nanodisks," *Adv. Mater.*, vol. 14, no. 15, p. 1084, 2002.
- [162] I. Pastoriza-Santos and L. M. Liz-Marzán, "Synthesis of Silver Nanoprisms in DMF," *Nano Lett.*, vol. 2, no. 8, pp. 903–905, Aug. 2002.
- [163] J. Yang and J. H. Fendler, "Morphology Control of PbS Nanocrystallites, Epitaxially Grown under Mixed Monolayers," *J. Phys. Chem.*, vol. 99, no. 15, pp. 5505–5511, Apr. 1995.
- [164] Y. Sun, B. Mayers, and Y. Xia, "Transformation of Silver Nanospheres into Nanobelts and Triangular Nanoplates through a Thermal Process," *Nano Lett.*, vol. 3, no. 5, pp. 675–679, May 2003.
- [165] Y. Xia, P. Yang, Y. Sun, Y. Wu, B. Mayers, B. Gates, Y. Yin, F. Kim, and H. Yan, "One-Dimensional Nanostructures: Synthesis, Characterization, and Applications," *Adv. Mater.*, vol. 15, no. 5, pp. 353–389, Mar. 2003.
- [166] B. D. Busbee, S. O. Obare, and C. J. Murphy, "An Improved Synthesis of High-Aspect-Ratio Gold Nanorods," *Adv. Mater.*, vol. 15, no. 5, pp. 414–416, Mar. 2003.
- [167] S.-S. Chang, C.-W. Shih, C.-D. Chen, W.-C. Lai, and C. R. C. Wang, "The Shape Transition of Gold Nanorods," *Langmuir*, vol. 15, no. 3, pp. 701–709, Feb. 1999.
- [168] N. R. Jana, L. Gearheart, and C. J. Murphy, "Wet chemical synthesis of silver nanorods and nanowires of controllable aspect ratio," *Chem. Commun.*, no. 7, pp. 617–618, 2001.
- [169] F. Kim, J. H. Song, and P. Yang, "Photochemical synthesis of gold nanorods," *J. Am. Chem. Soc.*, vol. 124, no. 48, pp. 14316–7, Dec. 2002.
- [170] Y. Sun, "Shape-Controlled Synthesis of Gold and Silver Nanoparticles," *Science (80-.)*, vol. 298, no. 5601, pp. 2176–2179, Dec. 2002.
- [171] M. A. Ahmadi, Temer S and Wang, Zhong L and Green, Travis C and Henglein, Arnim and El-Sayed, "Shape-controlled synthesis of colloidal platinum nanoparticles," *Science (80-.)*, vol. 272, no. 5270, p. 1924, 1996.

- [172] X. Peng, L. Manna, W. Yang, J. Wickham, E. Scher, A. Kadavanich, and A. P. Alivisatos, "Shape control of CdSe nanocrystals," *Nature*, vol. 404, no. 6773, pp. 59–61, Mar. 2000.
- [173] M. B. Mohamed, V. Volkov, S. Link, and M. A. El-Sayed, "The 'lightning' gold nanorods: fluorescence enhancement of over a million compared to the gold metal," *Chem. Phys. Lett.*, vol. 317, no. 6, pp. 517–523, Feb. 2000.
- [174] W. U. Huynh and A. P. A. Janke J. Dittmer, "Hybrid Nanorod-Polymer Solar Cells," *Science (80-.)*, vol. 295, no. 5564, pp. 2425–2427, Mar. 2002.
- [175] Y. Sun and Y. Xia, "Increased Sensitivity of Surface Plasmon Resonance of Gold Nanoshells Compared to That of Gold Solid Colloids in Response to Environmental Changes," *Anal. Chem.*, vol. 74, no. 20, pp. 5297–5305, Oct. 2002.
- [176] E. Hao and G. C. Schatz, "Electromagnetic fields around silver nanoparticles and dimers," *J. Chem. Phys.*, vol. 120, no. 1, p. 357, 2004.
- [177] B. Nikoobakht, J. Wang, and M. A. El-Sayed, "Surface-enhanced Raman scattering of molecules adsorbed on gold nanorods: off-surface plasmon resonance condition," *Chem. Phys. Lett.*, vol. 366, no. 1–2, pp. 17–23, Nov. 2002.
- [178] G. S. Métraux, Y. C. Cao, R. Jin, and C. a. Mirkin, "Triangular Nanoframes Made of Gold and Silver," *Nano Lett.*, vol. 3, no. 4, pp. 519–522, Apr. 2003.
- [179] Y. Sun and Y. Xia, "Triangular Nanoplates of Silver: Synthesis, Characterization, and Use as Sacrificial Templates For Generating Triangular Nanorings of Gold," *Adv. Mater.*, vol. 15, no. 9, pp. 695–699, May 2003.
- [180] P. D. Cozzoli, A. Kornowski, and H. Weller, "Low-temperature synthesis of soluble and processable organic-capped anatase TiO₂ nanorods.," *J. Am. Chem. Soc.*, vol. 125, no. 47, pp. 14539–48, Nov. 2003.
- [181] S.-J. Park, S. Kim, S. Lee, Z. G. Khim, K. Char, and T. Hyeon, "Synthesis and Magnetic Studies of Uniform Iron Nanorods and Nanospheres," *J. Am. Chem. Soc.*, vol. 122, no. 35, pp. 8581–8582, Sep. 2000.
- [182] A. Gole and C. J. Murphy, "Polyelectrolyte-coated gold nanorods: Synthesis, characterization and immobilization," *Chem. Mater.*, vol. 17, no. 6, pp. 1325–1330, Mar. 2005.
- [183] M. D. Malinsky, K. L. Kelly, G. C. Schatz, and R. P. Van Duyne, "Chain Length Dependence and Sensing Capabilities of the Localized Surface Plasmon Resonance of Silver Nanoparticles Chemically Modified with Alkanethiol Self-Assembled Monolayers," *J. Am. Chem. Soc.*, vol. 123, no. 7, pp. 1471–1482, Feb. 2001.
- [184] A. J. Haes and R. P. Van Duyne, "A Nanoscale Optical Biosensor: Sensitivity and

- Selectivity of an Approach Based on the Localized Surface Plasmon Resonance Spectroscopy of Triangular Silver Nanoparticles,” *J. Am. Chem. Soc.*, vol. 124, no. 35, pp. 10596–10604, Sep. 2002.
- [185] G. Chumanov, K. Sokolov, B. W. Gregory, and T. M. Cotton, “Colloidal metal films as a substrate for surface-enhanced spectroscopy,” *J. Phys. Chem.*, vol. 99, no. 23, pp. 9466–9471, Jun. 1995.
- [186] C. L. Haynes and R. P. Van Duyne, “Nanosphere lithography: A versatile nanofabrication tool for studies of size-dependent nanoparticle optics,” *J. Phys. Chem. B*, vol. 105, no. 24, pp. 5599–5611, 2001.
- [187] C. Xue, Z. Li, and C. A. Mirkin, “Large-scale assembly of single-crystal silver nanoprism monolayers,” *Small*, vol. 1, no. 5, pp. 513–6, May 2005.
- [188] H. S. Nalwa, *Nanostructured Materials and Nanotechnology: Concise Edition*, Gulf Profe. Gulf Professional Publishing, 2001.
- [189] N. Malikova, I. Pastoriza-santos, M. Schierhorn, N. A. Kotov, and L. M. Lizmarza, “Layer-by-Layer Assembled Mixed Spherical and Planar Gold Nanoparticles : Control of Interparticle Interactions,” *Langmuir*, vol. 18, no. 9, pp. 3694–3697, 2002.
- [190] T. J. Norman, C. D. Grant, D. Magana, J. Z. Zhang, D. Cao, F. Bridges, and A. Van Buuren, “Near Infrared Optical Absorption of Gold Nanoparticle Aggregates,” *J. Phys. Chem. B*, vol. 106, no. 28, pp. 7005–7012, 2002.
- [191] C. S. Ah, Y. J. Yun, H. J. Park, W. Kim, D. H. Ha, and W. S. Yun, “Size-Controlled Synthesis of Machinable Single Crystalline Gold Nanoplates,” *Chem. Mater.*, vol. 17, no. 22, pp. 5558–5561, 2005.
- [192] J. E. Millstone, S. Park, K. L. Shuford, L. Qin, G. C. Schatz, and C. a. Mirkin, “Observation of a quadrupole plasmon mode for a colloidal solution of gold nanoprisms,” *J. Am. Chem. Soc.*, vol. 127, no. 15, pp. 5312–5313, 2005.
- [193] S. Chen and D. L. Carroll, “Synthesis and Characterization of Truncated Triangular Silver Nanoplates,” *Nano Lett.*, vol. 2, no. 9, pp. 1003–1007, Sep. 2002.
- [194] S. Chen and D. L. Carroll, “Silver Nanoplates: Size Control in Two Dimensions and Formation Mechanisms,” *J. Phys. Chem. B*, vol. 108, no. 18, pp. 5500–5506, May 2004.
- [195] G. S. Métraux and C. a. Mirkin, “Rapid Thermal Synthesis of Silver Nanoprisms with Chemically Tailorable Thickness **,” *Adv. Mater.*, vol. 17, no. 4, pp. 412–415, 2005.
- [196] T. Klaus, R. Joerger, E. Olsson, and C.-G. Granqvist, “Silver-based crystalline nanoparticles, microbially fabricated,” *Proc. Natl. Acad. Sci.*, vol. 96, no. 24, pp.

13611–13614, 1999.

- [197] B. Liu, J. Xie, J. Y. Lee, Y. P. Ting, and J. P. Chen, “Optimization of High-Yield Biological Synthesis of Single-Crystalline Gold Nanoplates,” *J. Phys. Chem. B*, vol. 109, no. 32, pp. 15256–15263, 2005.
- [198] S. S. Shankar, A. Rai, B. Ankamwar, A. Singh, A. Ahmad, and M. Sastry, “Biological synthesis of triangular gold nanoprisms,” *Nat. Mater.*, vol. 3, no. 7, pp. 482–488, Jul. 2004.
- [199] S. P. Chandran, M. Chaudhary, R. Pasricha, A. Ahmad, and M. Sastry, “Synthesis of gold nanotriangles and silver nanoparticles using Aloe vera plant extract.,” *Biotechnol. Prog.*, vol. 22, no. 2, pp. 577–83, Jan. .
- [200] S. Brown, M. Sarikaya, and E. Johnson, “A Genetic Analysis of Crystal Growth,” *J. Mol. Biol.*, vol. 299, pp. 725–735, 2000.
- [201] L. Jiang, S. Xu, J. Zhu, J. Zhang, J. Zhu, and H. Chen, “Ultrasonic-Assisted Synthesis of Monodisperse Single-Crystalline Silver Nanoplates and Gold Nanorings,” *Inorg. Chem.*, vol. 43, no. 19, pp. 5877–5883, 2004.
- [202] Y. Y. K. Okitsu, A. Yue, S. Tanabe, H. Matsumoto, “Formation of Colloidal Gold Nanoparticles in an Ultrasonic Field: Control of Rate of Gold(III) Reduction and Size of Formed Gold Particles,” *Langmuir*, vol. 23, p. 13244, 2007.
- [203] K. Okitsu, A. Yue, S. Tanabe, H. Matsumoto, and Y. Yobiko, “Formation of Colloidal Gold Nanoparticles in an Ultrasonic Field : Control of Rate of Gold (III) Reduction and Size of Formed Gold Particles,” *Langmuir*, vol. 17, no. 25, pp. 7717–7720, 2001.
- [204] M. Tsuji, M. Hashimoto, Y. Nishizawa, and T. Tsuji, “Preparation of Gold Nanoplates by a Microwave-polyol Method,” *Chem. Lett.*, vol. 32, no. 12, pp. 1114–1115, 2003.
- [205] C. Li, W. Cai, Y. Li, J. Hu, and P. Liu, “Ultrasonically Induced Au Nanoprisms and Their Size Manipulation Based on Aging,” *J. Phys. Chem. B*, vol. 110, pp. 1546–1552, 2006.
- [206] I. Pastoriza-santos and L. M. Liz-marza, “Formation of PVP-Protected Metal Nanoparticles in DMF,” *Langmuir*, vol. 18, no. 7, pp. 2888–2894, 2002.
- [207] A. Sarkar, S. Kapoor, and T. Mukherjee, “Synthesis of silver nanoprisms in formamide,” *J. Colloid Interface Sci.*, vol. 287, pp. 496–500, 2005.
- [208] V. Bastys, I. Pastoriza-Santos, B. Rodríguez-González, R. Vaisnoras, and L. M. Liz-Marzán, “Formation of silver nanoprisms with surface plasmons at communication wavelengths,” *Adv. Funct. Mater.*, vol. 16, no. 6, pp. 766–773, 2006.

- [209] A. Callegari, D. Tonti, and M. Chergui, "Photochemically Grown Silver Nanoparticles with Wavelength-Controlled Size and Shape," *Nano Lett.*, vol. 3, pp. 1565–1568, 2003.
- [210] C. Xue, G. S. Métraux, J. E. Millstone, and C. A. Mirkin, "Mechanistic study of photomediated triangular silver nanoprism growth," *J. Am. Chem. Soc.*, vol. 130, no. 26, pp. 8337–8344, 2008.
- [211] X. Wu, P. L. Redmond, H. Liu, Y. Chen, M. Steigerwald, and L. Brus, "Photovoltage mechanism for room light conversion of citrate stabilized silver nanocrystal seeds to large nanoprisms," *J. Am. Chem. Soc.*, vol. 130, pp. 9500–9506, 2008.
- [212] M. Maillard, P. Huang, and L. Brus, "Silver Nanodisk Growth by Surface Plasmon Enhanced Photoreduction of Adsorbed [Ag⁺]," *Nano Lett.*, vol. 3, no. 11, pp. 1611–1615, 2003.
- [213] P. L. Redmond, E. C. Walter, and L. E. Brus, "Photoinduced thermal copper reduction onto gold nanocrystals under potentiostatic control," *J. Phys. Chem. B*, vol. 110, no. 50, pp. 25158–25162, 2006.
- [214] a J. Hallock, P. L. Redmond, and L. E. Brus, "Optical forces between metallic particles.," *Proc. Natl. Acad. Sci. U. S. A.*, vol. 102, pp. 1280–1284, 2005.
- [215] V. Wong and M. A. Ratner, "Size dependence of gradient and nongradient optical forces in silver nanoparticles," *J. Opt. Soc. Am. B*, vol. 24, no. 1, p. 106, 2007.
- [216] A. Henglein, "Physicochemical properties of small metal particles in solution: 'microelectrode' reactions, chemisorption, composite metal particles, and the atom-to-metal transition," *J. Phys. Chem.*, vol. 97, no. 21, pp. 5457–5471, May 1993.
- [217] A. Machulek Junior, H. P. M. de Oliveira, and M. H. Gehlen, "Preparation of silver nanoprisms using poly(N-vinyl-2-pyrrolidone) as a colloid-stabilizing agent and the effect of silver nanoparticles on the photophysical properties of cationic dyes.," *Photochem. Photobiol. Sci.*, vol. 2, pp. 921–925, 2003.
- [218] C.-M. Ho, C.-K. Wong, S. K.-W. Yau, C.-N. Lok, and C.-M. Che, "Oxidative dissolution of silver nanoparticles by dioxygen: a kinetic and mechanistic study.," *Chem. Asian J.*, vol. 6, no. 9, pp. 2506–11, Sep. 2011.
- [219] R. Jin, Y. Charles Cao, E. Hao, G. S. Métraux, G. C. Schatz, and C. a Mirkin, "Controlling anisotropic nanoparticle growth through plasmon excitation," *Nature*, vol. 425, no. 6957, pp. 487–490, Oct. 2003.
- [220] J. Zhang, M. R. Langille, and C. A. Mirkin, "Photomediated synthesis of silver triangular bipyramids and prisms: the effect of pH and BSPP.," *J. Am. Chem. Soc.*,

vol. 132, no. 35, pp. 12502–10, Sep. 2010.

- [221] C. Xue, J. E. Millstone, S. Li, and C. A. Mirkin, “Plasmon-Driven Synthesis of Triangular Core–Shell Nanoprisms from Gold Seeds,” *Angew. Chemie*, vol. 119, no. 44, pp. 8588–8591, Nov. 2007.
- [222] C. Xue and C. A. Mirkin, “pH-Switchable Silver Nanoprism Growth Pathways,” *Angew. Chemie*, vol. 119, no. 12, pp. 2082–2084, Mar. 2007.
- [223] X. Zheng, W. Xu, C. Corredor, S. Xu, J. An, B. Zhao, and J. R. Lombardi, “Laser-induced growth of monodisperse silver nanoparticles with tunable surface plasmon resonance properties and a wavelength self-limiting effect,” *J. Phys. Chem. C*, vol. 111, no. 41, pp. 14962–14967, 2007.
- [224] T. C. R. Rocha, H. Winnischofer, E. Westphal, and D. Zanchet, “Formation kinetics of silver triangular nanoplates,” *J. Phys. Chem. C*, vol. 111, no. 7, pp. 2885–2891, 2007.
- [225] A. Dmitriev, T. Pakizeh, M. Käll, and D. S. Sutherland, “Gold-silica-gold nanosandwiches: tunable bimodal plasmonic resonators.,” *Small*, vol. 3, no. 2, pp. 294–9, Feb. 2007.
- [226] S. I. Bozhevolnyi, V. S. Volkov, E. Devaux, J.-Y. Laluet, and T. W. Ebbesen, “Channel plasmon subwavelength waveguide components including interferometers and ring resonators.,” *Nature*, vol. 440, no. 7083, pp. 508–11, Mar. 2006.
- [227] J. Homola, S. S. Yee, and G. Gauglitz, “Surface plasmon resonance sensors: review,” *Sensors Actuators B Chem.*, vol. 54, no. 1–2, pp. 3–15, Jan. 1999.
- [228] T. M. Chinowsky, L. S. Jung, and S. S. Yee, “Optimal linear data analysis for surface plasmon resonance biosensors,” *Sensors Actuators B Chem.*, vol. 54, no. 1–2, pp. 89–97, Jan. 1999.
- [229] K. a Willets and R. P. Van Duyne, “Localized surface plasmon resonance spectroscopy and sensing.,” *Annu. Rev. Phys. Chem.*, vol. 58, no. October, pp. 267–97, Jan. 2007.
- [230] G. H. Chan, J. Zhao, E. M. Hicks, G. C. Schatz, and R. P. Van Duyne, “Plasmonic Properties of Copper Nanoparticles Fabricated by Nanosphere Lithography,” *Nano Lett.*, vol. 7, no. 7, pp. 1947–1952, Jul. 2007.
- [231] E. Ringe, J. M. McMahan, K. Sohn, C. Copley, Y. Xia, J. Huang, G. C. Schatz, L. D. Marks, and R. P. Van Duyne, “Unraveling the Effects of Size, Composition, and Substrate on the Localized Surface Plasmon Resonance Frequencies of Gold and Silver Nanocubes: A Systematic Single-Particle Approach,” *J. Phys. Chem. C*, vol. 114, no. 29, pp. 12511–12516, Jul. 2010.

- [232] O. Stranik, R. Nooney, C. McDonagh, and B. D. MacCraith, "Optimization of Nanoparticle Size for Plasmonic Enhancement of Fluorescence," *Plasmonics*, vol. 2, no. 1, pp. 15–22, Dec. 2006.
- [233] P. N. Njoki, I.-I. S. Lim, D. Mott, H.-Y. Park, B. Khan, S. Mishra, R. Sujakumar, J. Luo, and C.-J. Zhong, "Size Correlation of Optical and Spectroscopic Properties for Gold Nanoparticles," *J. Phys. Chem. C*, vol. 111, no. 40, pp. 14664–14669, Oct. 2007.
- [234] R. Cui, C. Liu, J. Shen, D. Gao, J.-J. Zhu, and H.-Y. Chen, "Gold Nanoparticle-Colloidal Carbon Nanosphere Hybrid Material: Preparation, Characterization, and Application for an Amplified Electrochemical Immunoassay," *Adv. Funct. Mater.*, vol. 18, no. 15, pp. 2197–2204, Aug. 2008.
- [235] J. Zhou, W. Wu, D. Caruntu, M. H. Yu, a. Martin, J. F. Chen, C. J. O'Connor, and W. L. Zhou, "Synthesis of Porous Magnetic Hollow Silica Nanospheres for Nanomedicine Application," *J. Phys. Chem. C*, vol. 111, no. 47, pp. 17473–17477, Nov. 2007.
- [236] J. Perezjuste, I. Pastorizasantos, L. Lizmarzan, and P. Mulvaney, "Gold nanorods: Synthesis, characterization and applications," *Coord. Chem. Rev.*, vol. 249, no. 17–18, pp. 1870–1901, Sep. 2005.
- [237] J. E. Millstone, S. J. Hurst, G. S. Métraux, J. I. Cutler, and C. a. Mirkin, "Colloidal gold and silver triangular nanoprisms," *Small*, vol. 5, no. 6, pp. 646–664, 2009.
- [238] M. Tréguer-Delapierre, J. Majimel, S. Mornet, E. Duguet, and S. Ravaine, "Synthesis of non-spherical gold nanoparticles," *Gold Bull.*, vol. 41, no. 2, pp. 195–207, 2008.
- [239] L. Liz-Marzán, "Tailoring surface plasmons through the morphology and assembly of metal nanoparticles," *Langmuir*, vol. 22, no. 1, pp. 32–41, Jan. 2006.
- [240] J. Nelayah, M. Kociak, O. Stéphan, F. J. García de Abajo, M. Tencé, L. Henrard, D. Taverna, I. Pastoriza-Santos, L. M. Liz-Marzán, and C. Colliex, "Mapping surface plasmons on a single metallic nanoparticle," *Nat. Phys.*, vol. 3, no. 5, pp. 348–353, 2007.
- [241] Y. Kenzo and I. Tomohiro, "Electric field enhancement of nano gap of silver prisms," *Chinese Phys. ...*, vol. 24, no. 10, pp. 29–34, 2007.
- [242] J. E. Millstone, G. S. Métraux, and C. A. Mirkin, "Controlling the edge length of gold nanoprisms via a seed-mediated approach," *Adv. Funct. Mater.*, vol. 16, pp. 1209–1214, 2006.
- [243] M. Tsuji, M. Hashimoto, Y. Nishizawa, M. Kubokawa, and T. Tsuji, "Microwave-assisted synthesis of metallic nanostructures in solution," *Chemistry - A European*

Journal, vol. 11. pp. 440–452, 2005.

- [244] B. J. Wiley, Y. Xiong, Z. Y. Li, Y. Yin, and Y. Xia, “Right bipyramids of silver: A new shape derived from single twinned seeds,” *Nano Lett.*, vol. 6, pp. 765–768, 2006.
- [245] J. E. Millstone, W. Wei, M. R. Jones, H. Yoo, and C. A. Mirkin, “Iodide ions control seed-mediated growth of anisotropic gold Nanoparticles,” *Nano Lett.*, vol. 8, pp. 2526–2529, 2008.
- [246] L. J. Sherry, R. Jin, C. a Mirkin, G. C. Schatz, and R. P. Van Duyne, “Localized surface plasmon resonance spectroscopy of single silver triangular nanoprisms,” *Nano Lett.*, vol. 6, no. 9, pp. 2060–2065, Sep. 2006.
- [247] S. Pal, Y. K. Tak, and J. M. Song, “Does the antibacterial activity of silver nanoparticles depend on the shape of the nanoparticle? A study of the gram-negative bacterium *Escherichia coli*,” *Appl. Environ. Microbiol.*, vol. 73, no. 6, pp. 1712–1720, 2007.
- [248] A. A. Ashkarran and A. Bayat, “Surface plasmon resonance of metal nanostructures as a complementary technique for microscopic size measurement,” vol. 2, no. d, p. 1, 2013.
- [249] K. Kimura, “Shape effect and quantum size effect on small metal particles,” *Zeitschrift fur Phys. D Atoms, Mol. Clust.*, vol. 11, no. 4, pp. 327–332, 1989.
- [250] F. Hache, D. Ricard, and C. Flytzanis, “Optical nonlinearities of small metal particles: surface-mediated resonance and quantum size effects,” *J. Opt. Soc. Am. B*, vol. 3, no. 12, p. 1647, 1986.
- [251] S. Alsheheri, M. Saboktakin, and M. Matin, “The effect of truncation in plasmon resonance of metal nanoprisms,” 2015, p. 95472H.
- [252] M. L. Brongersma and V. M. Shalaev, “Applied physics. The case for plasmonics,” *Science*, vol. 328, no. 5977, pp. 440–441, 2010.
- [253] S. A. Maier, *Plasmonic: Fundamentals and Applications*. Springer Science & Business Media, 2007.
- [254] R. Gans, “Form of ultramicroscopic particles of silver,” *Ann. Phys.*, vol. 47, no. 10, pp. 270–284, 1915.
- [255] U. Kreibig and L. Genzel, “Optical absorption u. kreibig of small metallic particles,” *Surf. Sci.*, vol. 156, pp. 678–700, 1985.
- [256] B. N. J. Persson, “Polarizability of small spherical metal particles: influence of the matrix environment,” *Surf. Sci.*, vol. 281, no. 1–2, pp. 153–162, 1993.
- [257] N. Nath and A. Chilkoti, “A colorimetric gold nanoparticle sensor to interrogate

- biomolecular interactions in real time on a surface,” *Anal. Chem.*, vol. 74, no. 3, pp. 504–509, 2002.
- [258] A. A. Lazarides, K. Lance Kelly, T. R. Jensen, and G. C. Schatz, “Optical properties of metal nanoparticles and nanoparticle aggregates important in biosensors,” *J. Mol. Struct. THEOCHEM*, vol. 529, pp. 59–63, 2000.
- [259] a. J. Haes, W. P. Hall, L. Chang, W. L. Klein, and R. P. Van Duyne, “A Localized Surface Plasmon Resonance Biosensor: First Steps toward an Assay for Alzheimer’s Disease,” *Nano Lett.*, vol. 4, no. 6, pp. 1029–1034, 2004.
- [260] G. Raschke, S. Brogl, A. S. Susha, A. L. Rogach, T. A. Klar, J. Feldmann, B. Fieres, N. Petkov, T. Bein, A. Nichtl, and K. Kürzinger, “Gold nanoshells improve single nanoparticle molecular sensors,” *Nano Lett.*, vol. 4, no. 10, pp. 1853–1857, 2004.
- [261] T. R. Jensen, M. L. Duval, T. R. Jensen, M. L. Duval, K. L. Kelly, K. L. Kelly, a a Lazarides, A. a. Lazarides, G. C. Schatz, G. C. Schatz, and R. P. Van Duyne, “Nanosphere Lithography: Effect of the External Dielectric Medium on the Surface Plasmon Resonance Spectrum of a Periodic Array of Silver Nanoparticles,” *J. Phys. Chem. B*, vol. 103, no. 45, pp. 9846–9853, 1999.
- [262] E. A. Coronado and G. C. Schatz, “Surface plasmon broadening for arbitrary shape nanoparticles: A geometrical probability approach,” *J. Chem. Phys.*, vol. 119, no. 7, pp. 3926–3934, 2003.
- [263] F. Tam, C. Moran, and N. Halas, “Geometrical parameters controlling sensitivity of nanoshell plasmon resonances to changes in dielectric environment,” *J. Phys. Chem. B*, vol. 108, no. 45, pp. 17290–17294, 2004.
- [264] S. Link, M. B. Mohamed, and M. A. El-Sayed, “Simulation of the Optical Absorption Spectra of Gold Nanorods as a Function of Their Aspect Ratio and the Effect of the Medium Dielectric Constant,” *J. Phys. Chem. B*, vol. 103, no. 16, pp. 3073–3077, Apr. 1999.
- [265] K. M. Mayer, S. Lee, H. Liao, B. C. Rostro, A. Fuentes, P. T. Scully, C. L. Nehl, and J. H. Hafner, “A Label-Free Immunoassay Based Upon Localized Surface Plasmon Resonance of Gold Nanorods,” *ACS Nano*, vol. 2, no. 4, pp. 687–692, Apr. 2008.
- [266] N. Nath and A. Chilkoti, “Label-free biosensing by surface plasmon resonance of nanoparticles on glass: Optimization of nanoparticle size,” *Anal. Chem.*, vol. 76, no. 18, pp. 5370–5378, 2004.
- [267] J. J. Mock, D. R. Smith, and S. Schultz, “Local refractive index dependence of plasmon resonance spectra from individual nanoparticles,” *Nano Lett.*, vol. 3, no. 4, pp. 485–491, 2003.

- [268] A. D. McFarland and R. P. Van Duyne, "Single silver nanoparticles as real-time optical sensors with zeptomole sensitivity," *Nano Lett.*, vol. 3, no. 8, pp. 1057–1062, 2003.
- [269] M. M. Shahjamali, M. Bosman, S. Cao, X. Huang, S. Saadat, E. Martinsson, D. Aili, Y. Y. Tay, B. Liedberg, S. C. J. Loo, H. Zhang, F. Boey, and C. Xue, "Gold Coating of Silver Nanoprisms," *Adv. Funct. Mater.*, vol. 22, no. 4, pp. 849–854, Feb. 2012.
- [270] S. Alsheheri, M. Saboktakin, and M. Matin, "Hybrid plasmonic nanosandwich structures," 2015, p. 95442R.
- [271] S. Alsheheri, M. Saboktakin, and M. Matin, "STUDY OF THE SNIP EFFECT IN RESONANCE OF HYBRID PLASMONIC NANOSANDWICH STRUCTURES IN OPTICAL RANGE," *Asian J. Sci. Technol.*, vol. 7, no. 2, pp. 2446–2454, 2016.

Appendix A: List of Publications

Journal Publications:

[1] S. Alsheheri, M. Saboktakin, and M. Matin, “A Simulation Study of the Plasmonic Resonance of Sharp and Truncated Silver Triangular Nanoprisms,” *J. Multidiscip. Eng. Sci. Technol.*, vol. 3, no. 1, pp. 3799–3802, 2016.

[2] S. Alsheheri, M. Saboktakin, and M. Matin, “Study of the Snip Effect in Resonance of Hybrid Plasmonic Nanosandwich Structures in Optical Range,” *Asian Journal Of Science And Technologies.*, February, 2016 (**In Press**)

Conference Publications:

[1] S. Alsheheri, M. Saboktakin, and M. Matin, “Hybrid plasmonic nanosandwich structures,” 2015, p. 95442R.

[2] S. Alsheheri, M. Saboktakin, and M. Matin, “The effect of truncation in plasmon resonance of metal nanoprisms,” 2015, p. 95472H.








Permission Asian Journal of Science and Technology

<http://journalajst.com/>

Copyrights:

Open Access authors retain the copyrights of their papers, and all open access articles are distributed under the terms of the Creative Commons Attribution license, which permits unrestricted use, distribution and reproduction in any medium, provided that the original work is properly cited.

Permission from SPIE

 New  Reply  Delete  Archive  Junk  Sweep  Move to  Categories 

RE: Question



Nicole Harris (nicoleh@spie.org) [Add to contacts](#) 2/2/2016

To: S. A.

Dear Soad Alsheheri,

Thank you for seeking permission from SPIE to reprint material from our publications. As author, SPIE shares the copyright with you, so you retain the right to reproduce your paper in part or in whole.

Publisher's permission is hereby granted under the following conditions:

- (1) the material to be used has appeared in our publication without credit or acknowledgment to another source; and
- (2) you credit the original SPIE publication. Include the authors' names, title of paper, volume title, SPIE volume number, and year of publication in your credit statement.

Sincerely,

Nicole Harris

Administrative Editor, SPIE Publications

1000 20th St.

Bellingham, WA 98225

+1 360 685 5586 (office)

nicoleh@spie.org

SPIE is the international society for optics and photonics. <http://SPIE.org>

SPIE.

From: S. A. [mailto:soad1001@hotmail.com]
Sent: Monday, February 1, 2016 9:55 PM
To: reprint_permission <reprint_permission@spie.org>
Subject: Question

Hi,

I am Soad Alsheheri, I have published two papers in SPIE Optics and Photonics Conference August (9-13) 2015 and I want to use all of them in my thesis, so I want to know what should I do??

This is information about my paper:

Title: The effect of truncation in plasmon resonance of metal nanoparticles

Authors: [Soad Alsheheri](#) , [Marjan Saboktakin](#) , [Mohammad Matin](#)

Vol. 9547, 95472E

DOI: [10.1117/12.2186139](https://doi.org/10.1117/12.2186139)

SPSPE Vol. 9547, 95472E-2

SPIE Optics and Photonics Conference August (9-13) 2015

Vol. 9544, 95442R.

DOI: 10.1117/12.2185685

SPIE Vol. 9544 95442R-1

Title: Hybrid Plasmonic Nanosandwich Structures

Soad Alsheheri, Marjan Saboktakin, Mohammad Matin

© 2016 Microsoft Terms Privacy & cookies Developers English (United States)

Permission from Prof. Karl Heinz at Journal of Multidisciplinary Engineering Science

+ New Reply Delete Archive Junk Sweep Move to Categories

Re: Permission from Prof.Karl Heinz to use my paper in my thesis

↑ ↓ ×



Journal of Multidisciplinary Engineering Science 2/2/2016

To: S. A.

Dear Dr. Alsheheri,

Thanks for your email and attachments.

In placing the thesis on the author's university website, please display the following message in a prominent place on the website: In reference to JMEST copyrighted material which is used with permission in this thesis, the JMEST does not endorse any of [university/educational entity's name goes here]'s products or services. Internal or personal use of this material is permitted.

Once you need anything else, please do not hesitate to contact us.

Kind Regards,

Editor-in-Chief, JMEST

On Tue, Feb 2, 2016 at 8:18 AM, S. A. <soad1001@hotmail.com> wrote:

Dear Prof.Karl Heinz,

I need your permission to use this paper titled: **A SIMULATION STUDY OF THE PLASMONIC RESONANCE OF SHARP AND TRUNCATED SILVER TRIANGULAR NANOPRISMS** in my thesis My university requires all the coauthors permission to include the published article in thesis. Kindly reply at your earliest convenience. I will include your reply in the appendix of the thesis. Please ask me if you have any questions or concerns.

Thanks, have a great vacation with friend and family.

Kind Regards,

Soad Alsheheri